MODELLING PHASE TRANSFORMATION AND TENSILE PROPERTIES OF MICRO-ALLOYED STRUCTURAL STEELS FOR FIRE RESISTANCE

by

Fahim Khan

Student ID: 1017112027

MASTER OF SCIENCE IN MATERIALS AND METALLURGICAL ENGINEERING

Department of Materials and Metallurgical Engineering

BANGLADESH UNIVERSITY OF ENGINEERING AND TECHNOLOGY (BUET)

January 2022

The thesis titled **"Modeling Phase Transformation and Tensile Properties of Micro-Alloyed Structural Steels for Fire Resistance"**-Submitted by Fahim Khan, Roll No.1017112027 and Session: October 2017 has been accepted as satisfactory as a partial fulfilment of the requirement for the degree of M.Sc. Engg. in Materials and Metallurgical Engineering on 08 January 2022.

BOARD OF EXAMINERS

1. Dr. Hossain Mohammad Mamun Al Rashed
Associate Professor
Department of Materials and Metallurgical Engineering, BUET
Chairman
(Supervisor)

2. Head/Director
Professor
Department of Materials and Metallurgical Engineering, BUET
Member
(Ex-officio)

3. Dr. Kazi Mohammad Shorowordi
Professor
Department of Materials and Metallurgical Engineering, BUET
Member

4. Dr. Md. Muktadir Billah
Associate Professor
Department of Materials and Metallurgical Engineering, BUET
Member

5. Dr. Md. Mohar Ali
Ex Professor, MME, BUET
Department of Materials and Metallurgical Engineering, BUET
Member
(External)

CANDIDATE'S DECLARATION

Declared that except where specified by reference to other works, the experimental studies embodied in thesis is the result of investigation carried out by the author. Neither the thesis nor any part has been submitted to or is being submitted elsewhere for any other purposes.

Fahim Khan

Fahim Khan

ACKNOWLEDGEMENT

First, I would like to express my sincerest gratitude to the Almighty, the benevolent and the merciful, for His graciousness, unlimited kindness and divine blessings.

I would like to express my sincere gratitude to my thesis supervisor, Dr. H M Mamun Al Rashed, Associate Professor, MME, for his kind supervision, indispensable guidance, constructive suggestions and continuous encouragement during this thesis work. I am truly indebted to him for his esteemed guidance and encouragement from the beginning to the end of this thesis.

Finally, I must express my very profound gratitude to my parents and my wife Humayra Alam Shinjon for providing me with unfailing support and continuous encouragement throughout my years of study and through the process of researching and writing this thesis. This accomplishment would not have been possible without them.

ABSTRACT

Fire is one of the most extreme situations in which structural steels can be damaged, culminating in catastrophic failure. Common structural steels incur subsequent changes in physical characteristics, stiffness, and mechanical properties because of high temperature treatment, which is irreversible after cooling. As a result, many alloy steels have been created to address these issues. Steel produces ferrite to austenite transformation temperatures of 700–750 °C and relative instability of carbide precipitates over 650 °C since it is not fire resistant. Few steel grades have been developed to prevent this, which has led to an increase in the use of certain steel grades at higher temperatures. The demand for fire-resistant high-temperature construction steels has increased as construction technology has improved, resulting in shorter construction periods and more efficient use of space. The aim of the research was to establish a common structural steel by adding a few specific alloying elements like Mo, Cr, Al, and Ti that will assist the steel to maintain its strength at high temperatures. Using thermodynamic data for phases and mobility, CALPHAD-based computational techniques provided insights of microstructure and its impact on different properties. The addition of Mo and Cr retarded the cementite growth and widened the melting range. Consequently, solidus line shifted at higher temperature. Addition of Mo passively raised the cooling rate by increasing time of formation of ferrite, pearlite, austenite and martensite. Mo and Cr enhanced the precipitation of intermetallic carbides of high melting temperatures and controlled and retarded the growth of such carbides. Thus, yield strength of fire-resistant steel was greater than that of conventional steels at elevated temperatures. Owing to low yield ratio, the alloys had a higher ductility. High temperature steels had the same workability and weldability as standard steels. Mo addition significantly modified the elevated temperature strength. To consider the economic perspective, an alternative to Mo can be Cr which is quantitatively found in the prediction. Addition of Cr over Mo might not give better high temperature mechanical properties than solely added Mo but provided superior properties than the base alloy. Combined Mo and Cr addition retarded the formation of cementite which is brittle in nature. Mo addition is exclusively responsible to increase the phase transformation time that will definitely reduce the residual stress of the sample while cooling. The predictions derived from statistical data will undoubtedly aid in the development of experiments for future research.

Contents

CANDIDATE'S DECLARATION II

ACKNOWLEDGEMENT III

ABSTRACT IV

1 INTRODUCTION 1

2 LITERATURE REVIEW 4

2.1 STEEL 4
2.2 EFFECT OF ALLOYING ELEMENT ON STEELS 4
2.2.1 Austenite Stabilizers: 5
2.2.2 Ferrite Stabilizers: 5
1.1.1 Carbide Formers: 8
2.3 TRANSFORMATION TEMPERATURE 9
2.4 CONTINUOUS COOLING TRANSFORMATION (CCT) 10
2.5 MECHANICAL PROPERTIES ON COOLING RATE 10
2.6 MECHANICAL PROPERTIES ON TEMPERATURE 10
2.7 PRECIPITATION AMOUNT AND SIZE WITH TIME 11
2.8 STACKING FAULT ENERGY 11
2.9 STRESS-STRAIN CURVES 11
2.10 TIME TEMPERATURE TRANSFORMATION 11
2.11 CALPHAD 12
2.12 FIRE ON STEELS 13
2.13 EFFECTS OF FIRE ON STEELS 16
2.13.1 Corrosion 17
2.13.2 Changes in dimensions 17
2.13.3 Strength reduction 17
2.13.4 Changes in the steel microstructure are permanent 17
2.14 HIGH TEMPERATURE EFFECTS ON STEELS 18
2.15 FIRE RESISTANCE RATING 20
2.16 TYPES OF STEELS: 23
2.16.1 Nickel Steels: 23
2.16.2 Chromium Steels: 24
2.16.3 Manganese Steels: 24
2.16.4 Molybdenum Steels: 24
2.16.5 Tungsten Steels: 25
2.16.6 Titanium Steels: 25
2.16.7 Niobium Micro alloyed steels 27
2.17 EFFECT OF ALLOYING ELEMENT ON FERRITE: 28
2.18 INFLUENCE OF ALLOYING ELEMENTS ON IRON-IRON CARBIDE DIAGRAM: 30
2.19 EFFECT OF ALLOYING ELEMENT ON TEMPERING: 32

2.20 Effects of Alloying Elements on Hardenability 32
2.21 Effect on the Eutectoid Point 34
2.22 Distribution of Alloying Elements 36
2.23 Effect on Tempering 37
2.24 Computational Method 38
2.24.1 Calculation Method for Multi Component System 39
2.25 Scope of the Work 41

3 EXPERIMENTAL METHODS 42

3.1 Modeling of material data for distortion protection 45
3.1.1 TTT and CCT diagrams 45
3.1.2 Thermophysical and physical properties 46
3.1.3 Mechanical properties during heat treatment 46

4 RESULTS AND DISCUSSION 49

4.1 Microstructural evolution of equilibrium phase formation for different alloys at variable temperature: 49
4.1.1 Alloy 0: 49
4.1.2 Alloy 1: 50
4.1.3 Alloy 2: 51
4.1.4 Alloy 3: 52
4.1.5 Alloy 4: 53
4.1.6 Alloy 5: 54
4.1.7 Alloy 6: 55
4.2 Statistical study of phase formation at equilibrium condition: 56
4.2.1 Cementite: 56
4.2.2 Austenite 57
4.2.3 Solidus and Liquidus line: 58
4.2.4 Summary of phase formation at equilibrium condition: 58
4.3 Microstructural evolution of non-equilibrium phase formation at different alloys at variable temperature: 60
4.3.1 Alloy 0: 60
1.1.2 Alloy 1: 61
4.3.2 Alloy 2: 62
4.3.3 Alloy 3: 63
4.3.4 Alloy 4: 64
4.3.5 Alloy 5: 65
4.3.6 Alloy 6: 65
4.4 Statistical study of phases formation at non-equilibrium condition: 66
4.4.1 Austenite 66
4.4.2 Solidus and Liquidus lines: 67
4.4.3 Martensite: 67
4.4.4 Ferrite: 68
4.5 Equilibrium Phase Formation on Cooling Rate 68
4.5.1 Ferrite Fraction 68
4.5.2 Pearlite Fraction 69
4.5.3 Bainite Fraction 70
4.5.4 Austenite Fraction 71
4.5.5 Martensite Fraction 72
4.6 Equilibrium Phase formation on Temperature Dependence 73

4.6.1 Bainite formation ... *73*
4.6.2 Ferrite formation ... *74*
4.6.3 Pearlite formation ... *75*
4.7 NON-EQUILIBRIUM PHASES – PRECIPITATION AMOUNT ... 76
4.7.1 Precipitation Amount for MC: ... *76*
4.7.2 Precipitation Amount for M_2C: ... *78*
4.7.3 Precipitation Amount for M_3C: ... *79*
4.7.4 Precipitation Amount for M_7C_3: ... *79*
4.7.5 Precipitation Amount for $M_{23}C_6$: ... *81*
4.7.6 Precipitation Amount for M_6C: ... *82*
4.7.7 Precipitation Amount for M(C,N): ... *83*
4.8 NON-EQUILIBRIUM PHASES- PRECIPITATION SIZE ... 84
4.8.1 Precipitation Size for MC: ... *84*
4.8.2 Precipitation Size for M_2C: ... *85*
4.8.3 Precipitation Size for M_7C_3: ... *86*
4.8.4 Precipitation Size for $M_{23}C_6$: ... *87*
4.8.5 Precipitation Size for M_6C: ... *88*
4.9 TRANSFORMATION TEMPERATURE ... 89
4.9.1 Upper transformation temperature: ... *90*
4.9.2 Lower transformation temperature: ... *90*
4.10 FORMATION TEMPERATURE AND TIME: ... 90
4.10.1 A1 & A3 Temperature: ... *91*
4.10.2 Transformation Temperature Crossing Time (A_1 line) ... *92*
4.10.3 Initial Formation Temperature for Pearlite and Ferrite: ... *92*
4.10.4 Initial Formation Temperature for Bainite: ... *93*
4.10.5 Initial Formation Temperature for Austenite and Martensite: ... *94*
4.10.6 Initial Formation Time for Austenite, Pearlite and Ferrite: ... *94*
4.10.7 Initial Formation Time for Bainite and Martensite: ... *95*
4.11 MECHANICAL PROPERTIES ON COOLING RATE ... 96
4.11.1 Tensile stress ... *96*
4.11.2 Hardness ... *97*
4.12 MECHANICAL PROPERTIES ON TEMPERATURE ... 98
4.12.1 High Temperature Yield Strength: ... *98*
4.13 STRESS-STRAIN CURVE ... 100
4.13.1 SS Curve 600^oC ... *100*
4.13.2 SS Curve 800^oC ... *101*
4.13.3 SS Curve 1000^oC ... *102*
4.14 PRECIPITATION FORMATION ... 103
4.15 STACKING FAULT ENERGY ... 104
4.16 SUMMARY OF THE EFFECTS OF ALLOYING ELEMENTS ON FIRE RESISTANCE STEEL ... 105
4.16.1 Molybdenum: ... *105*
4.16.2 Chromium ... *108*
4.16.3 Other Alloying Elements ... *111*
5 CONCLUSIONS ... 112
5.1 SCOPE FOR FUTURE WORK ... 114
REFERENCE ... 115

List of Figures

Figure 2.12.1 Stages of Fire Development [54]. 15
Figure 2.14.1 Yield Strength Retention Factors for Structural Steels at Elevated Temperature [61] 18
Figure 2.14.2 Modulus of Elasticity Retention Factors for Structural Steels at Elevated Temperature [61] 19
Figure 2.17.1 Probable Hardening effect of the various elements as dissolved in alpha iron [64]. 29
Figure 2.17.2 The minor effect of chromium in annealed steels compared with the powerful effect as a strengthener through its influence on structure in air cooled steels. Probable Hardening effect of the various elements as dissolved in alpha iron [62] 30
Figure 2.18.1 Eutectoid composition and eutectoid temperature as influenced by several alloying elements. Probable Hardening effect of the various elements as dissolved in alpha iron [64]. 31
Figure 2.18.2 Range of austenite in chromium steels. [65] 32
Figure 2.21.1Influence of alloying element additions on the eutectoid temperature and the eutectoid carbon content [66] 35
Figure 2.21.1 Effect of alloying additions on the γ-phase field: (a) Mn; (b) Mo; (c) Cr; (d) Ti [66] 36
Figure 4.1.1 Equilibrium phases for alloy 0 50
Figure 4.1.2 Equilibrium phases for alloy 1 51
Figure 4.1.3 Equilibrium phases for alloy 2 52
Figure 4.1.4 Equilibrium phases for alloy 3 53
Figure 4.1.5 Equilibrium phases for alloy 4 54
Figure 4.1.6 Equilibrium phases for alloy 5 55
Figure 4.1.7 Equilibrium phases for alloy 6 56
Figure 4.3.1 Non-equilibrium phases for alloy 0 61
Figure 4.3.2 Non-equilibrium phases for alloy 1 61
Figure 4.3.3 Non-equilibrium phases for alloy 2 62
Figure 4.3.4 Non-equilibrium phases for alloy 3 63
Figure 4.3.5 Non-equilibrium phases for alloy 4 64
Figure 4.3.6 Non-equilibrium phases for alloy 5 65
Figure 4.3.7 Non-equilibrium phases for alloy 6 65
Fgure 4.5.1 Ferrite fraction vs cooling rate 69
Figure 4.5.2 Pearlite fraction vs cooling rate 70
Figure 4.5.3 Bainite fraction vs cooling rate 71
Figure 4.5.4 Austenite fraction vs cooling rate 72
Figure 4.5.5 Austenite fraction vs cooling rate 73
Figure 4.6.1 Bainite formation (1%) vs Temperature 74
Figure 4.6.2 Ferrite formation (1%) vs Temperature 75
Figure 4.6.3 Perlite formation (1%) vs Temperature 75
Figure 4.7.1 Precipitation amount of MC with time 77
Figure 4.7.2 Precipitation amount of M_2C with time 78
Figure 4.7.3 Precipitation amount of M_3C with time 79
Figure 4.7.4 Precipitation amount of M_7C_3 with time 80
Figure 4.7.5 Precipitation amount of $M_{23}C_6$ with time 81
Figure 4.7.6 Precipitation amount of M_6C with time 83
Figure 4.7.7 Precipitation amount of M(C,N) with time 83
Figure 4.8.1 Precipitation size of MC with time 85
Figure 4.8.2 Precipitation size of M_2C with time 86
Figure 4.8.3 Precipitation size of M_7C_3 with time 87

FIGURE 4.8.4 PRECIPITATION SIZE OF $M_{23}C_6$ WITH TIME 88
FIGURE 4.8.5 PRECIPITATION SIZE OF M_6C WITH TIME 89
FIGURE 4.10.1 DIFFERENCE BETWEEN A1 & A3 TEMPERATURE 91
FIGURE 4.10.2 TIME OF CROSSING A_1 LINE 92
FIGURE 4.10.3 INITIAL FORMATION TEMPERATURE OF PEARLITE, FERRITE, BAINITE, AUSTENITE AND MARTENSITE 93
FIGURE 4.10.4 INITIAL FORMATION TIME FOR AUSTENITE, PEARLITE AND FERRITE, BAINITE AND MARTENSITE 95
FIGURE 4.11.1 TENSILE STRESS VS COOLING RATE 96
FIGURE 4.11.2 HARDNESS VS COOLING RATE 97
FIGURE 4.12.1 HIGH TEMPERATURE YIELD STRENGTH FOR ALLOY 99
FIGURE 4.13.1 STRESS- STRAIN CURVE AT 600^oC 101
FIGURE 4.13.2 STRESS- STRAIN CURVE AT 800^oC 101
FIGURE 4.13.3 STRESS- STRAIN CURVE AT 1000^oC 102
FIGURE 4.15.1 STACKING FAULT ENERGY VS TEMPERATURE 105

List of Tables

TABLE 2.1.1 CHEMICAL COMPOSITIONS OF COMMON STRUCTURAL STEELS 4
TABLE 2.15.1 VALUES OF CONSTANT "A" [61] 22
TABLE 2.15.2 VALIDITY LIMITS [61] 23
TABLE 2.16.1 SUMMARY OF ALLOYING ELEMENT EFFECT OF DIFFERENT TYPES OF STEELS 27
TABLE 2.17.1 BEHAVIORS OF THE INDIVIDUAL ELEMENT IN ANNEALED STEELS 28
TABLE 4.2.1 CEMENTITE FORMATION FOR DIFFERENT ALLOYS 57
TABLE 4.2.2 AUSTENITE FORMATION FOR DIFFERENT ALLOYS 57
TABLE 4.2.3 SOLIDUS AND LIQUIDUS LINE 58
TABLE 4.2.4 SUMMARY OF EQUILIBRIUM PHASES 59
TABLE 4.4.1 AUSTENITE FORMATION FOR DIFFERENT ALLOYS 66
TABLE 4.4.2 LIQUID FORMATION FOR DIFFERENT ALLOYS 67
TABLE 4.4.3 MARTENSITE FORMATION FOR DIFFERENT ALLOYS 67
TABLE 4.4.4 FERRITE FORMATION FOR DIFFERENT ALLOYS 68
TABLE 4.7.1 SUMMARY OF THE EFFECT OF ALLOYING ELEMENT ON PRECIPITATION AMOUNT 84
TABLE 4.8.1 SUMMARY OF THE EFFECT OF ALLOYING ELEMENT ON PRECIPITATION SIZE 89
TABLE 4.13.1 EFFECT OF ALLOYING ELEMNT ON TRUE STRESS AT THE DIFFERENT TEMPERATURES 103

1 Introduction

Steel is an extremely configurable alloy with a wide range of inherent advantages and desirable properties including hardness, toughness, compressive strength, yield strength, conductivity, thermal expansion, elongation, flow ability, flexural behavior, fatigue strength, malleability and creep. Its most valuable properties are its high formability and resilience, as well as its high tensile and yield strength and good thermal conductivity [1]. When steel is heated, it expands. Thermal expansion occurs when temperature causes length, surface area, and volume to grow. Thermal expansion happens when the motions of the metal's atoms are increased by heat. Steel's mechanical properties deteriorate during a fire event due to the elevated temperature. The effects of this sudden fire on steel are serious, and it may even lead to catastrophic failure.

Steel is a high thermal conductivity which allows the temperature to rise dramatically as it is heated by fire. This means that simple link failures will cause floor assemblies to collapse under some circumstances [2]. To avoid this phenomenon, some improvements in the steel derives some modified mechanical properties that are changed as a result of a combination of chemical composition, manufacturing processes, and heat treatment. Iron is the most important component of steel; even small amounts of other elements can have a significant impact on its properties [3]. These elements have a huge impact on alloys. It influences the chemical, mechanical and other transformation properties drastically. Alloys are frequently utilized to improve the steel's properties and make it more feasible. When a composition of carbon and iron is alloyed with additional elements, it receives benefits such as corrosion resistance and increased strength.

To achieve the objectives, the approach was mainly towards to uphold the impact of the alloying elements like molybdenum, titanium, chromium, aluminum in some of steel alloys on their different phases. The method is carried out by adjusting different alloying content to alter the phase diagram. At elevated temperature, by using a CALPHAD-based computational technique different type of diagrams and investigations are generated when alloying elements are applied to EN 10025-2:2004 Grade S355. These diagrams include transformation temperatures, continuous cooling transformation curves, mechanical properties on cooling rate

and temperature, precipitation formation and size, SS-curves in different temperatures, TTT curves etc. With the increasing amount of alloying elements, the changes in the mentioned properties were observed thoroughly.

Chapter 2 discusses the basics of steel and ability of different stabilizers on microstructure. How the transformation of phases is controlled by alloying elements and effects of fire on steel strength are also highlighted here.

In Chapter 3, the methodology of the work is presented.

In Chapter 4, the modelling work in vividly described. The effects of elements on phase transformation and mechanical properties are compared and analyzed thoroughly.

In Chapter 5, the summary of the work is offered.

Most valuable properties of steel are its high formability and resilience, as well as its high tensile and yield strengths and good thermal conductivity. The heat of fire on steel causes the temperature to rise rapidly due to high thermal conductivity of steel and forms carbide at 650°C. To prevent this, a few steel grades were developed having higher yield strengths at elevated temperatures, resulting in the increased use of those steels in structures. This work presents the assessment of presence of different phases at certain temperature and time by adding different composition of Mo (0-0.75% with 0.25% in succession) on EN 10025-2:2004 Grade S355 at elevated temperature using CALPHAD based computational technique. The amalgamation of the data containing the change in phase transformation at certain temperature after quenching from elevated temperature. Optimized amount of molybdenum with other alloying elements can intelligently manipulate microstructure having different amounts of bainite, ferrites and pearlites to improve strength. Alloys 0 to 3 are the successive addition of 0.25% Mo up to 0.75% Mo. Addition of Mo lowers the elevated temperature stability of ferrite, bainite and austenite. The transformation temperature of ferrite, bainite and austenite shifts at the lower temperature than the base alloy upon addition of Mo. Thus, it may reduce the susceptibility of such phases to be stable at elevated temperature than the base alloy. On the other hand, in the case of pearlite it is clearly seen form the graph that addition of Mo causes stability of pearlite at much elevated temperature than the base alloy. In case of martensite, any significant effect of Mo has not been observed. The overall predictions provide observations about the improvement of common structural steels with addition of Molybdenum.

When first Mo is successively added then the cementite stability at the higher temperature reduces. At the elevated temperature the cementite growth remains faster. And at the elevated temperature the large grain size of brittle nature of cementite weakens the strength of the structural steels. But when Mo is added then the formation of cementite at the elevated temperature reduces down. Thus, it improves the elevated temperature strength to some extent. Cr is added over the Mo then these properties also enhanced but not linearly. It retards the growth of cementite less than the Mo.

Later, addition of Mo and Cr both are responsible to form carbides and intermetallic carbides to some extent. These carbides have better strength and due to high temperature stability, it withstands at the elevated temperature. But there came a risk about the grain size. Because irrespective of the amount of the carbide of high melting temperature if the size of the carbide or the growth of the carbide remains higher it will lessen the strength as a whole. Continuing the computation, it was found that the addition of Mo and Cr retards the grain growth of the carbide and lowers the size of the carbide particles. Thus, while cooling from the elevated temperature these carbides will cause precipitation hardening and increases the overall strength. While adding Ti and Al, they form more intermetallic carbides of high melting temperature.

Mo addition successively provides the best possible results. Then a question may arise about the addition of Cr over the Mo. The answer is the prices of Mo per ton is about ten times than the price of Cr per ton. As it is the common structural steels instead of increasing the high temperature properties and stability one thing needs to be taken in consideration is the economic perspective. If the price becomes much higher then it will be difficult for large scale use. Thus, an alternative to the Mo can be the Cr. Which gives a result closer to the Mo. This is the way it is tried to add Cr over Mo to see the impact.

Later in the Alloy 6, Ti and Al is added. Due to the complexities of the computational techniques later part has not been done. But predicted that it will help the common structural steels to sustain at the elevated temperature.

2 Literature Review

2.1 Steel

Steel is an alloy composed primarily of iron with a small percentage of carbon and other alloying elements. Carbon and other alloying elements are responsible to provide mechanical properties of steels. Iron has two allotropic forms depending on temperature: body centered cubic (BCC) and face centered cubic (FCC) [4]. In nature, pure iron is ductile. The addition of various alloying elements increases the strength and physical properties of the material. Steel is an alloy of iron and carbon (maximum solubility 2 percent). Steel is commonly employed in construction because of its high strength and low cost. Steel is by far the most widely used material for building infrastructure and industries around the world; it's used to make anything from sewing needles to oil tankers. Steel is also used in the tools that are used to construct and manufacture such items.

Table 2.1.1 Chemical compositions of Common Structural Steels

C	Si	Mn	S	P	Nb
0.15	0.4	1.4	0.0025	0.0025	0.01

Table 2.1.1 depicts the chemical composition of common structural steel. There are a variety of structural steel grades, the most popular being ASTM A36 and ASTM A572. These and other structural steel grades are primarily used to build frames of buildings and bridges. They are also used in the construction equipment. Structural steel comes in various shapes like L-beam, Z shape, HSS shape, L shape (angle), structural channel (C-beam, cross section), T shaped, rail profile, bar, rod, plate and an open joist of web steel. Standard structural steel varies in different countries with various specifications. This research work is about the variation of steel grade EN 10025-2:2004 S355, equivalent to ASTM A572 Grade 50.

2.2 Effect of Alloying Element on Steels

In comparison to those in plane carbon steels, alloy steels produce minimal concentrations of alloying elements. In addition to those which was already mentioned in plain carbon steels, Cr,

Ni, Mo, Nb, Ti, W, Co, Cu, V, Si, Al and B are included in the list of items that are relevant in alloy steels. Such elements trigger a number of improvements in steel's efficiency and properties. As the equilibrium state of steel is defined in the phase graphical charts accessible in Fe-C-x and other systems, alloying elements now have a significant impact on the characteristics of stainless-steel phase transitions. These effects influence both the kinetics of transformations and the method of transition as additional phases that are not present in plain carbon steels may be formed. Alloying components can have significant impacts on the recovery, recrystallization and grain growth of phenomena.

Classification of Alloying Elements:

Austenite Stabilizers, Ferrite Stabilizers, Carbide Formers, Graphite Stabilizers

2.2.1 Austenite Stabilizers:

When carbon is added to the iron it favors to form austenite than ferrite [5]. This is because it decreases the austenite to alpha ferrite transition temperature (the A_3 point), and also raises the austenite to delta ferrite transition temperature. It extends the gamma spectrum and hence is known as an austenite stabilizer. Once iron is analyzed for the binary phase diagrams of these elements, they can be separated into two classes.

Nickel and Manganese: Adding an alloy element depresses the FCC at a room temperature to BCC before other phases occur.

Other Austenite stabilizing elements are Pt, Ir, Os, and Ru.

2.2.2 Ferrite Stabilizers:

Some alloying elements tend to stabilize the ferrite phase in preference to austenite. Many of these elements have same crystal structure as ferrite (BCC). They reduce the extent of the austenite area on the equilibrium diagram by forming a gamma loop [6]. Austenite is enclosed within the loop. Manganese (Mn), nickel (Ni), cobalt (Co) and copper (Cu) stabilize austenite. These elements alter the critical points of iron in a similar way to carbon by raising the A_4 point and lowering the A_3 point, thus increasing the range in which austenite is stable. The following elements have ferrite stabilizing effect: chromium (Cr), tungsten (W), Molybdenum (Mo), vanadium (V), aluminum (Al) and silicon (Si).

2.2.2.1 Molybdenum

Molybdenum has the lowest coefficient of thermal expansion among engineering materials, and its thermal conductivity outperforms all but a few components. Being a large atom,

molybdenum improves stainless steels' high-temperature resilience [7]. As molybdenum is added to steel alloys, the microstructures, phase diagram, and cooling curves all change dramatically. In the study [8], it is experimentally justified that the reduction rate of ferrite growth in molybdenum-containing steels is detected, and this happens because of the thermodynamic stability of austenite in comparison to ferrite is influenced by molybdenum. However, the addition of Mo increases the solubility of niobium in austenite and the carbon precipitate on ferrite. It is well known that austenite decomposition is slowed in molybdenum steels, resulting in enhanced hardenability. However, the temperature at which the austenite transition begins, and ends is exempted by molybdenum addition whereas it has a significant impact on the temperature at the formation and end of the bainitic transformation. The bainitic transition temperature decreases as molybdenum concentration rises. [9]. If any quantitative Mo is given to the steel, bainite transformation occurs at a lower temperature, and as the point falls, the microstructure of bainite created from transformation becomes finer than that of Mo-free steel [13]. The pearlite phase area in the continuous cooling transformation (CCT) diagram shifts towards longer periods as the molybdenum alloy content increases. By refining pearlite, molybdenum addition of up to 0.5% acts as a very strong pearlite stabilizer and increases strength [10]. When cooling rates are lower, Mo effectively inhibits ferrite formation thus promoting bainite formation and improves martensite formation at higher cooling rates thus lowering martensite's critical cooling rate [11]. The formation time and temperature is influenced by all of the materialistic behavior of molybdenum. It also has an effect on the A_1 and A_3 temperatures where during heating, A_1 represents the critical temperature at which pearlite converts into austenite; A_3 reflects the final critical temperature at which free ferrite transforms fully into austenite. In the study [12], it can be seen after adding Mo, the new A_1 and A_3 temperatures are distinctly higher. So, it is evident that molybdenum has impact on A_1 and A_3 curves as well.

Molybdenum ultimately increases the properties of structural steels, such as high temperature strength and hardness. To make a strong and hard steel, it improves hardenability by lowering the necessary quench rate during the heat-treating process. It plays a role in lowering the amount of strain-induced ferrite in the microstructure. As a result, corrosion resistance and microstructural phase equilibrium of the alloy are all improved. The study [14] investigated the impact of Mo in the phases (liquid, austenite, ferrite, and carbides) existing at high temperatures and stated that molybdenum improves the properties in a shape that can be performed in our life significantly. However, intensive research on new alloy designs for

improving high-temperature properties, such as thermal fatigue properties and cast productivity, as well as clarifying mechanisms involved in improved properties, should be proceeded in the future in addition to enhancing microstructures and characteristics of heat-resistant austenitic stainless steels. Mo offers creep resistance and corrosion resistance in addition to high temperature strength on steels. Up to 800°C, Mo greatly improves room temperature and high temperature tensile properties [15].

2.2.2.2 Chromium

In steel, chromium is a potent alloying element. It improves the hardenability of steel and the corrosion resistance of alloys in oxidizing conditions significantly. Its presence in some steels has the potential to induce excessive hardness and cracking in and around welds [16]. To attain improved qualities, such as nickel toughens steel and chromium hardens steel. Chromium acts as ferrite stabilizer. The gamma loop diminishes when chromium as ferritic stabilizers are added, and the maximal matrix comprises ferrite. In addition, when Chromium is added, the austenite zone shrinks and the eutectoid transformation line, which separates the pearlitic and bainitic regions, rises. Not only does the addition of ferrite stabilizing components delay diffusion, shifting the pearlite region to the right, but it also separates the pearlite and bainite bays. This allows for more precise control of the bainitic transition [17]. It increases hardenability, strength, and wear resistance are all improved, as is corrosion resistance. As can be seen from the growing value of tensile strength, chromium boosted the alloy's strength. The strength of the alloy has not been influenced by increasing the chromium content, and the tensile strength of the alloy has been determined to be better than the normal configuration. Corrosion resistance is unquestionably improved by increasing chromium concentration [18]. The most significant quality shared by all chromium-containing alloys, including stainless steels, is that they contain enough chromium to be corrosion, oxidation, and heat resistant. The addition of Cr, on the other hand, as a general passivation element, will invariably increase the passivation propensity of the material's surface, reducing the reaction process. In conclusion, Cr addition influences the passivation and rust layer structure of steels, inhibiting corrosion [19].

2.2.2.3 Aluminum

Aluminum's chemical composition increases its qualities, primarily for the aim of enhancing its strength. However, aluminum is a highly versatile metal that offers a lot of benefits, including being lightweight and flexible. The interstitial nitrogen in low carbon steels is fixed

by aluminum, which enhances strength. Aluminum has a negligible influence on hardenability, thus it is never used for this purpose, and its grain refining capabilities actually reduce deep hardening [20]. Aluminum is a ferrite-forming element, and when more aluminum is added to ultra-pure 429 ferritic stainless steels, the microstructure can maintain a single ferritic phase from high to low temperatures [21]. Excess Al in steel has an impact on the microstructure of steels of various compositions, depending on the degree of additional Al. The study [20] also investigated on the grain size for excess aluminum. It has stated that ferrite grains become finer when 0.07% Al is added, but more than 0.1% Al results in slightly coarser ferrite grains when compared to lesser Al content steels. A similar process occurs in ultra-low carbon steels, where increasing the Al content causes the grain structure to become coarser and more equiaxed, which is thought to be due to the influence of Al and N content on AlN. Steels can be made more formable with aluminum. The tensile strength improves linearly as the aluminum content increases, while the elongation and plastic strain ratio increase and then decline, and the working hardening index differs slightly among the steels [21]. Precipitation hardening results in a metal that is harder and stronger. Because aluminum is a relatively soft metal, this procedure can greatly improve yield strength, tensile strength, and wear resistance [22].

1.1.1 Carbide Formers:

Moderate carbide formers: Cr, Mo

Strong carbide formers: W, Ta, Nb

Very strong carbide formers: V, Ti, Zr

The carbide influences the mechanical properties of structure. Sometimes it may descend the physical properties to some extends.

Alloying elements have significant influence on different types of steels. It sometimes lowers the grain size and improves the mechanical properties.

2.2.2.4 Titanium

Titanium is the element that is most typically added to steel to boost its strength and corrosion resistance. Titanium gives alloys additional desirable property: lightness. Because titanium's density is less than half that of steel, it weighs less and is more durable and stronger than pure steel. Titanium-steel alloys are especially helpful in spacecraft and airplane applications, which account for around 65% of all titanium marketed [23]. To address the negative effects of intergranular corrosion, titanium has been added to ferritic stainless steels. Localization of other alloying elements has been reported to provide new insight into their role in localized

corrosion resistance when combined with electron microscopy and micro elemental analysis [24]. There are three types of titanium alloying elements: -stabilizers, -stabilizers, and neutral. While certain elements that are classified as -stabilizers cause an increase in the allotropic transformation temperature, others that are classified as -stabilizers cause a drop [25]. The coarsening of the microstructure and the rise in graphite content were shown to be connected to the considerable loss of mechanical strength and hardness reported on high-Ti samples. As a result, the microstructure is more refined, with smaller eutectic cells, decreased graphite concentration, and improved mechanical characteristics [26].

2.3 Transformation Temperature

The temperature at which a material transforms between phases is called transformation temperature. This change takes place over a wide temperature range (known as the transformation range) instead of at a single temperature in alloys, such as steel. The transformation range's upper and lower boundaries are indicated by the upper and lower transformation temperatures [27].

Upper transformation temperature: The temperature at which a reaction or transformation finishes or begins during heating or cooling. The A_3 and A_{cm} lines on the iron-carbon phase diagram represent the upper transition temperature. It represents the point where austenite and ferrite, or austenite and cementite, finalize their transition by becoming pure austenite, while heating. This temperature indicates when pure austenite starts to convert into a mixture of austenite and ferrite or austenite and cementite after cooling [28].

Lower transformation temperature: The temperature during which a reaction or transformation occurs or finishes during heating or cooling. The A_1 line indicates the lower transformation temperature, which defines the point at which ferrite, cementite, pearlite, or a combination of these minerals begin to transform into austenite when heated. This transformation temperature specifies when austenite, or a combination of austenite and ferrite or cementite, totally transforms into ferrite, cementite, or pearlite, while cooling.

Formation temperature and time: The formation of ferrite, perlite, bainite, austenite and cementite vary with the temperature and time. The temperature and time of formation alter as the alloying characteristics change.

2.4 Continuous Cooling Transformation (CCT)

When heat treating steel, a continuous cooling transformation phase diagram is frequently utilized. These diagrams show the numerous types of phase shifts that can occur in a material when it cools at different rates. Various cooling rates result in a variety of phase combinations. Depending on cooling rate such as extremely slow cooling rate, speedier cooling rate resulting in coarse or finer particles [29]. The smaller the grain size of the alloy and the fewer the precipitated phases in the matrix, the higher the cooling rate. At a constant cooling rate, relatively uniform size of the alloy could be achieved [30]. Depending on cooling rate ferrite fraction, pearlite fraction, bainite fraction, austenite fraction and martensite fraction are changed.

2.5 Mechanical properties on cooling rate

The changes in mechanical properties of objects deformed at various temperatures and cooled simultaneously rate reveal that increasing the deformation temperature increases the actual yield strength, ultimate strength, and hardness. These properties are significantly influenced by the cooling rate. Higher cooling rates suppress atomic diffusion, resulting in smaller ferrite grains and the production of high strength, hardness, dislocation density, and fine phases. Slow cooling rates cause polygonal ferrite to convert into soft, coarse, and less dislocated phases [31].

2.6 Mechanical properties on temperature

The operating temperature has a significant impact on the mechanical properties of most materials. At specified temperatures, stress-strain graphs are obtained. Material stiffness and strength are reduced at high temperatures, while stiffness and strength are increased at low temperatures. When subjected to high temperatures while under load, almost all materials creep with time. At "low" temperatures, ductile materials act like brittle materials, while brittle materials behave more like ductile materials at "high" temperatures [32]. Effects of Temperature The operating temperature has a significant impact on the mechanical properties of most materials. At specified temperatures, stress-strain graphs are obtained. Material stiffness and strength are reduced at high temperatures, while stiffness and strength are increased at low temperatures [33].

2.7 Precipitation amount and size with time

The precipitation formation varies depending on the type of alloying element and the time. Different alloying elements have different effects. The dynamics are affected when alloying elements are added. It takes longer or less time to form depending on the formation. MC, M_2C, M_3C, M_6C M_7C_3, $M_{23}C_6$ are formed generally in steel alloy as precipitation. While adding different type of alloying elements like Mo, Cr, Ti and Al the precipitation amount and size are changed.

2.8 Stacking Fault Energy

On a very small scale, the stacking-fault energy is a material attribute. In terms of energy per area, it is denoted as SFE. In a close-packed crystal structure, a stacking defect occurs when the regular stacking sequence of atomic planes is disrupted. These disruptions have a stacking-fault energy to them. As a result, the stacking-fault energy influences the equilibrium width to some extent. When the SFE is high, splitting a full dislocation into two partials is energetically undesirable, and the material can deform either by dislocation glide or cross-slip [34].

2.9 Stress-Strain Curves

A stress–strain curve for a material is used in engineering and materials science to show the relationship between stress and strain. It's calculated by progressively adding load to a test coupon and measuring deformation, from which stress and strain may be calculated [35]. The stress-strain curve includes a vast list of relevant parameters for application design to design engineers. Many mechanical properties can be determined from a stress-strain graph, including strength, toughness, elasticity, yield point, strain energy, resilience, and elongation under load. It also aids in the production of goods [36]. However, with the increasing temperature, the stress strain curve changes. When temperatures are reduced, tensile and yield strengths increase modestly, then gradually decline as temperatures rise. The elasticity modulus is more stable than the strength modulus. Ductility diminishes consistently as temperature drops and increases as temperature rises [37].

2.10 Time Temperature Transformation

The time-temperature-transformation (TTT) diagram, often known as an S-curve, refers to only one steel of a specific composition at a time, and it refers to all carbon steels. This diagram is

also known as Bain's curve and C-curve isothermal (decomposition of austenite) graphic [38]. The TTT diagram is a simplified representation of the kinetics of pearlite and bainite creation, as well as martensite's diffusion-less transition. It's a graph made out of overlapping curves. The alloy composition, grain size, and carbon content all influence the shape and location of the curves [39]. The TTT diagram aids in determining the holding temperature and time. The formation of bainite, ferrite and pearlite affects significantly as the temperature increases.

The aim of this research is to see how the increasing content of alloying elements in the range of $0.25 - 0.75\%$ wt. in Grade S355 steel affects the development of a completely new alloy. The effect in the new alloy was investigated on high temperature equilibrium phases and their formation temperature and time was recorded. From the analysis it will be able to understand the steel with more effective properties in case of resilience, high temperature strength, and thermal fatigue and in some extend creep resistance and corrosion resistance as well.

2.11 CALPHAD

CALPHAD (Calculation of PHASE Diagram) is a well-established approach for forecasting the thermodynamic, kinetic, and other aspects of multicomponent material systems. CALPHAD methodology is used at Thermo-Cal Software to create databases that, when combined with our software, can anticipate the properties of multicomponent systems corresponding to real materials [40]. CALPHAD predicts the properties of higher order alloys via extrapolation from binary and ternary systems [41]. It is a way of calculating phase diagrams using advanced computation methods that has been effectively applied to a variety of applications including alloy design, corrosion, and environmental sciences [42]. There are a great number of researchers have done a lot of groundwork on this approach.

In the study [43], a systematic method following three steps was developed to design single-phase HEAs using CALPHAD. First, equiatomatic single phase HEAs were synthesized, then the CALPHAD technique was utilized to build an isothermal ternary diagram, and finally, X-Ray Diffraction (XRD) and Scanning Electron Microscope (SEM) were being used to verify the CALPHAD assumption [43]. In another study [44], effect of Ag and Cu addition on microstructural properties were investigated by calculations based on Scheil's model utilizing CALPHAD software (Pandat and Thermo Calc.) and the solder database were used to predict the liquid fraction change of the alloys during solidification (ADAMIS). In a study [45], it is said that CALPHAD modeling is based on a combination of experimental data and atomistic

modeling, often quantum mechanical calculations. By manipulating phases and microstructure evolutions, CALPHAD and its created databases can be employed in different modeling techniques for creating material properties. In a recent study [46], effects of some solid solution strengthening elements on some properties of nickel-based super alloys were measured by using Thermo-Calc (databases: TTNI8 and TCNI6) and MatCalc to compare experimentally determined values with computed values using the CALPHAD software tools (database ME-NI). In another very recent work, for the Al-Co-Cr-Fe-Ni system, this research discovered three high entropy alloy categories and offered the best alternative within every category by using the HT-CALPHAD computation, Thermo-Calc and TC-python software [47]. The HT-CALPHAD technique can run hundreds, if not tens of thousands, of calculations in user-defined compositions in a single system, considerably reducing the time required to build next-generation HEAs. However, CALPHAD database validation is required [48].

The development of traditional materials and processes requires money. The CALPHAD approach was quickly recognized as a helpful tool for alloy creation, as understanding the phases present in a material, as well as their compositions, is critical for simulating its behavior and properties [49]. It's been utilized to describe diffusion mobility's [50,51], molar volumes [52], and elastic characteristics with great effectiveness [53]. However, the creation of supplemental property databases will broaden the application possibilities.

2.12 Fire on Steels

When steel is exposed to high temperatures, such as when a catastrophe fire breaks out in a steel-framed structure, the mechanical properties of steel deteriorate. It also causes a decline in yield strength, stiffness, and elasticity modulus. Even though structural steel members are distorted, once the fire is quenched, the steel will regain its pre-fire qualities.

When a fire incident occurs, the fire goes through four stages. They are:

a) **Incipient/Ignition** – An ignition source ignites a flammable fuel in the first or early stages of a fire.

b) **Growth** – As a heat source, the first flame is included. As more fuel ignites, the fire increases in size and heat.

c) **Burning** – All exposed surfaces are burning due to the high temperature and heat flux.

d) **Decay** – When the compartment's fuel supply is depleted and the fire goes out.

The flashover occurs when the burning is ready to commence and begin. The quick change from relatively modest burning of a limited number of combustibles in the room to close participation is referred to as flash over. It can be thought of as a substitute for instantaneous ignition. The amount and characteristics of flammable elements within the compartment, the volume of the compartment, and ventilation conditions all influence the time it takes to reach flashover.

The duration of time a normal fire burns and the amount of heat it produces are determined by the following factors:

- Amount and configuration of combustibles
- Ventilation conditions
- Properties of the enclosure/compartment
- Weather conditions

Firmly defined fires typically reach temperatures of 1500°C, with extreme conditions reaching 2300°C.

According to Figure 2.12.1, when a material ignites at a given temperature or heat, it grows. Heat spreads because of growth. The heat eventually reaches a point where it starts to burn. This is the region with the highest temperature. The deterioration comes before the combustion region. The point at which the temperature and heat begin to drop. That seems to be, the materials absorb all the heat required for combustion [54].

Figure 2.12.2 relates a time Vs temperature plot. Temperature growth is high at certain time. Prior to that time temperature falls. Though standard temperature curve shows the growth and remains steady after a certain time. But in practical, the temperature or heat releases as the material absorb heat for combustion [54].

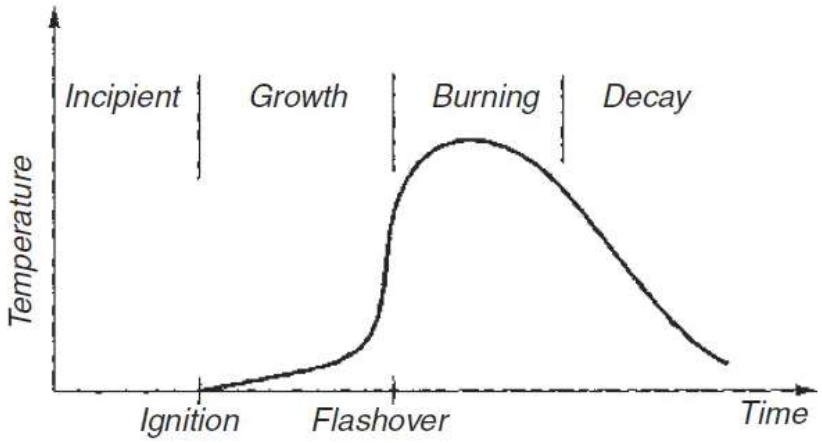

Figure 2.12.1 Stages of Fire Development [54].

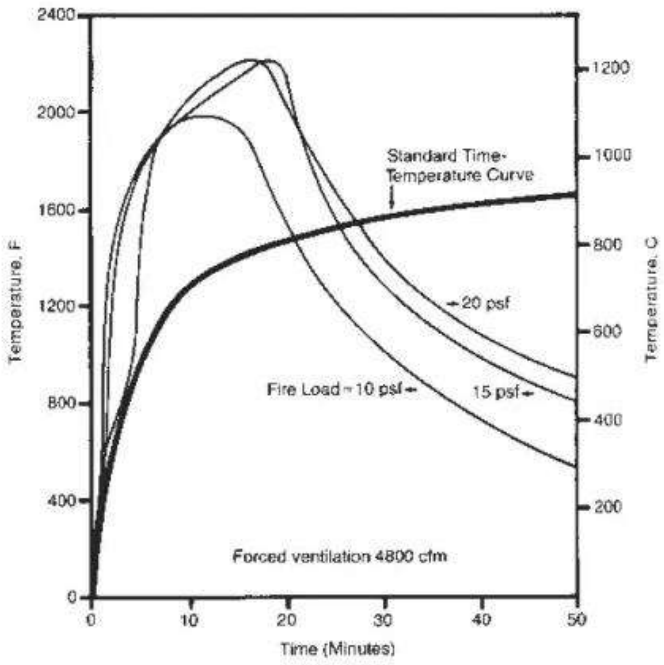

Figure 2.12.2 Stages of fire at Peak Temperature 10 to 20 Minutes [54]

The following methods of heat transfer from the fire to the surrounding structures:

- **Conduction**: Transfer of heat through solid materials. It depends on the density of materials, its specific heat capacity and thermal conductivity.

- **Convection** – Transfer of heat through fluids. Usually convection happens in the gases or liquid medium.
- **Radiation** – Heat transfer by electromagnetic waves. It is based on the gas temperature

2.13 Effects of Fire on Steels

To comprehend the behavior of steel and composite structures in fire, it is necessary to understand the mechanical properties of various structural steel grades at elevated temperatures. The material data of the employed steel material obtained through testing should be used to thoroughly investigate the behavior of a given steel structure at elevated temperatures. The tests must be completed so that the results can be utilized to assess the structure's performance [55].

The steel surface temperature governs the fundamental behavior and strength of steel members, and that the strength and stiffness of steel columns reduces dramatically with increasing temperatures, notably in the range of 500-600 degrees C [56].

When single-story steel buildings are studied at high temperatures, it can be concluded that the collapse of one element does not always result in the collapse of the entire structure. Correct knowledge of the damage degree of steel buildings subjected to fire, in order to identify which elements can be maintained and which must be replaced, results in a lower consumption of materials and financial resources in the majority of cases.

The mechanical characteristics of HSS at elevated temperatures and after cooling are reviewed in the study. High-strength steels, as shown in this study, have more unstable heating conditions than normal steels. These facts suggest that when employing high-strength steel, fire design is a critical loading requirement.

If the temperature does not reach 720°C (1330°F), structural steel can restore nearly all of its preheated qualities. The most common type of structural steel is hot-rolled low carbon steel with different strengths. The characteristics of these steels alter as the temperature rises. As the temperature of the steel rises, the following can happen:

- Corrosion
- Changes in dimensions

- Strength reduction
- Changes in the steel microstructure are permanent.

2.13.1 Corrosion

Paint and other protective coatings are largely consumed during a fire. The exposed steel surfaces will then undergo surface corrosion. Rust is caused by the oxidation of steel, which is a temperature dependent chemical reaction. Thermally accelerated oxidation of steel can occur when steel is exposed to high temperatures in a fire. In addition, melted plastics and other materials often contain chlorides and other potentially corrosive compounds in the gases produced by fire. Any corroded steel should be visually checked to see if the cross-section has been severely damaged if chlorides or other fire generated aggressive corrodes are expected. Testing for the presence of chlorides on the surface is possible [57].

2.13.2 Changes in dimensions

Steel expands when the temperature rises owing to thermal expansion. These modifications are only transient unless other causes are present. Internal stresses may be created in steel components if the steel is constrained during the fire, which can result in buckles or other permanent deformations.

2.13.3 Strength reduction

The strength of the steel diminishes as the temperature of the steel rises above room temperature:

- Carbon steel retains roughly 90% of its yield strength at 204°C (400°F).

- It retains roughly 60% of its yield strength at 427°C (800°F).

- Carbon steel retains roughly 50% of its yield strength at 566°C (1050°F).

The decrease of strength caused by high temperatures is usually very transitory.

2.13.4 Changes in the steel microstructure are permanent

A few of the steel's composition will be converted into martensite if heated to sufficiently high temperatures, typically between 704°C (1300°F) and 843°C (1550°F) for most structural steel, and rapidly cooled by suppression water during firefighting operations. Martensite is a steel phase that is hard but brittle [58]. If the steel's exposure temperature is lower than the

temperature at which this transformation occurs, the steel's mechanical characteristics essentially return to pre-fire values after cooling, depending on the exposure period and rate. The lack of deformation in a loaded condition indicates that the steel was not heated to a temperature high enough to cause martensite formation during the fire, and hence the steel's mechanical qualities were likely unaffected [59].

2.14 High Temperature Effects on Steels

During the fire event the mechanical properties of the steels degrade to a high quantity under the elevated temperature. These cause to increase yield strength, stiffness and modulus of elasticity [60].

If the temperature never exceeds 1300°C for 20 minutes, then the reductions of stiffness and strength are temporary for the elevated temperature. Even if the structural steel members are deformed, the steel will regain its pre-fire properties once the fire is extinguished. However, longer exposures will likely result in annealing and reduction of yield strength.

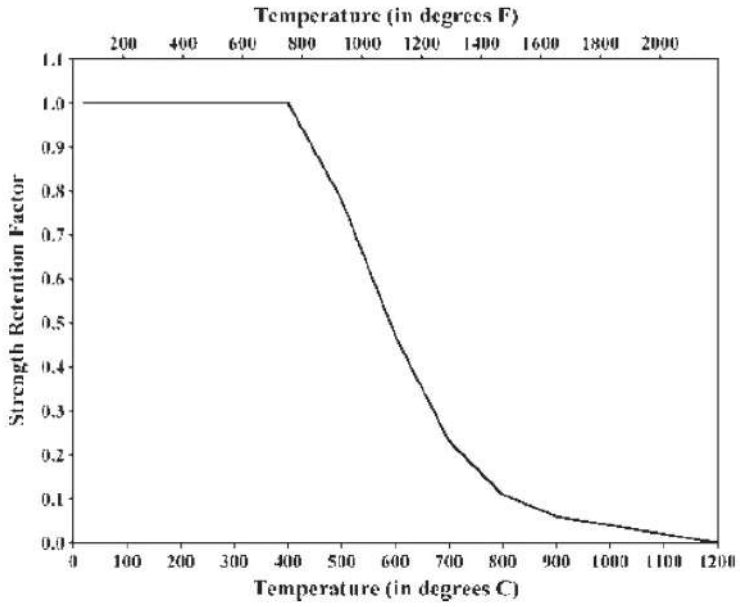

Figure 2.14.1 Yield Strength Retention Factors for Structural Steels at Elevated Temperature [61]

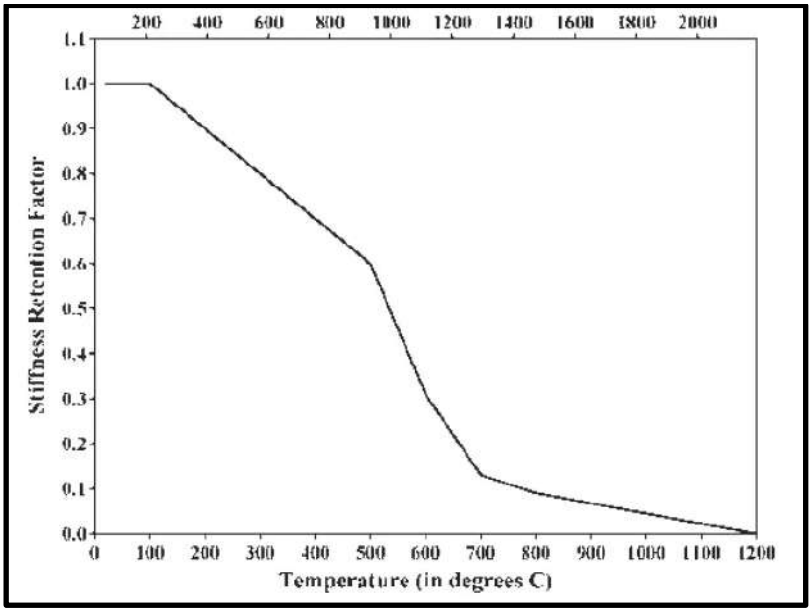

Figure 2.14.2 Modulus of Elasticity Retention Factors for Structural Steels at Elevated Temperature [61]

When fire event happens then the physical and material property changes occur within the structural steel framing. It causes to change the physical properties of steels like thermal elongation, strength reduction, and a reduction in stiffness. Due to the property changes deformations and buckling can occur at 600°C. Deformation and buckling can occur as low as 250°C if a structural steel frame member, such as a beam or girder, is entirely restrained at its connections. Typically, though buckling of the member occurs around 1,300°C due to the 50% reduction in strength and stiffness (Depicted in the graphs above; Fig 2.14.2).

After catching fire, the structural steel framing will begin to compress to its natural shape as the fire event advances into the decay stage and temperatures drop. If inelastic deformations occur during the fire, the steel members will be permanently deformed. Even after the fire has been extinguished, structural parts and connections can fail. Members or connections can collapse in tension as a result of the combination of persistent deformation and residual stress caused by the fire.

The primary issues that need to be answered are how long the fire lasted and what caused it. For more than 20 minutes, did the fire produce temperatures higher than 1,300°C? Visible deformations within the structural steel framing are not proof that the steel was subjected to temperatures above 1,300°C for more than 20 minutes. The exterior appearance of the steel structural members may also change at temperatures less than 1,300°C. Tightly adherent mill scale will remain, and the color will look normal

Temperatures greater 1,300°F for more than 20 minutes :

- Steel surface will become oxidized
- Possible pitting
- Loss of cross-sectional area thickness

The appearance of significantly “burned” steel is typically light gray or white. The structural steel framing can also take the color of the fuel contents in the room due to combustible residue. It should be noted that paint applied to the steel will typically burn off at around 300°F.

As the investigation of structural steel framing after a fire event is carried out, the American Institute of Steel Construction (AISC) recommends the structure to be assessed into three categories:

- **Category 1** – Straight members that appear to be unaffected by the fire, including those that have slight distortions that are not easily visually observable. These members are typically unaffected by the fire or require minor repairs.
- **Category 2** – Members that are noticeably deformed but that could be heat straightened, if economically justified.
- **Category 3** – Members that are so severely deformed that repair would be economically unfeasible when compared to the cost of replacement.

2.15 Fire Resistance Rating

1. The length of time a passive fire prevention system can endure a conventional fire resistance test. The standard fire resistance test is based on a time measurement or other functional or fitness for purpose criteria.

Hollow steel columns, filled with plain concrete, are loaded concentrically as well as steel-fiber reinforced concrete, or bar reinforced concrete that are manufactured and constructed within the tolerances defined in CSA S16, "Design of Steel Structures," are permitted to be given a R fire-resistance rating, and that comply;

Where, C axial compressive force excluding load factors related to dead and live loads, kN,

$C_{max} = \left(\frac{a(f'c+20)D^{2.5}}{R(KL-1000)}\right)^2$

but not greater than

a) 1.0 C', for plain concrete filling (PC),

b) 1.1 C' for steel-fiber reinforced concrete filling (FC), and

c) 1.7 C', for bar-reinforced concrete filling (RC)

$C'_x = 0.85\emptyset_c f'_c A_c \lambda_c^{-2} [\sqrt{1 + 0.25\lambda c^{-4}} - 0.5\lambda c^{-2}]$

where a = constant attained from Table D-2.6.6.-A,

f'_c = defined the concrete's compressive strength in accordance with CSA A23.3,

"Design of Concrete Structures," MPa,

r_c = radius of gyration of the concrete area,

A_c = area of concrete, mm²,

D = outside diameter of a round column or outside width of a square column, mm,

E_c = preliminary elastic modulus for normal-weight concrete, considering the effects of long-term loading =

$(1+\frac{S}{T})\ 2500C\ \sqrt{f'c}$

R = specified fire-resistance rating, min,

KL column's effective length in CSA S16, "Design of Steel Structures," mm,

$\lambda_c = \frac{KL}{r_c}\sqrt{\frac{f'c}{\pi^2 Ec}}$ and

$\emptyset_c = 0.60$

Subject to the limitations of validity listed in Table 2.15.1

Table 2.15.1 Values of Constant "a" [61]

Filling type	Concrete Type	Steel Reinforcement	Circular Columns	Square Columns
PC	S	n/a	0.070	0.060
FC	S	=2%	0.075	0.065
RC	S	1.5%-3%	0.080	0.070
RC	S	3%-5%	0.085	0.075
PC	N	n/a	0.080	0.070
FC	N	=2%	0.085	0.075

Table 2.15.1 (continued)

Filling type	Concrete Type	Steel Reinforcement	Circular Columns	Square Columns
RC	N	1.5%-3%	0.090	0.080
RC	N	3%-5%	0.095	0.085

2. At either end of the hollow steel column and at each intermediate floor level, a set of steam vent holes must be supplied, and the holes must be

a) a diameter of at least 13 mm,

b) 150 mm above or below a base plate, cap plate, or concrete slab on opposite faces,

c) Orient in such a way that neighboring pairs are perpendicular to one another, and

d) Not hindered by additional construction features.

3) Load application and reaction must be done using end bearings in line with the manufacturer's instructions with CSA S16, "Design of Steel Structures."

Table 2.15.2 Validity Limits [61]

Parameter	Type of Concrete Filling		
	PC	FC	RC
f'_c (MPa)	20 to 40	20 to 55	20 to 55
D (round) (mm)	140 to 410	140 to 410	165 to 410
D (square) (mm)	140 to 305	102 to 305	175 to 305
Reinforcement (%)	n/a	=2% of the concrete mix by mass	1.5% to 5% of cross sectional area
Concrete Cover (mm)	n/a	n/a	≥ 25
R (min)	≤ 120	≤180	≤180
KL (mm)	2000 to 4000	2000 to 4500	2000 to 4500
Class(2)	1,2 or 3	1,2 or 3	1,2 or 3

2.16 Types of Steels:

2.16.1 Nickel Steels:

Nickel is the oldest and one of the fundamental alloying elements. It has unlimited solubility in gamma iron and highly soluble in ferrite. As a result, it gives high strength and toughness. Ni lowers the critical temperature of the steels and retards the decomposition of the austenite [62]. As a result, at low temperature or more specifically at room temperature austenite gets stable.

Ni never forms carbide. Besides, it reduces the carbon content of the eutectoid composition. As a result of which high percentage of pearlite forms compared to the equal composition plain carbon steels. At the lower temperature, the grain size of is finer and tougher than the in unalloyed steels.

2.16.2 Chromium Steels:

Chromium is less expensive than the Ni. Chromium is a carbide former and forms (Cr_7C_3, Cr_4C) or complex carbide [$(FeCr)_3C$]. This carbide has high hardness and wears resistance. It has 13% solubility in austenite and unlimited solubility in ferrite. In the alloying steels chromium containing more than 5% it improves the corrosion resistance and high temperature properties.

2.16.3 Manganese Steels:

Manganese is less expensive and mostly acts as deoxidizers. The presence of the manganese in the alloy steel reduces the prone to the hot-shortness. As a result of which the alloy steel containing manganese can participate in the hot working process.

Besides, absence of the manganese in the steel may form FeS. FeS has low melting temperature. When the steel sample is hot rolled then due to the low melting temperature of the FeS it melted first. As a result, few places on the steel containing FeS becomes slippery and slips during rolling [62].

Mn and Ni both reduces the critical temperature and lowers the amount of carbon in eutectoid. Alloying steels containing more than 10% Mn becomes austenitic after slow cooling.

Hadfield Mn steel is a special type of steel (12%Mn) has great abrasion resistance. When it is slow cooled from 1750F then large brittle carbide forms surrounding the austenite grain. Ultimately forms the structure with low strength and ductility.

2.16.4 Molybdenum Steels:

Molybdenum is a little expensive alloying element. It has limited solubility in austenite and ferrite. As a result of which it is strong carbide former. Molybdenum combines with the Ni or Cr or both with the Ni and Cr. Plain Molybdenum steel is carburized to improve the wear resistance.

A lot of research has been taken place in the case of inter phase precipitation. In this case Molybdenum plays significant roles. Four steels were manufactured with identical composition and Ti, V, Mo and N content is added to investigate the effect of composition on interphase precipitation. Alloys were rapidly cooled from the single austenite phase field and isothermally transformed at $630\ ^\circ C$ and $650\ ^\circ C$ for 90min [44]. When Mo is added, transformation of ferrite to austenite reduces to a certain value, particularly in the case of V steels. Interphase

precipitation was observed in all the alloys at both transformation temperatures. In the case of the Ti bearing steel, the two types of precipitate were observed, namely TiC (finer) and Ti_2C (coarser), while for the V bearing steels, VC (finer) and V_4C_3 (coarser) were observed. Where Mo was present in the alloy, it was found dissolved in all carbide types. The (Ti, Mo)C and (V, Mo)C formed by classical planer interphase precipitation (PIP) while the $(Ti, Mo)_2C$ and $(V, Mo)_4C_3$, that had a much wider row spacing, formed through curved interphase precipitation (CIP). Each adopted one variant of the Baker-Nutting orientation relationship. The Ti-micro alloyed steels undergo the smallest precipitates of all the steels, which were approximately the same size irrespective of whether Mo was present in the alloy and irrespective of the transformation temperature [63]. However, the addition of Mo to the V bearing steels causes significant increase in precipitate volume fraction and a reduction in precipitate size.

2.16.5 Tungsten Steels:

Tungsten is mainly popular for providing high temperature properties and harden ability. It is mainly carbide former. Approximately $2-3\%$ W is equivalent to $1\%\ Mo$. Tungsten is mainly used in the tools industry.

2.16.6 Titanium Steels:

Titanium alloys are mainly used in the structural materials, aerospace, and chemical industries due to lower density, high strength and corrosion resistance. Tensile strength/ density ratios of Titanium alloys are considerably greater than that of the steels and Al alloys at ordinary temperature. For this reasons Ti alloys are mostly used in the aerospace industries. And for this Ti is added to the steels to improve its properties to some extent.

When Ti is added to the steels then it improves its high temperature properties as a refractory metal. Chemical behavior of the Ti always limits its application at moderate to high temperature. At low temperature Ti passives to acids and minerals but at the elevated temperature Ti oxidizes very fast. Besides dissolution of hydrogen and nitrogen causes surface hardening.

Pure Ti undergoes allotropic transformations at about $1158K$. Thus if Ti remains in steels at around 1158K the properties may varies. Because pure Ti at $1158K$ transforms from closed packed hexagonal structure to body centered cubic structure. The high temperature BCC of Ti is called alpha phase. On the other hand, HCP at the low temperature forms beta phase.

Allotropic transformation temperature depends on few alloying elements. Some alloying elements raises the transformation temperature called alpha stabilizers whereas few lowers the transformation temperatures called beta stabilizers.

The element that lowers the transformation temperature has two classes. One is the elements that undergo the eutectoid transformations. Example: iron, Cu, N, Co and Mn etc. And the other one is those that are isomorphs with beta phase at high temperature and from alpha + beta equilibrium phase at ordinary temperature.

The main role of Ti in steel is grain refinement strengthening and precipitation strengthening. The smelting of Ti micro alloyed steel should satisfy that most of the Ti dissolves in the molten steel and precipitate in the form of carbide or carbo - nitride after the subsequent solidification. The affinity of Ti towards oxygen is less than that of the Aluminum towards the oxygen. Beside Ti has greater affinity than Manganese towards oxygen.

The high content of Nitrogen forms titanium nitride that forms inclusions in the molten steels. On the other hand, titanium oxides and nitrides will obstruct the process of continuous casting. During the refining process by pyro metallurgy of Ti micro-alloyed steel it is required to remove Sulphur, oxygen and Nitrogen. But emphasize should be given on the relationship between Ti and Al refractory elements. Compared with the Nb or V, in case of Ti it is more difficult to control Ti micro-alloyed steels which attributes to the more type of the secondary phase and wider temperature range of the precipitate.

As a kind of micro alloying element, Ti significantly improves the comprehensive properties of steel. However, when compared with niobium and Vanadium micro alloyed technology, Ti has not been used extensively in industry for a long time. Ti micro alloyed steel fluctuates largely, and production process is not stable. Ti is very reactive and forms TiO, TiS which are very harmful. Formation of these phases consumes a portion of Ti that reduces the volume fraction of TiC precipitation at low temperature but also significantly changes the chemical free energy of TiC. Precipitation behavior of TiC changes and strengthen effect greatly affected. Besides, TiC is sensitive to temperature and affects the properties of steel.

Besides, High-strength Ti micro-alloyed steels are the precipitation hardened ferritic steels. The ferrite grain refinement and TiC precipitation have a good combination in strengthening; that plays an important role in obtaining both high strength and high toughness simultaneously for those steels. The ferrite grain refinement depends on the refinement of austenite grain size and on the control of transformation temperature. The refinement of austenite grain size mainly depends on the control of the austenite grain growth before hot rolling, and recrystallized austenite grains during hot rolling.

2.16.7 Niobium Micro alloyed steels

Niobium is a soft grey ductile and transition element. The main commercial source of niobium is mineral pyrochlore. Around 80% of the niobium produces used in automotive industry, for oil and gas pipelines and in construction. Adding niobium to steels causes the formation of niobium carbide and niobium nitride which improves the grain refinement and retardation of recrystallization. Besides, it enhances precipitation hardening which increases toughness, strength, formability, and weld ability of micro alloyed steel.

Large diameter pipes are used in transportation of oil and gas. It is manufactured by the thermo mechanical controlled processing (TMCP). Its performance can be enhanced by inducing its strength and toughness through grain refinements. Grain refinement can be done by controlling austenite parameters by the addition of niobium.

In case of Austenitic – Ferrite stainless steel, usually solidification starts at 1450°C with the formation of ferrite (α). It acts as an origin to start the formation of austenite near 1300°C. σ forms at the interphase of austenite and ferrite at 600°C-950°C and the toughness of the steel gets reduced.

The addition of niobium in super martensitic stainless steel after tempering at 600°C for 2h improves the mechanical resistance properties with lower degree of sensitization. Besides, giving such properties it never compromises its elongation and pitting corrosion resistance compared to the reference steels.

Summary of alloying element effect of different types of steels are as follows:

Table 2.16.1 Summary of alloying element effect of different types of steels

Nb Micro alloyed Steels	***Ti Micro alloyed Steels***	***Ni Micro alloyed Steels***	***Cr Micro alloyed Steels***	***Mn Micro alloyed Steels***	***Mo Micro alloyed Steels***	***W Micro alloyed Steels***
Addition of Nb in steels causes formation of niobium carbide and niobium nitride which improves the grain	Addition of Ti in steels passives to acids and minerals at low temperatu re and	Ni lowers the critical temperature of the steels and retards the decompositi on of the austenite. As a result	In the alloying steels chromiu m containin g more than 5% improves the	The presence of the mangane se in the alloy steel reduces the prone to the	Molybden um is used in the combinatio n with the Ni or Cr or both with the Ni and Cr. Plain Molybden	Tungsten is mainly popular for providing high temperatur e properties and

Nb Micro alloyed Steels	***Ti Micro alloyed Steels***	***Ni Micro alloyed Steels***	***Cr Micro alloyed Steels***	***Mn Micro alloyed Steels***	***Mo Micro alloyed Steels***	***W Micro alloyed Steels***
refinement, retardation of recrystallization ultimately increases toughness, strength, formability and weld-ability.	improves high temperature properties.	at low temperature or room temperature austenite gets stable	corrosion resistance and high temperature properties.	hot-shortness	um steel is carburized to improve the wear resistance.	hardenability of the steels.

2.17 Effect of alloying element on Ferrite:

FCC has 8 and 4 octahedral and tetrahedral voids per unit cell respectively. Whereas BCC has 12 and 6 respectively. Octahedral in FCC is bigger than tetrahedral. Carbon occupies octahedral with less distortion. Octahedral in BCC is smaller than tetrahedral even in that case Carbon occupies octahedral void due to lesser distortion (only top atom and bottom need to be distorted). Number of voids in BCC are more than FCC whereas size of voids in BCC are significantly smaller than FCC. For this reason, austenite has higher solubility of C than ferrite. But all the alloying elements have some sorts of solubility on ferrite. It mainly depends on the amount of carbon present in the structure. Nickel, Aluminum, Silicon, Copper, Cobalt etc. dissolve in ferrite in large extent and play a significant role in increasing hardness and strength by solid solution hardening. Group 2 element in the following Table dissolve in ferrite in the absence of carbon otherwise it forms carbide.

Table 2.17.1 Behaviors of the individual element in Annealed Steels

Alloying Element	Group 1 Dissolved in Ferrite	Group 2 Combined in Carbide
Nickel	Ni	
Silicon	Si	
Aluminum	Al	
Copper	Cu	
Manganese	Mn	Mn
Chromium	Cr	Cr

Alloying Element	Group 1 Dissolved in Ferrite	Group 2 Combined in Carbide
Tungsten	W	W
Molybdenum	Mo	Mo
Vanadium	V	V
Titanium	Ti	

*Adapted from E.C Bain and H.W. Paxoton, "Alloying element in steel." 2d ed., American Society for Metals, Metals Park, Ohio, 1961

In Figure 2.17.2 it is seen that the probable hardening effect of various element dissolved in alpha (α) iron. When silicon dissolved in alpha (α) iron then the hardening value lies in maximum among the addition of Mn, Ni, Mo, V, W and Cr. Among the alloyed element addition of chromium causes least hardening effect.

The dissolved element has a little hardening effect in the contribution of ferrite to the overall strength of the steel. In the case of the low carbon chromium steels, when the structural change occurs by any process then hardening of such steels occur. The change of structure can be done in the case of annealed steels by cooling it from higher temperature by air cooling. In the Fig 2.17.3 it is clearly understood. In Figure 2.17.3 the low carbon chromium annealed steels when air cooled then its tensile strength rises to a high value. On the other hand, when cooled in furnace a little change in tensile property is seen.

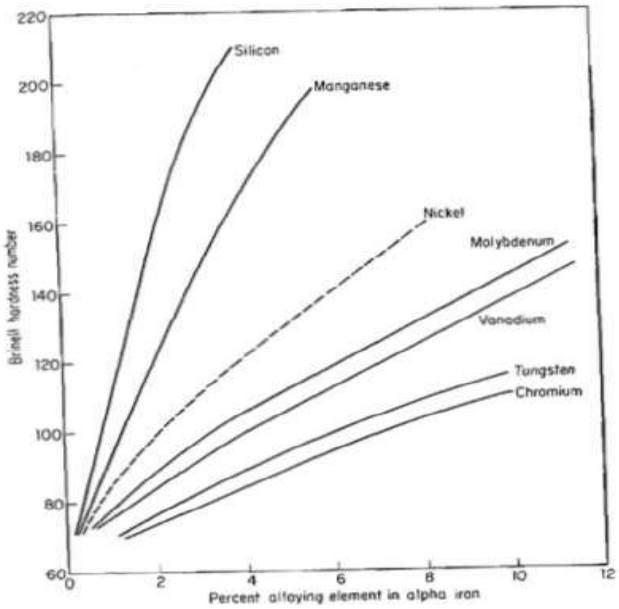

Figure 2.17.1 Probable Hardening effect of the various elements as dissolved in alpha iron [64].

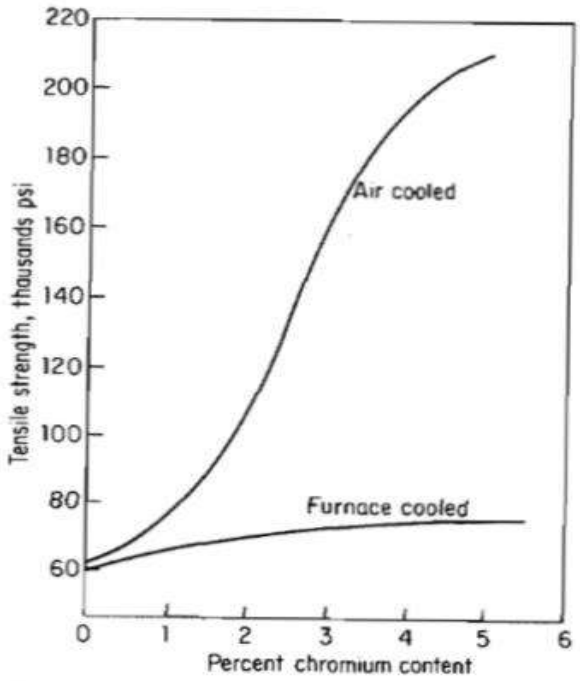

Figure 2.17.2 The minor effect of chromium in annealed steels compared with the powerful effect as a strengthener through its influence on structure in air cooled steels. Probable Hardening effect of the various elements as dissolved in alpha iron [62].

2.18 Influence of Alloying Elements on Iron-Iron Carbide Diagram:

The presence of alloying elements plays an important role in the change of critical range, position of eutectoid point and location of the alpha and gamma fields indicated by the binary iron – iron carbon diagram. Besides, presence of Nickel and Manganese lowers the critical temperature on heating. As a result of which it stabilizes the austenite. If the critical temperature lowers than that of the standard region, then the austenite becomes stable at the room temperature. Thus Nickel and Molybdenum stabilizes the austenite at room temperature and the addition of such alloying element is used in the preparation of austenitic stainless steel.

On the other hand, Mo, Cr, Si, Ti raise the critical temperature range which contracts the austenite zone and enlarge the alpha and gamma region as well.

Austenitic stainless steel plays a great role in industrial applications by giving corrosion resistance of the steels and providing well mechanical strength. It is mainly used in the pressure vessels, reactors, storage tanks which are used underground and specially in the aqueous environments containing chlorides. Austenitic stainless steels are used in manufacturing pump in the oil industry that inject the salt water to expel gas and oil. For the preparation of austenitic stainless steels, the Ni and Mo plays an important role.

From the Fig 2.18.1 It is clearly seen that the addition of Ti, Mo, Si, W,Cr raise the eutectoid temperature of the steels. The rise of the eutectoid temperature of the steels lowers the stability region of the austenite. It ultimately stabilizes the austenite at the elevated temperature. At this scenario the austenite becomes unstable at lower or room temperature. Besides the addition of Mn and Ni lowers the eutectoid temperature, passively indicates that the stability of the austenite at the room temperature. As a result, Mn and Ni are the helpful alloying element in the case of the austenitic stainless steels.

Chromium in particular lowers the eutectoid temperature. Thus with the addition of the chromium the austenite zone contracts as austenite is stable above the critical temperature. If the critical temperature rises up, then austenite gets stable at the elevated temperature and unstable at the room temperature. Thus with the addition of chromium the austenite zone contracts more and prone to the formation of austenitic stainless steel reduces. And austenitic stainless steels become unstable at the room temperature.

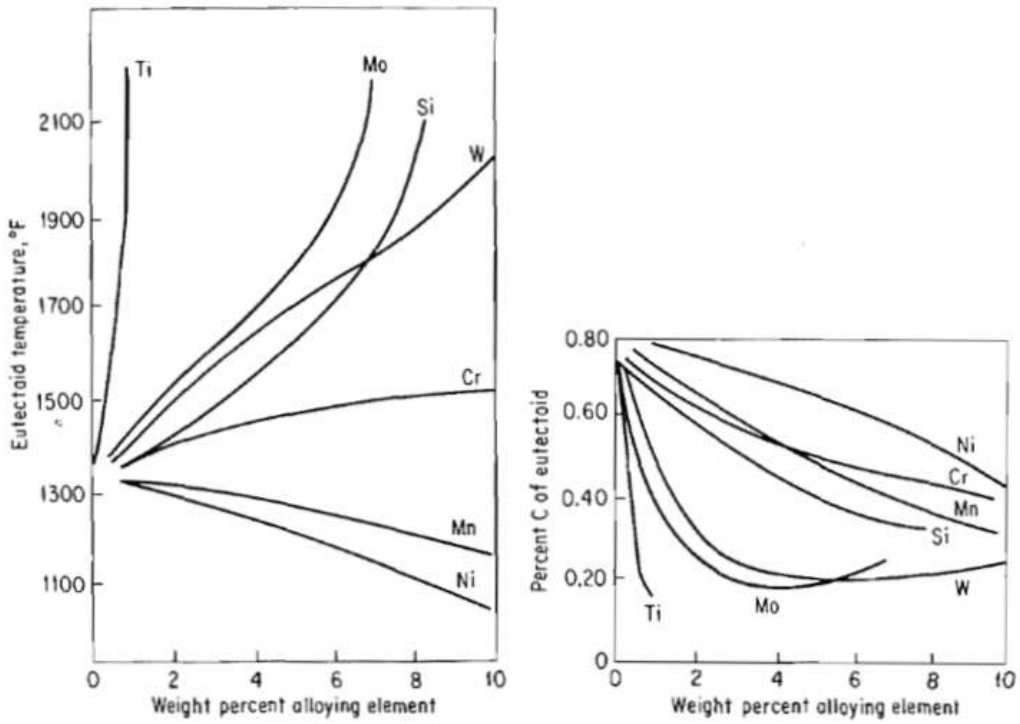

Figure 2.18.1 Eutectoid composition and eutectoid temperature as influenced by several alloying elements. Probable Hardening effect of the various elements as dissolved in alpha iron [64].

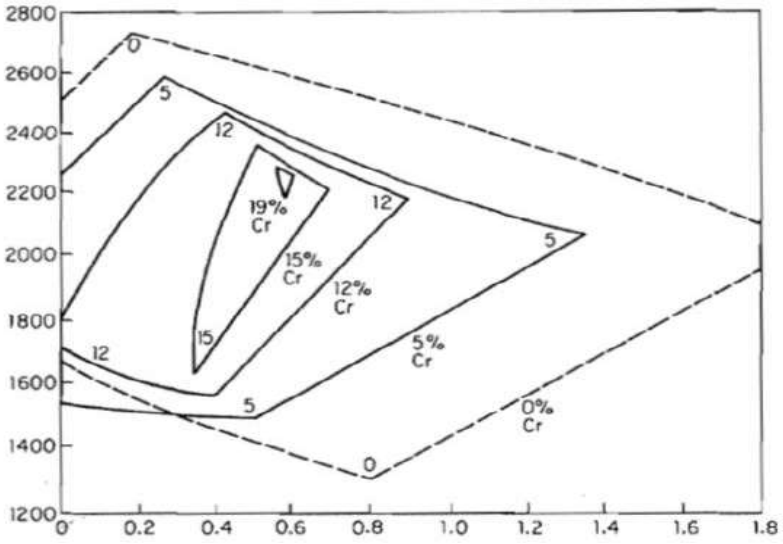

Figure 2.18.2 Range of austenite in chromium steels. [65]

2.19 Effect of Alloying Element on Tempering:

In the case of the tempering of the plain carbon steels, when the temperature is increased then the hardness value decreased thus hardened steels are softened. At the same time the hardness drops continuously. Some alloying elements play an important role to retard the softening effect of the hardened steel at the elevated temperature. When tempering is done at the elevated temperature then the steel may get soften? Usually, the elements that remain dissolved in ferrite, such as Ni, Si, Mn have very little effect in the retardation of the softening of the steels at the elevated temperature.

The complex carbide forming elements such as Cr, W, Mo, V retards the softening at the elevated temperature while tempering. Besides, they not only retard the softening effect but also improves the hardness of the plain carbon steels to some aspects.

2.20 Effects of Alloying Elements on Hardenability

Some systems are particularly suitable for the properties of tempered martensite, which are often required for the performance of the application. Unfortunately, only those components that can first be converted to martensite can achieve these desirable properties. Owing to the relatively poor hardenability of these steels, this puts severe restrictions on the use of simple carbon steels. When the entire component (usually considered to be hardening) has to be martensite shaped, fast quenching is required within, reducing the number of pieces that can be effectively handled. The risk of deviations and splitting are high at very high quench speeds, which can lead to severe functional problems. Carbon steels are typically weak in hardness

since they can be easily converted by diffusion guided reactions. If the levels at which these improvements take place will reduce their hardenability. Work has shown that the correct alloying elements can be made available. All alloying elements which are applied to steel improve the hardness provided that they are dissolved in austenite except for cobalt which has a negative effect. It is a crucial condition. The main reason for creating the AISI / SAE standard low alloy steels is the influence of alloying components on the hardenability of steels.

The basic low-alloy steels from AISI / SAE are used in ASM manuals and other texts and articles. These steels are classified by numerical code that shows carbon content as for plain carbon steels in the final pair (trio, if five digits) of numbers, and the first two numbers represent the main elements of alloy. Standard steels are manganese steels with 13xx code numbers, 40xx molybdenum steels, 41xx molybdenum and chromium plate, 43xx molybdenum, chromium and nickel steels and 51xx chromium steels. Many type variants include 6xxx, 7xxx etc. The 2xxx and 3xxx series refer to nickel-containing steels as the primary alloy element. Nevertheless, several other combinations of alloy elements improve hardenability more than nickel alone and improve it at a lower rate. Nickel steels are also not as used as before. In addition, certain tables of traditional low-alloy steels are sometimes skipped these days. When the toughness of the alloy steel is of the utmost importance, steels which are produced with strictly regulated formulations should be purchased in order to ensure the same toughness.

V, B and Pb are extra elements applied to the regular alloy metals. Vanadium is a strong carbide former, and it makes fine carbides that inhibit grain growth during austenitization, together with aluminum compounds in killed steels. It is successful because its carbides that survive at temperatures nearly 2000 ° F which is far higher than the normal low-alloy stone austenitizing temperatures. The plum remains in steel in the shape of small lead blocks at present; it has very little solubility in ferrite. The consequence is that the machinability of the steel is increased. To boost hardenability, boron is applied. That's the only reason it's included. In the case of boron found in a regular steel in an alloy, the code name is changed by adding letter B from second to third digit e. g. 50B44

When considering the influence of alloy elements on the strength of steels, the impacts of them on the phase transitions of steel must be taken into consideration. The first is the austernisation effect; then the impact on the forming of pro eutectoid ferrite, pearlite and bainite; and the martensitic transition itself, of course, would be influenced. Summary of the designations for common carbon and low alloy steels.

2.21 Effect on the Eutectoid Point

The point in a phase diagram indicating the chemical composition and temperature corresponding to the lowest melting point of a mixture of components. Now here it can be found that there's a considerable change in the eutectic temperature for the effect of the alloying elements. Firstly, stabilizers for austenites and ferrites extend the respective phase regions. By raising or lowering the alloying addition, the effect of elements on the Fe-Fe_3C phase diagram is strongly reflected in the eutectoid temperature. The austenite stabilizers lower the eutectoid temperature and thus expand the temperature range in which austenite is stable. Similarly, the ferrite formers increase the temperature of the eutectoid, thus reducing the area of γ –phase field. The Figure that is given below shows the influence of alloying addition on eutectoid temperature and eutectoid carbon content.

One easy way to quantitatively explain the effect of an alloying element on the γ-phase field of the Fe-C system is to project the γ-phase field boundaries for increasing concentration of a specific alloying element onto the Fe-C plane of the ternary system. This is illustrated in next Figure for Titanium, Chromium, Molybdenum and Manganese, from which, for example, it is obvious that just over 1 wt. percent Ti will break the γ -loop, while 20 wt percent Cr is required to reach that level. It also shows related variations in the temperature and composition of eutectoids.

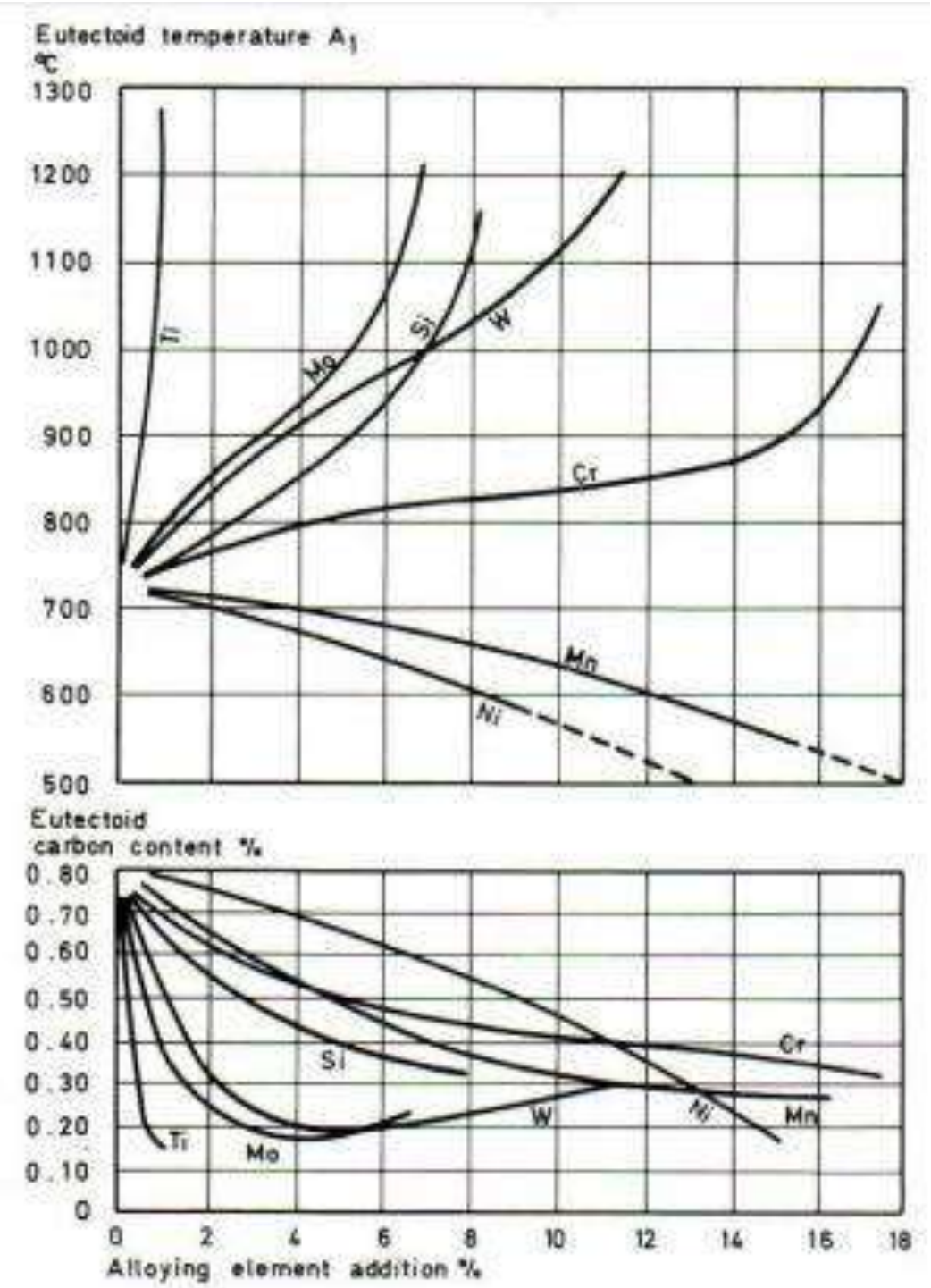

Figure 2.21.1Influence of alloying element additions on the eutectoid temperature and the eutectoid carbon content [66]

2.22 Distribution of Alloying Elements

Alloying elements can be found in various ways which are structures of multicomponent in commercial alloy steels. It helps to find out the purpose and effect of the elements on the phase diagram easily. Those elements can be found (i) in the free state condition; (ii) As an intermetallic alloy with or without iron; (iii) As oxides, sulfides and other inclusions of nonmetals; (iv) in carbides format; or (v) as an iron Solution. As to the nature of their steel delivery, the alloy elements can be split into two groups:

Elements not carbide-forming in steel (e.g. Ni, Si, Co, Al, Cu and N)
Elements stable carbides forming in steel (e.g. Cr, Mn, Mo, W, V, Ti, Zr, and Nb)
Firstly, the elements from group one (nickel, silicon, cobalt, aluminum, copper and nitrogen) do not form any chemical compounds with iron and carbon, and therefore the only possible way in which they can be found in steel is in solid iron solutions. There are also exceptions as well like Cu(copper) and N(nitrogen). Copper dissolves up to 1.0 percent in α-iron at normal temperatures. If the contents of Cu reach 7 per cent, iron may contain copper as metal inclusions in the free state. In ferrite too, nitrogen has minimal solubility. When the N content reaches

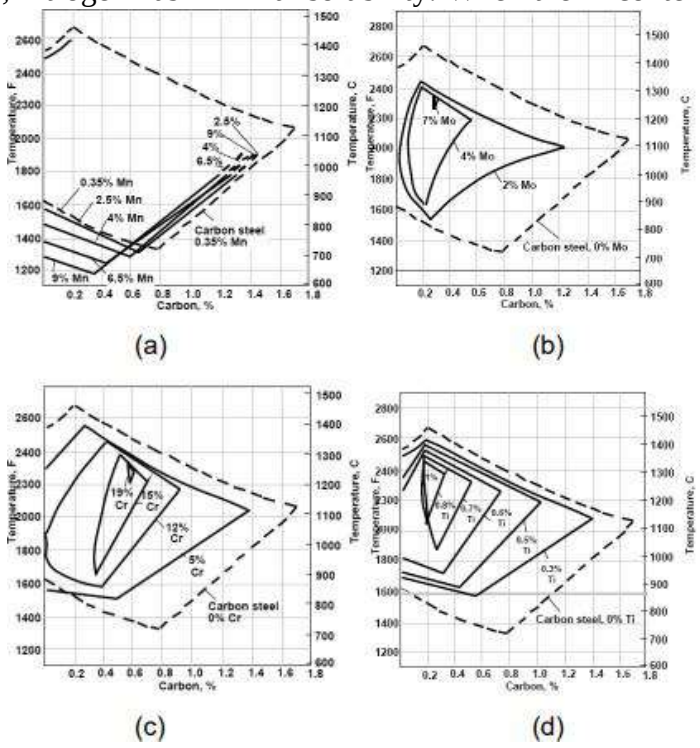

Figure 2.21.1 Effect of alloying additions on the γ-phase field: (a) Mn; (b) Mo; (c) Cr; (d) Ti [66]

0.015%, nitrogen is present in steel in the form of chemical compounds containing iron or other alloying elements (V, Al, Ti, and Cr). Such chemicals are called nitrides

Those alloying elements which have higher affinity for oxygen than that of iron, those can form oxides and nonmetallic compounds as well. These elements (e.g., Al, Si, V, Ti) deoxidize steel by removing oxygen from iron when applied at the very end of the steel melting process. The deoxidizing reaction produces Al2O3, TiO2, V2O5 as well as other oxides. Now considering the fact that since deoxidizers are added at the final stages of the steel melting process, the majority of oxides have little time to coagulate or move to slag, and as a result are retained as fine non-metal inclusions in the solid steel. Besides a great affinity for oxygen, some alloying elements have a greater affinity for sulfur than iron does, and they form sulfides when incorporated in to steel.

Now let's consider the second group that are able to form stable carbide in steel this can be found in carbon and iron chemical compounds, or in solid solutions. The elements those are chosen on the basis of the carbon content of steel and other carbide-forming elements being present at the same time. When a steel contains a fairly small amount of carbon and an alloying element in large amounts, then carbon would be attached to carbides until the carbide-forming elements are completely used. And this is why the solid solution includes excess carbide-forming elements. If a steel has a significant amount of carbon and none of the alloying elements, the latter will mainly be present as carbides in the steel. Most alloying elements in the periodic Table, namely C, N, O, B and metalloids that stand far from iron, dissolve in iron in large amounts.

The iron- right elements (Co, Ni, Cu, etc.) form solutions in iron only, and do not join carbides. So it's obvious to specify that alloying elements are dissolved predominantly into basic phases (ferrite, austenite, cementite) of iron-carbon alloys or form special carbides.

2.23 Effect on Tempering

In steel, Martensite is very strong but in its virgin condition it is fragile. To enhance the mechanical properties, the steel is tempered in the range of 150°C -700°C [67]. After tempering, the microstructures advance in stable condition. During hardening, martensite starts with the dismissal of plenty carbon to encourage carbides however the substitutional solutes don't diffuse during this process. The final product of this process is like a coarse carbide in ferritic lattice which looks like the original. Expansion of alloy in steel affects the kinetics and pearlite reaction. Adding alloying elements shift the time temperature transformation (TTT) curve to longer positions, resulting to miss the nose of the curve during quenching which gives

higher hardenability. Since martensite can be obtained in slower cooling rate and in sensible terms thick sample can be made full martensite. The alloys slow down the rate of softening during tempering by stabilizing the ε-iron carbide and the supersaturated martensite structure at higher temperature and by stalling considerably the precipitation and development of cementite.

2.24 Computational Method

CALPHAD method is based on the development and application of theoretical thermodynamic models. However, none of this would be possible without the existence of the computational methods and software which allow these models to be applied in practice. In essence, the issues involved in computational methods are less diverse and mainly revolve around Gibbs energy minimization. In addition, there are 'optimizer' codes which are used for the thermodynamic assessment of phase equilibrium. The essential aim of these codes is to reduce the statistical error between calculated phase equilibrium, thermodynamic properties and the equivalent experimentally measured quantities. It is also worthwhile to make some distinctions between methods of calculating phase equilibrium. For many years, equilibrium constants have been used to express the abundance of certain species in terms of the amounts of other arbitrarily chosen species. Such calculations suffer significant disadvantages in that some prior knowledge of potential reactions is often necessary, and it is difficult to analyze the effect of complex reactions involving many species on a particular equilibrium reaction. Furthermore, unless equilibrium constants are defined for all possible chemical reactions, a true equilibrium calculation cannot be made and, in the case of a reaction with 50 or 60 substances present, the number of possible reactions is massive.

CALPHAD methods attempt to provide a true equilibrium calculation by considering the Gibbs energy of all phases and minimizing the total Gibbs energy of the system (G). In this circumstance G can be calculated either from knowledge of the chemical potential (Gi) of component,

$$\sum_i G = n_i G_i$$

Where n_i is amount of component i, or alternatively by

$G=\sum_{\emptyset} N^{\emptyset}\, Gm^{\emptyset}$

where$N^{\emptyset}$ is the amount of phase $\emptyset$ and $G^{\emptyset}$ its Gibbs energy. The number of unknowns is now considerably reduced in comparison to an equilibrium constant approach.

One of the most significant advantages of the CALPHAD methodology is that, because the total Gibbs energy is calculated, it is possible to derive all of the associated functions and characteristics of phase equilibria, e.g., phase diagrams, chemical potential diagrams, etc. Examples of some graphical forms of representing such functions will also be given. Finally, 'optimizer' programs will be discussed with particular emphasis on the two major codes currently used world-wide, the Lukas program [68].

2.24.1 Calculation Method for Multi Component System

Essentially, the calculation must be defined so that (1) the number of degrees of freedom is reduced, (2) the Gibbs energy of the system can be calculated, and (3) some iterative technique can be used to minimize the Gibbs energy. The number of degrees of freedom is reduced by defining a series of constraints, such as the mass balance, electro neutrality in ionic systems, or the composition range in which each phase exists. Preliminary estimates for equilibrium values must be given so that the process can begin and subsequently proceed smoothly. These values are called the start points and are critical in the minimization process of finding true equilibrium.

One of the earliest examples of Gibbs energy minimization applied to a multicomponent system was investigated in the study [69] where the chemical equilibrium in an ideal gas mixture of O, H and N with the species H, H2, H20, N, N2, NH, NO, O, 02 and OH being present. The problem here is to find the most stable mixture of species. The Gibbs energy of the mixture was defined using Eq. and defining the chemical potential of species i as –

$$\bar{G}_i = \bar{G}_i^{\circ} + RT \log_e a_i$$

where G^0_i is the standard chemical potential of species i. Standard mass balance equations were then introduced where

$$\sum_i (a_{ij} x_i) = n_j \text{ (j = 1,2,3, ….., m)}$$

wherea_{ij} represents the number of atoms of element j in the species i, x_i the number of moles of species $i$and n_j the total number of moles of$j$ in the system. These authors presented two

methods of Gibbs energy minimisation, one which utilised a linear programming method developed and one based on the method of steepest descent using Lagrange's method of undetermined multipliers [70]. Their linear programming method used the following equation:

$$\frac{G}{RT} = \sum_i x_i \left[\left(\frac{\bar{G}_i^o}{RT} \right) + \log_e \frac{x_i}{x_{\text{total}}} \right]$$

$$\frac{G}{RT} = \sum_i x_i \left(\frac{\bar{G}_i^o}{RT} \right) + x_{\text{total}} \sum \left(\frac{x_i}{x_{\text{total}}} \right) \log_e \left(\frac{x_i}{x_{\text{total}}} \right)$$

G is then calculated as a linear function of $(x_i/x_{total})log(x_i/x_{total})$ and standard Simplex code was used to find the Gibbs energy minimum. The method of steepest descent provides a rapid solution to the minimization problem and was later used by other authors in the software codes SOLGAS and SOLGASMIX. SOLGAS, the earlier code, treated a mixture of stoichiometric condensed substances and an ideal gas mixture, while SOLGASMIX was able to further include non-ideal solution phases. A quadratic approximation of G(Y) is then expanded using Taylor's approximation and minimize dutilizing Lagrange multipliers to incorporate the mass balance constraint. The relevant set of linear equations are solved to produce interim values for x_i^g and x_i^c which are then used as estimates for Y_i^g and Y_i^c in the next iteration. Convergence is considered to have been reached when the difference in Gibbs energy between the two steps is below a predefined limit of accuracy. A short additional procedure eliminates the possibility of obtaining negative values of xi and guarantees convergence; all mole numbers are screened to remain positive and the directional derivatives has to remain negative, i.e., the minimum point is not passed [71]. The minimization methods used by later programs such as ChemSage, the successor to SOLGASMIX. Thermodynamic models are now more complex, which makes it necessary to consider further degrees of freedom but, essentially, constraints are made to the system such that the Gibbs energy may be calculated as a function of extensive variables, such as the amount of each phase present in the system. Initial guesses are made for the Gibbs energy as a function of phases present, their amounts and composition, etc. The Gibbs energy is then calculated and some numerical method is used, whether it be through Lagrangian multipliers or a Newton-Raphson method, so that new values which will cause the Gibbs energy to be decreased can be estimated [71]. When the difference in calculated Gibbs energy between the iterative steps reaches some small enough value, the calculation is taken to have converged. Recently, from study [72] author described the development of new code which provides an interesting insight to some of the computational problems which can arise during Gibbs energy minimization.

2.25 Scope of the Work

High temperature properties of steel are crucial during fire hazards. This work is expected to predict the relationship between microstructure and composition of micro-alloyed carbon-steel at high temperatures. This may, in turn, suggest development of new steel grades to prevent fire disaster.

The principal objective involves modelling microstructure and tensile properties of micro-alloyed structural steels at elevated temperatures. Calculation of phases present at different temperatures using thermodynamic databases for multi-component alloy system will be carried out. Following the compositional evaluation of phases, correlations among phases will be attempted using predicted time-temperature-transformation (TTT) curves and continuous-cooling-transformation (CCT) curves. Finally, modelling of stress-strain curves at different temperatures for steels containing different alloying elements will be estimated.

3 Experimental Methods

Table 3.1 shows the composition designed for the modelling work.

Table 3.1 Chemical Composition of the structural steels (wt.%)

Alloy	C	Si	Mn	S	P	Nb	Mo	Cr	Ti	Al
Alloy 0	0.15	0.4	1.4	0.0025	0.0025	0.05	-	-	-	-
Alloy 1	0.15	0.4	1.4	0.0025	0.0025	0.05	0.25	-	-	-
Alloy 2	0.15	0.4	1.4	0.0025	0.0025	0.05	0.5	-	-	-
Alloy 3	0.15	0.4	1.4	0.0025	0.0025	0.05	0.75	-	-	-
Alloy 4	0.15	0.4	1.4	0.0025	0.0025	0.05	0.25	0.25	-	-
Alloy 5	0.15	0.4	1.4	0.0025	0.0025	0.05	0.25	0.50	-	-
Alloy 6	0.15	0.4	1.4	0.0025	0.0025	0.05	0.25	0.50	0.50	0.50

Microstructural observation and its influence on mechanical properties for different alloying elements can effectively be accomplished by computational thermodynamics [73,74]. Using thermodynamic data for phases and mobility, CALPHAD-based computational techniques provide insights of microstructure and its impact on different properties [75]. This method is found efficient for advanced automotive steel [76], including ultra-high temperature automotive exhaust components [77]. Structural steels of required composition has been taken and using the thermodynamic data different physical and mechanical properties have been discussed.

CALPHAD method is based on converting a wide range of experimental data on materials systems into physical-based mathematical models. The methodology consists of 4 main steps. Firstly, collecting experimental data on the features to be simulated. Then, examining and selecting an acceptable model for the gathered data. Thirdly, improving the models' free parameters and adding the researched system's optimal model parameters to a library of model parameters for additional systems following. CALPHAD-based technologies have been used to expedite alloy design and optimize processes for more than 30 years [78].

As discussed earlier the first stage in any assessment is to do a literature search and evaluation. Phase diagram data, such as melting point, diffusion mobility databases, invariant reactions, phase compositions, and so on, are among the experimental data employed [79]. As a consequence, all of the system's phases as well as reactions have been recognized. After that, a Gibbs energy model for each phase is determined depending on the crystal or chemical structure of the substance. For obtaining Gibbs energy model, crystal structure within each phase is required, as is thermochemical information such as formation enthalpy, heat capacity, vapor pressure data, mixing capacities and so forth. Crystal structure leads to find the Gibbs energy model. Each energy function has a set of coefficients that are later used to fit the experimental data using least square fitting. This step's output can be saved in a file known as a SETUP file. The necessary experimental data is then compiled in a separate file. The pure element's reference states need to be matched to the ones utilized in the trials. Eventually, the experimental data is fitted with the coefficients of Gibbs Energy functions. It's also worth noting that macro files, also known as TCM and EXP files, can be created that can be used to quickly draw desired property or phase diagrams. The POP file is compiled to the work file after the setup file is completed. The optimization process, or modifying the model coefficients, begins at this point. During evaluation, phase diagrams and other features are routinely drawn and compared to experimental data until the desired data is obtained [80].

However, it works in two stages to complete the calculations. It starts by extrapolating the Gibbs free energy of the available lower order systems to the energy of the higher order systems using well-established models. Finally, it improves the coupled phases' Gibbs free energy to produce the overall system's lowest Gibbs free energy [81].

CALPHAD was used to predict phase fractions of all the alloys. The temperature range used was 1600-100 ^{0}C for both equilibrium and non-equilibrium conditions. A 5 ^{0}C step temperature was used for the equilibrium condition and 4 ^{0}C was used for the non-equilibrium condition.

Simulations were saved in graphical and tabular form to interpret the results in different format. Stability information of all the phases during cooling was observed. Also, variations in composition of a particular phase were extracted. The most important information taken from the simulations was phase fractions at a pre-defined temperature (200 to 300 ^{0}C). The composition of each phase for every alloy was taken as both at % and wt %. General Steel database was used.

The step temperature method was applied for modelling. The step size was kept very low – only 5 ^{0}C for equilibrium calculation. Low step size should be able to prevent any abrupt change in phase fraction during calculation. A high step sizes like 20 K, which were found to be used in the literature, sometimes lead to incomplete liquid reaction. For non-equilibrium calculations, the step size was chosen as 4 ^{0}C. A 5 ^{0}C step was tried but for most of the alloys it returned a calculation error. A solidification cut-off of 0.10% was used to prevent liquid being retained to unrealistically low temperatures, which can occur in the Scheil model since diffusion is ignored.

Correct austenite composition is important to predict presence of carbides, and other relevant second phases. The current database used was able to predict accurate martensite start temperature and austenite composition. The model contained calculations for amount of transformation of the phases, including ferrite, pearlite and bainite.

The precipitates considered in the model include M3C, M(C,N), M2(C,N), M7C3, M23C6, M6C, Z-phase and Laves phase. The precipitation kinetics model is based on the classical Johnson-Mehl-Avrami theory with an adaption that allows the morphology of the precipitate to be considered as well as specifics associated with potential nucleate sites.

MTDATA was used to provide a comparison of results. Alloys 0, 1 and 2 were chosen to verify by MTDATA. The simulation was only run for the equilibrium condition and phase stability data against temperature during cooling were saved. The limited steel database was used.

Unwanted distortion generated during heat treatment is a major industrial problem because it critically affects the dimensional accuracy of precision components. If distortion can be predicted and controlled, then corrections can be made during the earlier machining stage so that the components reach their final desired shape and dimension after heat treatment. Prediction of distortion induced by heat treatment has generally been based on prior experience or by a trial-and-error approach. In recent years, with the significant improvement of computing power, Finite Element/Finite Difference (FE/FD) simulation tools have been developed to tackle this problem. While being successful in some cases, almost all of the FE/FD packages

suffer from one common problem: the lack of accurate material property data. This is because the prediction of distortion requires detailed knowledge of the material properties of each phase formed during heat treatment, all of which are a function of alloy composition, heat treatment procedures (microstructure) and temperature. The following information on materials properties has to be known for distortion prediction:

• phase transformation kinetics, i.e., TTT and CCT diagrams

• temperature dependent thermophysical properties of each phase formed, such as

density, Young's modulus, thermal expansion coefficient, and thermal conductivity

• temperature dependent mechanical properties of each phase formed, including tensile

strength, yield strength and hardness.

In the present paper, the development of a computer program, Java-based Materials Property (JMatPro) simulation software, is reported which can calculate the above material properties for general steels. The success of the program is based on an accurate description of all the major phase transformations taking place during heat treatment (Saunders et al., 2004), as well as an accurate calculation of the properties of different phases formed in steels. This paper is a natural extension of our previous work (Guo et al., 2005), where model development was explained in details and extensive validation had been carried out. Consequently, the present paper will focus on a specific application of JMatPro, which generates material data that otherwise has to be measured through experiments such as: dilatometry, Jominy hardenability test, and Greeble testing.

3.1 Modeling of material data for distortion protection

3.1.1 TTT and CCT diagrams

Significant work has been carried out over recent decades to develop models that can calculate TTT/CCT diagrams for steels (Kirkaldy et al., 1978; Kirkaldy and Venugopolan, 1984; Bhadeshia, 1981; 1982; Lee and Bhadeshia, 1993). Although successful for low alloy steels, these models are limited when it comes to more highly alloyed types. This problem has been

solved in the most recent version of JMatPro, which is now able to calculate TTT/CCT diagrams for steels of all types, including the highly alloyed ones (Guo et al., 2005; Saunders et al., 2004). Two new features in the models deserve special attention. One is the determination of the austenite composition at the quenching temperature. When carbides or other second phases are present at this temperature, it would be inappropriate to use the overall alloy composition as the composition of the austenite to be decomposed. In the present treatment, the composition of the austenite present at the quenching is always calculated directly (Li et al., 2002) and then used in the subsequent modelling. The other feature is that the formation of martensite and bainite is affected by the prior formation of ferrite. The carbon rejected by the formation of ferrite is then incorporated into the remaining austenite, which may have a significant impact on further transformations. For example, increased carbon in austenite reduces bainite and martensite start temperatures and increases the strength of the transformed phases.

3.1.2 Thermophysical and physical properties

Thermophysical and physical properties are critical parameters for the prediction of distortion induced by heat treatments or processing. JMatPro's ability to model these properties has been well documented in previous published work for various metallic systems (Sente Software Ltd., 2005; Guo et al., 2005). The relevant properties that can be modelled include: density, molar volume, thermal expansion coefficient, Young's, bulk and shear moduli, Poisson's ratio, thermal conductivity and diffusivity, electrical conductivity and resistivity, all are provided for each phase present when necessary.

3.1.3 Mechanical properties during heat treatment

A heat treatment cycle typically includes heating, isothermal holding and cooling procedures. The mechanical properties, as well as physical and thermophysical properties, of steels during those procedures can now be calculated (Sente Software Ltd., 2005; Guo et al., 2005). The microstructure is assumed to be 'frozen' when below the final heat treatment temperature, and reach equilibrium when above this temperature. The calculation of mechanical properties during isothermal holding or cooling has been demonstrated previously (Guo et al., 2005).

Properties critical to the prediction of distortion induced by heat-treatment have been calculated using JMatPro, which embodies integrated software for the prediction of both the structure and properties of a wide range of alloys. TTT and CCT diagrams, as well as the density and yield stress of key microstructural constituents such as ferrite, pearlite, bainite and martensite for the two steels 4140 and 5140 have been calculated as examples of a larger range of physical, thermophysical and mechanical properties that can be handled in a similar way. Such calculations are available as a function of temperature, including elevated temperatures for which experimental results are often not readily available. The way that arbitrary cooling profiles can be handled is demonstrated by the calculation of Jominy hardenability profiles which are the result of a complex interplay between thermal and microstructural properties. The variation of properties of different constituents for different cooling rates substantially increase the understanding of the hardness variation along the Jominy bar. The success of the model is based on accurate description of all the major phase transformations taking place, as well as an accurate calculation of the properties of different phases formed during heat treatment process. The output from JMatPro has already been linked to other FE/FD-based process simulation packages such as MAGMASOFT and PROCAST for casting, DEFORM and FORGE-3D for forging and rolling, and ANSYS which is a general simulation tool. The desired properties could therefore also be linked to any packages that describe the development of the internal stress patterns originating from both elastic and plastic mechanisms.

As part of the development of the software programme JMatPro, phase transformation models have been included for a variety of alloy types e.g. Al-alloys, Ni-based superalloys, Ti-alloys and for TCP phases such as σ and χ in stainless steels. JMatPro also incorporated a capability to calculate transformations involving ferrite, pearlite and bainite in HSLA steels closely based on the model of Kirkaldy. To bring this calculation capability in-line with JMatPro's capability for other alloys, where high alloy contents can be routinely handled, work has been undertaken to extend this model capability to steels of high alloy content. There is a hugely extensive published literature concerned with the transformations in steels but, of this, only a small part is given over to the calculation of TTT and CCT diagrams. The pioneering work of Kirkaldy and co-workers showed that it was possible to calculate quite accurate TTT and CCT diagrams as well as the Jominy hardenability for low alloy steels. Later work by Bhadeshia used a different methodology to determine start curves for ferrite and bainite transformations and tested the model against experiment. The model of Bhadeshia has been extended by Lee to

cover slightly higher concentrations. However, although successful for low alloy steels these models are limited when it comes to more highly alloyed types.

One of the drawbacks of both models has been the use of dilute solution thermodynamics in calculating transformation temperatures. This can now be overcome using thermodynamic models that provide high quality results for steels in general, ranging from stainless steels, to tool steels as well as the low to medium alloy range types. The aim of the present work is to combine the more extensive thermodynamic models with a kinetic model to see if the composition range of applicability could be extended to cover a wider range of steels, including the highly alloyed types. The model of Kirkaldy was chosen as the basis for the new calculations as there is a clearly identifiable set of input parameters that are required and which can be readily calculated. It is also having empirical parameters that can be adjusted easily and controllably.

4 Results and Discussion

4.1 Microstructural evolution of equilibrium phase formation for different alloys at variable temperature:

When cooling from an elevated temperature different phases forms at different temperature. And these phases are important in developing mechanical and physical properties at different temperature. The addition of different alloying elements helps in maintaining proper properties. In this research work, different alloying elements are added to predict its high temperature properties. As mechanical properties depends on the phases present in the microstructure, addition of different alloying elements plays an important role in developing different phases.

Below, a study of different phase formation for different alloys at variable temperature is going to discuss.

4.1.1 Alloy 0:

From Figure 4.1.1, it is clear that a few percentages of cementite form throughout a wide temperature range of 600ºC to 700ºC. At 600ºC, ferrite developed at a rate of 97.83%, which subsequently reduced until the wt. (%) reached 0 at 826ºC. Austenite began to form around 690ºC, just as cementite has finished, and it gradually increased. The wt. (%) of austenite is almost 100% for a wide temperature range of 826ºC to 1472ºC. After that, it started to lose weight. At 1483ºC, the wt. (%) of austenite becomes zero. Liquid started forming just before the austenite formation was completed. After 1510ºC, the liquid was formed 100 wt. (%). However, from 600ºC to 1357ºC the formation of MNS was very negligible. The formation amount in M(C, N) is also minimal like MNS, and the temperature range was 600ºC to 1239ºC.

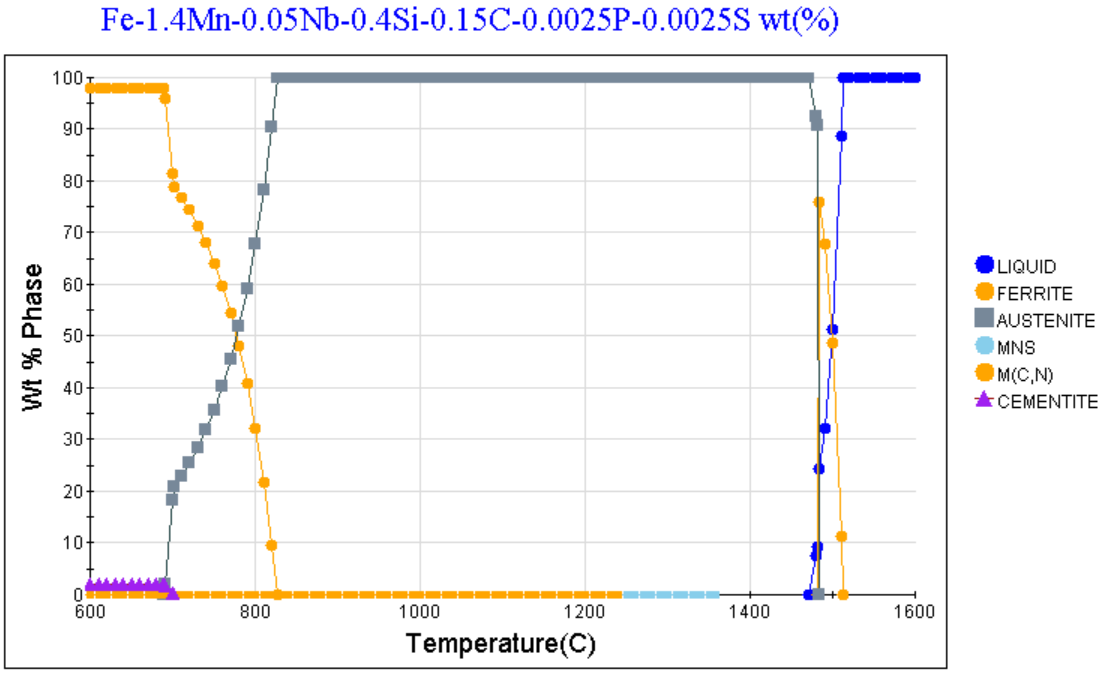

Figure 4.1.1 Equilibrium phases for alloy 0

4.1.2 Alloy 1:

Figure 4.1.2 shows that cementite forms in minimal amounts over a large temperature range of 600°C to 700° C. The initial and ending formation temperature of cementite for Alloy 1 is identical to Alloy 0. However, the amount of wt. (%) phase in Alloy 1 is 0.559777, which is slightly higher than Alloy 0. Because of the inclusion of 0.25 % molybdenum, the amount has increased. Similar research can be found in a study where it can be evaluated how adding molybdenum affects cementite formation. Ferrite evolved at a rate of 97.83% at 600° C, then decreased until the weight (%) reached zero at 831.7142°C.

Molybdenum does not appear to have a substantial effect on the ferrite percentage. Austenite continues to form around 690°C, much like cementite was reaching the decline stage, and its temperature gradually climbed. For a broad temperature range of 1357°C to 1468°C, the wt. (%) of austenite is nearly 100%. It began to lose weight after that. The weight (%) of austenite is zero at 1480°C.

Liquid began to form at 1470ºC, just before austenite formation reached 100%. Liquid was formed 100% in the temperature range of 1520ºC to 1600ºC. Molybdenum did not show any great impact on the liquid formation as well. The effect of molybdenum is seen to be explored

in the case of liquid, with the effect being non-significant in the case of a modest amount of Mo addition. However, the formation of MNS was insignificant between 600ºC and 1350ºC. M(C,N) has a limited formation amount, similar to MNS, and the temperature range was 600ºC to 1230ºC.

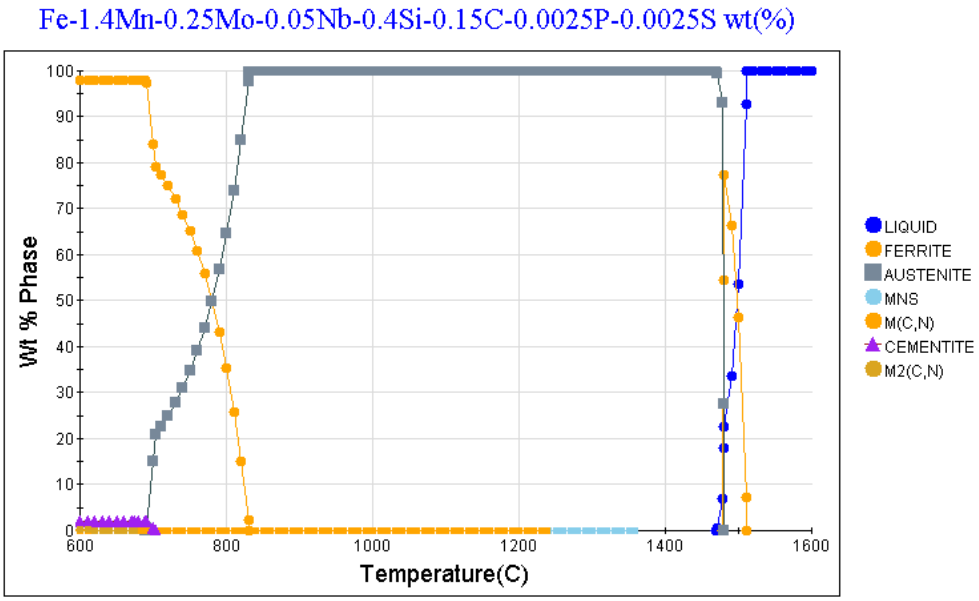

Figure 4.1.2 Equilibrium phases for alloy 1

4.1.3 Alloy 2:

Figure 4.1.3 depicts the same temperature range for cementite formation as alloys 0 and 1. Cementite formation is, however, higher at 700°C than the other two alloys. The amount has grown due to the addition of 0.25 % molybdenum. So it can be predicted that as the amount of molybdenum increases, the formation of cementite also increases with temperature. Austenite continued to form about 690°C, and its temperature progressively climbed, similar to the way as the cementite was approaching the decline stage. After that, it gradually has lost weight. At 1480°C, the weight (%) of austenite is zero. It is predicted that there is no discernible variation in austenite production kinetics when Mo is added. Between 600°C and 1350°C, however, MNS growth was modest. Identical to MNS, M(C,N) has a confined formation amount and the temperature range was 600°C to 1230°C. MNS and M(C,N) have the same formation and termination temperatures as alloys 0 and 1, implying that molybdenum has a negligible effect on these formations.

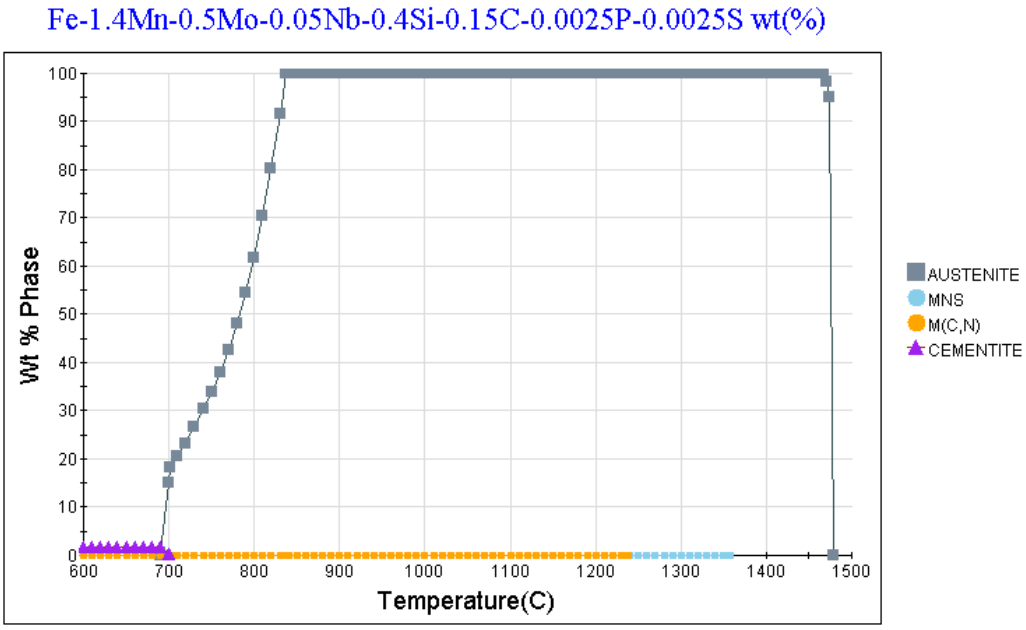

Figure 4.1.3 Equilibrium phases for alloy 2

4.1.4 Alloy 3:

Figure 4.1.4 showed somewhat changes in the graph when 0.75% chromium was added. The cementite formation was throughout the temperature range of 600° C to 690°C However, alloy 3 has 1.360073 wt. (%) phase, which is slightly greater than other alloys. Because of the inclusion of 0.75 % Mo, the amount has increased and the ending formation temperature is decreased. At 600°C, ferrite formed at a rate of 97.83 %, then the weight (%) declined till it reached zero at 842.0495°C. It is predicted that with increasing Mo concentration, the amount of martensite drops while the amount of ferrite steadily increases. However, Molybdenum does not appear to have a significant impact on the percentage of ferrite as discussed earlier. Austenite began to develop at 690°C, and the amount of wt. (%) rapidly grew until it reached 100 % wt. at 1357.901°C. It remained stable for 1460°C after attaining 100%. Just before austenite production reached 100%, liquid began to develop around 1464.278°C. Liquid was formed 100% in the temperature range of 1510ºC to 1600ºC. Between 600ºC and 1350ºC, however, MNS formation was minimal. Similar to MNS, M(C,N) has a constrained formation amount, and the temperature range was 600ºC to 1230ºC. The formation of M_6C is seen to be between the range of 750.2751ºC to 776.9311ºC. From the temperature ranges of 600ºC to 750.5769ºC the formation of wt. (%) of M2(C,N) is 0.011822.

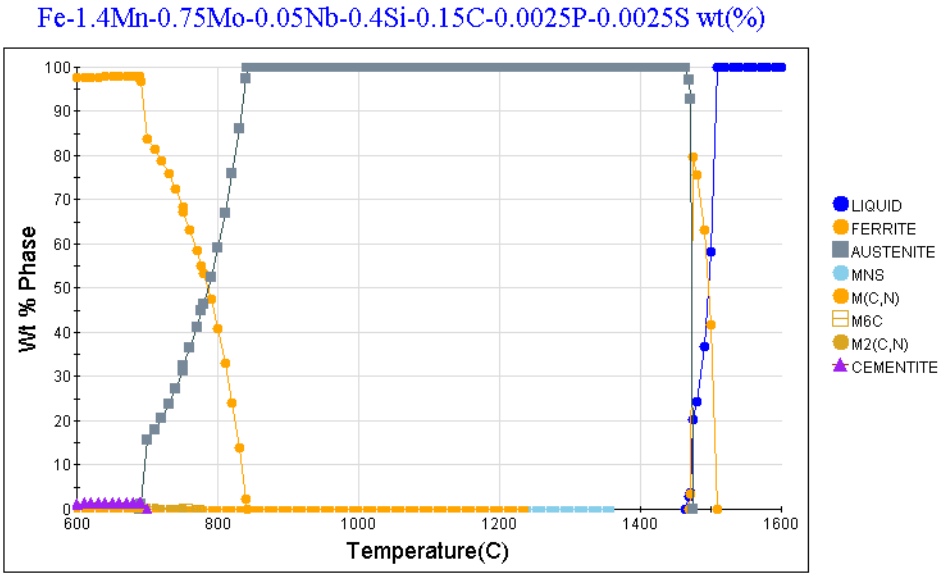

Figure 4.1.4 Equilibrium phases for alloy 3

4.1.5 Alloy 4:

Figure 4.1.5 showed somewhat changes in the graph when 0.25% chromium was added along with the 0.25% molybdenum. Cementite formation occurred at temperatures ranging from 600°C to 705.2908°C. However, alloy 4 has a phase content of 0.77 wt. (%), which is substantially lower than the other alloys. Because of the inclusion of 0.25% chromium, the amount has increased and the ending formation temperature is also increased but the wt. (%) decreased. However, the amount of chromium affected the cementite formation. Ferrite developed at a rate of 97.94 % at 600° C, then the weight (%) decreased until it reached zero at 828.7205°C. Ferrite is generated when strong ferrite formers like molybdenum and chromium are added in excess. Austenite formed at 690°C, and the weight (%) gradually increased until it reached 100 % at 1358.98°C. It remained stable for 1468.631°C after attaining 100% wt. Just before austenite production reached 100%, liquid began to develop around 1480°C. Liquid was formed 100% in the temperature range of 1468.631ºC to 1600ºC. Molybdenum and chromium, on the other hand, had little effect on the liquid formation.

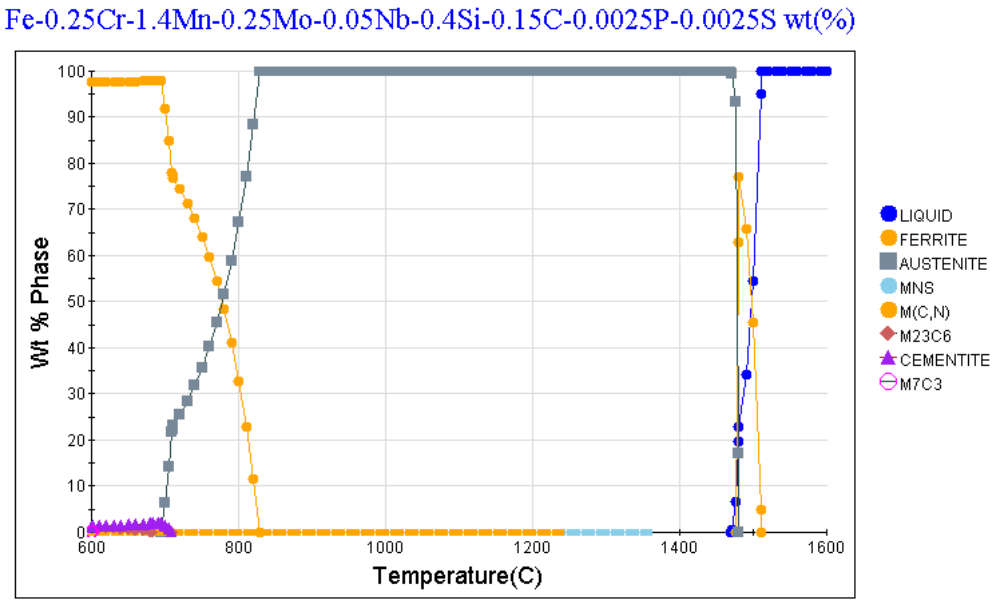

Figure 4.1.5 Equilibrium phases for alloy 4

MNS formation, on the other hand, was minimal between 600ºC and 1350ºC. M(C,N) had a restricted formation amount, similar to MNS, and the temperature range was 600ºC to 1230ºC. So it can be concluded that MNS and M(C,N) does not have any impact for adding Mo and Cr. The formation of M_7C_3 is seen to be between the range of 600ºC to 601.9072ºC. At 600ºC, the formation of $M_{23}C_6$ initially started which gradually reduced to zero at 684.1024ºC. M23C6 began to form again after crossing the temperature of 705.2908ºC, and it formed until 710ºC, around 0.082857 wt. (%), before returning to zero.

4.1.6 Alloy 5:

When 0.50 % chromium was added to the 0.25 percent molybdenum in Figure 4.1.6, the graph changed marginally. Cementite formation occurred at temperatures ranging from 600° C to 707.4798° C. The phase content of alloy 4 is 1.2 wt. (%), which is significantly higher than the other alloys. Because of the inclusion of 0.50 % chromium, the amount has increased and the ending formation temperature is also increased along with the wt. (%). Ferrite developed at a rate of 97.57 % at 600° C, then the weight (%) decreased until it reached zero at 830°C. The addition of small amount of chromium and molybdenum do not show any significant change in the graph. Austenite started forming from 696.74°C. The initial formation temperature slightly increased due to the addition of chromium to it.

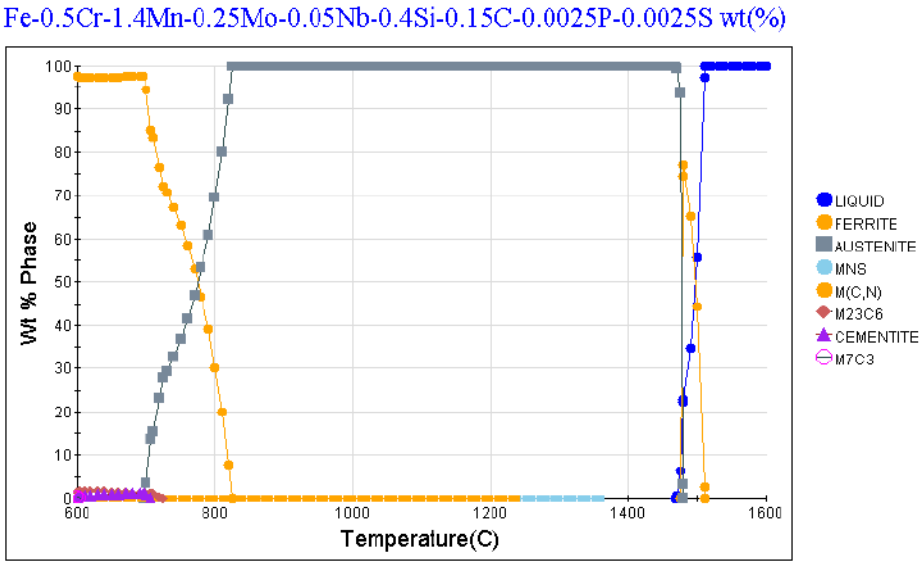

Figure 4.1.6 Equilibrium phases for alloy 5

The formation temperature for austenite is predicted and which shows similar result with this his graph as well. From 825.8097°C to 1468.452°C temperature range the austenite was remained almost 100 wt. After reaching 100% wt., austenite became zero at 1480.073°C as a few temperatures rises. While examining this sudden fall in the graph, liquid is seen to be developing within the temperature range of 1468.452°C to 1600°C. MNS formation, on the other hand, was minimal between 600ºC and 1360ºC. M(C,N) had a restricted formation amount, similar to MNS, and the temperature range was 600ºC to 1230ºC. As a result, M(C,N) has no effect on the addition of Mo and Cr, whereas MNS does. M_7C_3 formation is shown to be very modest just at the very beginning, at 600ºC. From 600ºC to 720ºC, the formation of $M_{23}C_6$ is observed. In the case of alloy 5, unlike alloy 4, the formation of $M_{23}C_6$ did not follow a complex curve.

4.1.7 Alloy 6:

The curve in Figure 4.1.7 changed dramatically when 0.50 % chromium, 0.50 % Titanium, and 0.50 % Aluminum were added to the 0.25 % molybdenum. Ferrite was formed at temperatures ranging from 600° C to 960.8578° C. The formation then ground to a standstill, and at 1500° C, it re-started and formed until it reached 1510.437° C. In a similar study [11], where it is shown that with the addition of titanium to the microstructure, up to 0.05 percent, promoted the production of acicular ferrite. Austenite started forming from 740°C which is much higher than alloy 5. In the 201L ASS, the influence of Titanuim addition on the creation of nano-crystalline structure was investigated [12] where it is stated that Ti has impact on the formation

of austenite. The austenite formation was stopped at 1450° C with 10.28602 wt. (%) phase. In this case the liquid started forming from 1430.248° C which is much lower than other alloy's required temperature.

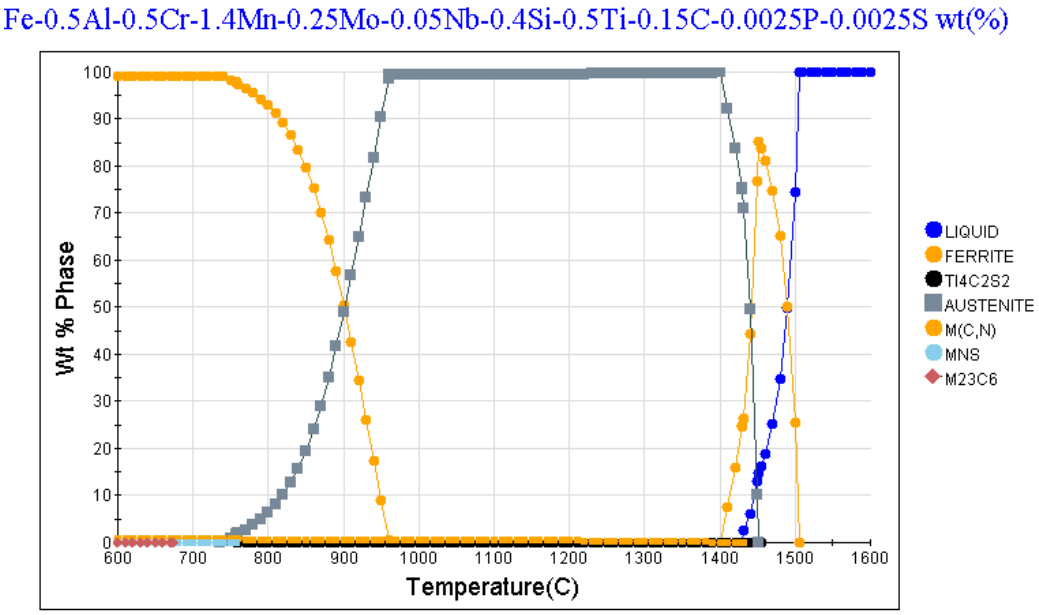

Figure 4.1.7 Equilibrium phases for alloy 6

This means the liquid was formed earlier because of the impact of the alloying elements. However, it stopped forming liquid at 1600° C with 100 wt. (%) phase. From the Figure the formation of $TI_4C_2S_2$ was found, which was started forming from 757.4767°C to 1454.726°C. The formation of M(C,N), MNS and $M_{23}C_6$ all initially started at 600° C. At 1430.248°C, the M(C,N) phase formed 0.073597 wt. (%) and subsequently stopped developing. MNS was formed till 757.4767°C from 600° C. The amount of wt. (%) phase, on the other hand, was nearly consistent at 0.006783. For $M_{23}C_6$ the formation temperature was from 600° C to 670° C.

4.2 Statistical study of phase formation at equilibrium condition:

4.2.1 Cementite:

While adding alloying elements like Mo, Cr, Al, Ti the initial cementite formation temperature remains same. The alloying addition cannot affect the formation of cementite. It forms at 600°C. The cementite may hamper the properties due to its high brittle properties. Thus it is a challenge to reduce its quantity. Thus from the Table 4.2.1 it is seen that the

addition of Mo and Cr causes diminish the cementite above 1230°C. But for Alloy 6 it is seen that, cementite remains stable at around 1430°C.

Table 4.2.1 Cementite formation for different alloys

Alloys	Initial Formation Temperature for Cementite (°C)	Cementite formation ends (°C)
0	600	1239.389
1	600	1230
2	600	1230
3	600	1230
4	600	1230
5	600	1230
6	600	1430.248

4.2.2 Austenite

In this case the addition of different alloying elements significant change or effect has not been found from the Table 4.2.2.

Table 4.2.2 Austenite formation for different alloys

Alloys	Initial formation temperature of Austenite (ºC)	Ending formation temperature of Austenite (ºC)
0	688.3	1483.3
1	690	1480
2	690	1478.006
3	690	1475.3

Alloys	Initial formation temperature of Austenite (ºC)	Ending formation temperature of Austenite (ºC)
4	700	1480.4
5	696.74	1480
6	740	1450

4.2.3 Solidus and Liquidus line:

From the Table 4.2.3 it can be predicted that the successive addition of Mo, Cr, Al, Ti widens the melting range. Alloy 6 has the maximum melting range whereas the base alloy has the minimum melting range. Another observation is found that the addition of alloying elements shifts the liquidus curve lower. It is one of the limitations of the addition of the particular alloying elements.

Table 4.2.3 Solidus and Liquidus Line

	Alloy 0	Alloy 1	Alloy 2	Alloy 3	Alloy 4	Alloy 5	Alloy 6
Initial formation temperature of Liquid (ºC)	1471.002	1470	1466.533	1464.278	1468.631	1468.452	1430.248
Ending formation temperature of Liquid (ºC)	1600	1600	1600	1600	1600	1600	1600

4.2.4 Summary of phase formation at equilibrium condition:

Table 4.2.4 clearly signifies the effects of alloying element on the stability of different phases at different temperature.

Table 4.2.4 Summary of Equilibrium Phases

	Alloy 0	Alloy 1	Alloy 2	Alloy 3	Alloy 4	Alloy 5	Alloy 6
Initial formation temperature of Liquid (ºC)	1471.002	1470	1466.533	1464.278	1468.631	1468.452	1430.248
Ending formation temperature of Liquid (ºC)	1600	1600	1600	1600	1600	1600	1600
Initial formation temperature of Ferrite (ºC)	600	600	600	600	600	600	600
Ending formation temperature of Ferrite (ºC)	1511.91	1511.231	1510.549	1509.862	1510.834	1510.437	1500
Initial formation temperature of Austenite (ºC)	688.2621	690	690	690	700	696.74	740
Ending formation temperature of Austenite (ºC)	1483.313	1480	1478.006	1475.296	1480.414	1480.073	1450
Initial formation temperature of MNS (ºC)	600	600	600	600	600	600	600
Ending formation temperature of MNS (ºC)	1357.642	1350	1350	1350	1350	1360	757.4767
Initial formation temperature of M(C,N) (ºC)	600	600	600	600	600	600	600

	Alloy 0	Alloy 1	Alloy 2	Alloy 3	Alloy 4	Alloy 5	Alloy 6
Ending formation temperature of M(C,N) (ºC)	1239.389	1230	1230	1230	1230	1230	1430.248
Initial formation temperature of Cementite (ºC)	600	600	600	600	600	600	
Ending formation temperature of Cementite (ºC)	700	700	700	690	709.1909	707.4798	

4.3 Microstructural evolution of non-equilibrium phase formation at different alloys at variable temperature:

In stress-temperature space, non-equilibrium phase diagrams of crystallization and melting under flow conditions are formed, with melt, non-crystalline, hexagonal, and orthorhombic phases. Changes in non-equilibrium phases are observed depending on the alloying components. Different alloying components are introduced to this research work in forecasting future of their high temperature properties. With the changing temperature, different phases are formed as various alloying elements are added.

4.3.1 Alloy 0:

Figure 4.3.1 shows that the bainite formation remained constant for roughly 64% of the temperature range of 25^{o}C to 475^{o}C. After that, the formation of ferrite started to steadily decline till 570^{o}C. Austenite started to form shortly after bainite had completed its formation. From 480^{o}C to 1840^{o}C the austenite formation was completed. Liquid started to form 1475^{o}C and gradually increased. From 1515^{o}C to 1595^{o}C temperature range the liquid is formed 100%. The formation of pearlite is also observed in the graph. From the temperature range of 25^{o}C to 590^{o}C, pearlite formation is indicated and the amount is very minimal.

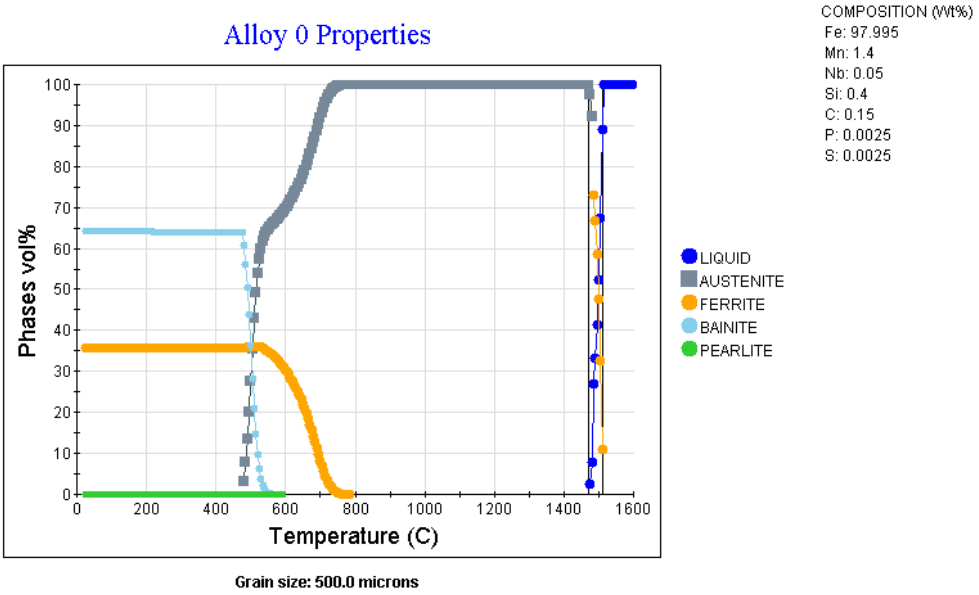

Figure 4.3.1 Non-equilibrium phases for alloy 0

1.1.2 Alloy 1:

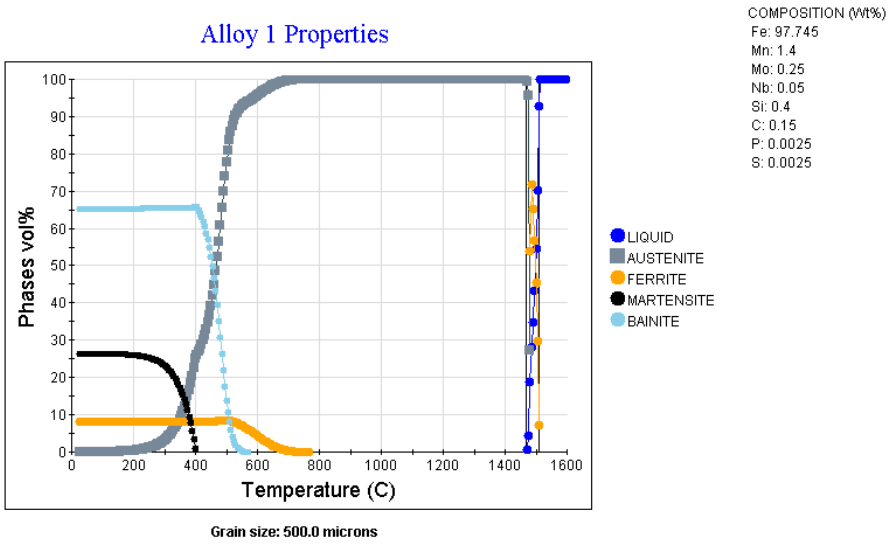

Figure 4.3.2 Non-equilibrium phases for alloy 1

Figure 4.3.2 depicts the evolution of the graph as molybdenum was introduced. Bainite started to form at 25^{o}C and for a wide temperature range the formation phase for bainite stayed constant with approximately 65% of phase volume. The inclusion of 0.25% Mo results in minor alterations in the bainite formation. Martensite started to form at 250°C, but not as greatly as bainite. At 570^{o}C martensite formation was completed.

Ferrite started to form from 25°C. The amount of formation remained practically consistent from 25°C to 540°C. The amount proceeded to decrease after that, and at 765°C, the formation amount was zero. The ferrite formation began again at 1480°C, and it was completed at 1510°C with a phase volume of 7.08862 (%). The amount of ferrite (%) is altered by molybdenum's effect, and it progressively decreases.

From 1470°C onwards, liquid began to form, and by 1515°C, the amount of produced liquid had reached 100%. The Mo appears to have very few effect on liquid. In case of austenite, the formation initially started at 25°C. After 600°C, the amount of phase volume of austenite became almost 100% till 1475°C and at 1480°C the amount suddenly dropped to 27.25184 phase volume (%).

4.3.2 Alloy 2:

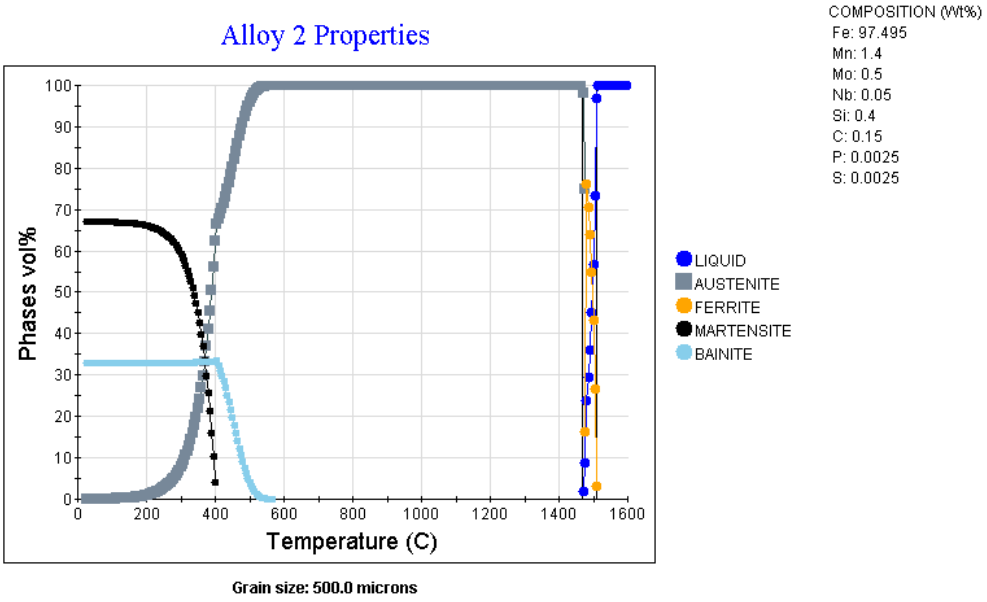

Figure 4.3.3 Non-equilibrium phases for alloy 2

From the Figure 4.3.3 the formation of austenite started at the very beginning of the temperature 25°C. After around 515°C, the amount of austenite became almost 100% phase volume. As the 0.50% percentage of Mo was introduced to the alloy, the changes in the austenite formation is observed. It took less temperature to form maximum amount of austenite. The volume percentage suddenly became 75.015% at 1475°C.

In case of martensite, while rapidly cooled from an elevated temp[erature the initial formation temperature is 400°C and it stopped forming till 25°C. The phase (%) of martensite

has increased dramatically as a result of the addition of Mo. Bainite started to form from 565°C till 25°C. In case of ferrite, the formation is observed for a very short period of temperature range which is from 1475°C to 1510°C.

4.3.3 Alloy 3:

The Figure 4.3.4 depicts that the curves vary as more Molybdenum (%) is added. The formation of austenite began at a temperature of 25°C. After around 465°C, the amount of austenite became almost 100% phase volume. The austenite formation alters as the 0.75 % Mo content is added to the alloy. The largest amount of austenite was formed in a relatively short time at a very low temperature. At 1475°C, the volume percentage abruptly increased to 7.6312%.

As the alloying element percentage was increased to 0.75%, the phase volume of martensite was also increased and at 25°C the amount is found to be 87.34143%. With the increasing temperature, the amount of martensite formation percentages decreased and at 395°C it only formed 8.53656%.

With the increasing amount of Mo, the bainite phase (%) is seen to be decreased. At 25°C the amount is only 12.62329% and this amount of formation was constant till 400°C. The liquid and ferrite has started forming at very high temperature. The initial formation temperature for liquid and ferrite is 1465°C and 1470°C respectively.

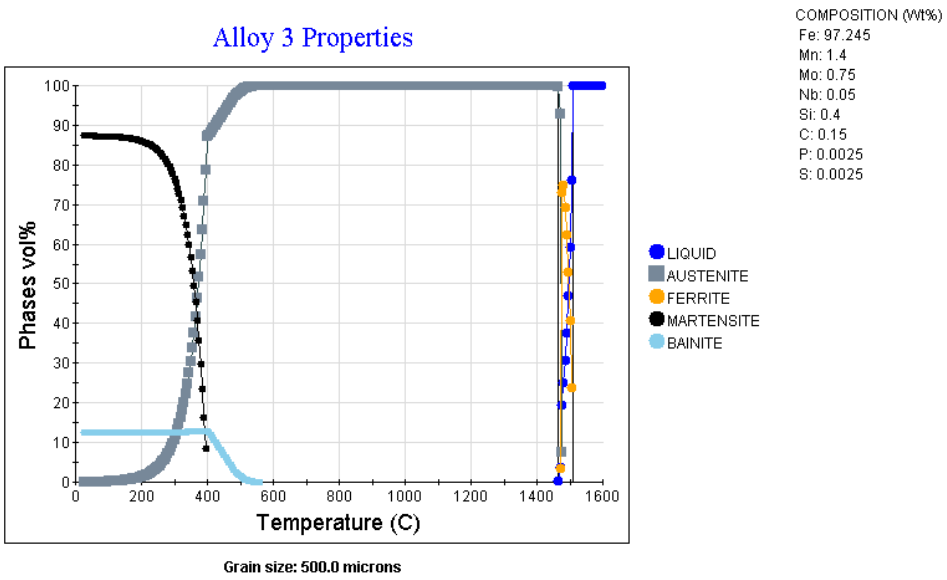

Figure 4.3.4 Non-equilibrium phases for alloy 3

4.3.4 Alloy 4:

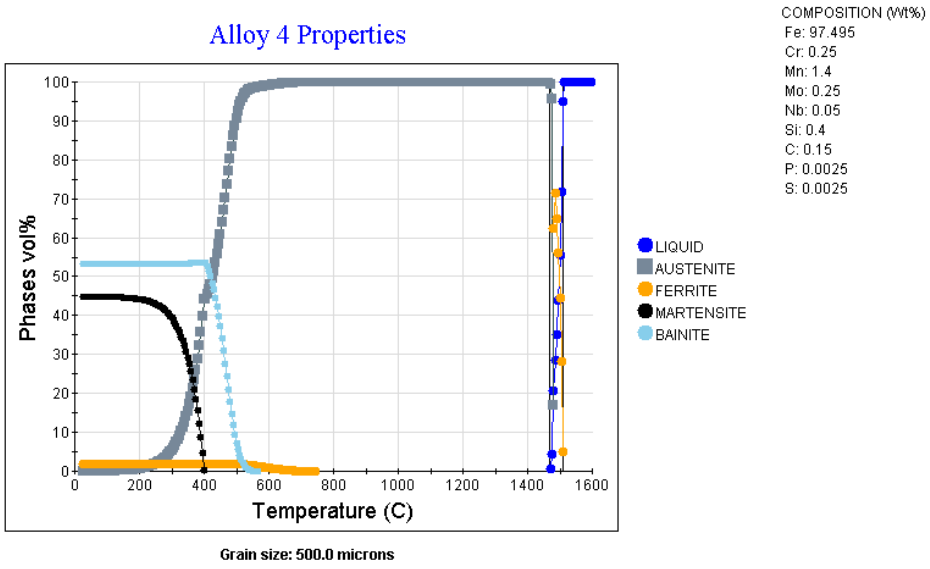

Figure 4.3.5 Non-equilibrium phases for alloy 4

As 0.25% chromium was added along with the Mo content, a significant change in the graph can be observed. Cr decreased the phase volume of martensite as depicted in the Figure 4.3.5. At 25^{o}C the volume percentages became 44.88665%. Bainite phase volume is seen to be increased drastically. The amount of bainite was almost constant from 405^{o}C to 25^{o}C.

The austenite formation was initially started from 25^{o}C and it gradually increased. Till 1475^{o}C the amount of formed austenite was seen to be 100%. And at 1480^{o}C, it suddenly became 16.93798%. Austenite did not show any major changes because of the addition of alloying elements. The ferrite formation is seen to be visible in low temperature ranges. The first one is from 25^{o}C to 745^{o}C and the second one is from 1480^{o}C to 1510^{o}C. The liquid is formed in very high temperature. At 1470^{o}C the formation started and gradually increased till 1595^{o}C.

4.3.5 Alloy 5:

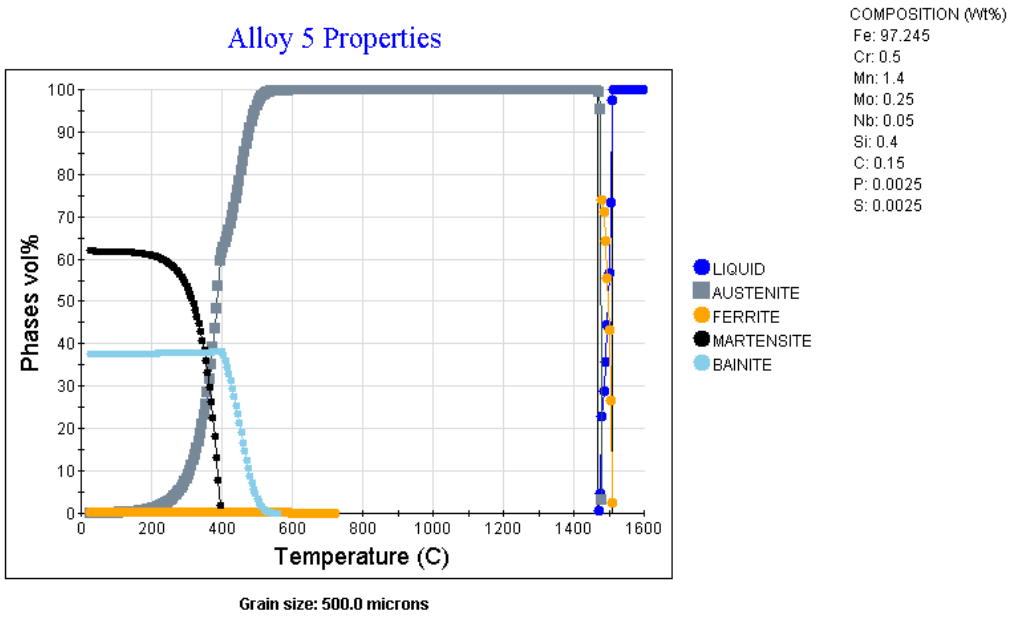

Figure 4.3.6 Non-equilibrium phases for alloy 5

In Figure 4.3.6, martensite, bainite, austenite and ferrite initial formation was started from 25°C. Ferrite formed from 25°C to 720°C with a very minimal amount. Again at 1480°C, the formation started and at 1510°C it became 2.6077% phase volume. Austenite started forming from 25°C and gradually decreased. It stayed almost 100% from 495°C to 1475°C. At 1480°C suddenly the phase volume became 3.04184%. The liquid started forming at 1470°C and till 1595°C the amount of liquid remained 100%.

4.3.6 Alloy 6:

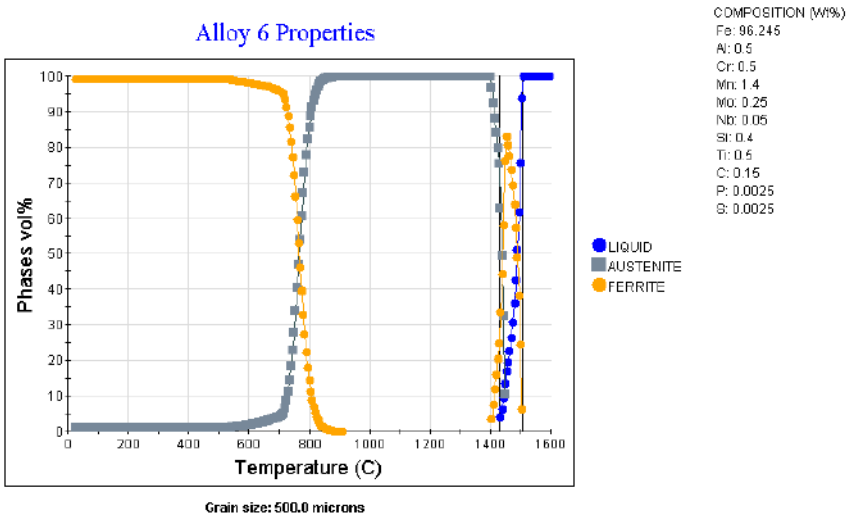

Figure 4.3.7 Non-equilibrium phases for alloy 6

Figure 4.3.7 shows changes in the phases as Cr, Mo, Ti and Al was added. Austenite started forming at 25^{o}C and gradually increased. The amount of austenite formed 100% from 820^{o}C to 1420^{o}C. At more high temperature the austenite gradually decreased and lastly became 10.20957%. Ferrite formed 98.95597% at 25^{o}C. Till 725^{o}C the amount of ferrite was almost constant. After that the ferrite gradually decreased. Again from 1405^{o}C to 1505^{o}C temperature the ferrite again formed. In case of liquid, it started forming at very high temperature which is 1435^{o}C. For adding those alloying elements, the liquid started forming earlier than other alloys. After 1505^{o}C the liquid was formed 100%.

4.4 Statistical study of phases formation at non-equilibrium condition:

4.4.1 Austenite

The formation temperature is modified with the base alloy while adding alloying. The other resultant values, on the other hand, appeared to be nearly identical. Table 4.4.1 depicts that, austenite phase is not stable at room temperature for base alloys. But successive addition of particular alloying elements is responsible to stable the austenite at room temperature in case of non-equilibrium condition.

Table 4.4.1 Austenite formation for different alloys

Alloys	Initial formation temperature of Austenite (ºC)	Ending formation temperature of Austenite (ºC)
0	480	1480
1	25	1480
2	25	1475
3	25	1475
4	25	1480
5	25	1480
6	25	1450

4.4.2 Solidus and Liquidus lines:

From the Table 4.4.2 it can be predicted that the successive addition of Mo, Cr, Al, Ti didn't affect the solidus and liquids line in any broadened manner. However, the formation of liquid is noticeably found in very high temperature.

Table 4.4.2 Liquid formation for different alloys

	Alloy 0	Alloy 1	Alloy 2	Alloy 3	Alloy 4	Alloy 5	Alloy 6
Initial formation temperature of Liquid (ºC)	1475	1470	1470	1465	1470	1470	1435
Ending formation temperature of Liquid (ºC)	1595	1595	1595	1595	1595	1595	1595

4.4.3 Martensite:

Table 4.4.3 depicts that, no substantial change or effect has been observed when different alloying elements are added.

Table 4.4.3 Martensite formation for different alloys

	Alloy 1	Alloy 2	Alloy 3	Alloy 4	Alloy 5
Initial formation temperature of Martensite (ºC)	25	25	25	25	25
Ending formation temperature of Martensite (ºC)	400	400	395	400	395

4.4.4 Ferrite:

Table 4.4.4 depicts that the formation of ferrite has shown different results as Mo, Cr, Ti and Al was added to it. In case of initial formation temperature when 0.50%Mo was added the formation temperature needed very high and that continued with the increasing amount of Mo. In case of alloy 4, when Cr was added the initial formation temperature again declined to 25^{o}C. So higher percentages of Mo have shown a great impact on the formation of ferrite. And after 1510^{o}C no formation of ferrite was observed.

Table 4.4.4 Ferrite formation for different alloys

	Alloy 0	Alloy 1	Alloy 2	Alloy 3	Alloy 4	Alloy 5	Alloy 6
Initial formation temperature of Ferrite (^{o}C)	25	25	1475	1470	25	25	25
Ending formation temperature of Ferrite (^{o}C)	1510	1510	1510	1505	1510	1510	1505

4.5 Equilibrium Phase Formation on Cooling Rate

Various cooling rates result in different phase combinations. Depending on the cooling rate (very slow cooling rate vs. faster cooling rate), coarser or finer particles are produced [82]. The faster the cooling rate, the smaller the alloy grain size and the fewer precipitated phases in the matrix. A relatively uniform size of the alloy could be achieved at a constant cooling rate [83].

4.5.1 Ferrite Fraction

The ferrite fraction of duplex stainless steels is an important microstructure variable that influences mechanical characteristics and corrosion resistance [84]. Alloy 0 has the highest ferrite fraction with increasing cooling rate. The ferrite fraction drops when 0.25% molybdenum is added to alloy 0, compared to pure alloy 0. Alloying element molybdenum reduces carbon's activity, slowing down operations that depends on carbon diffusion [85,86].

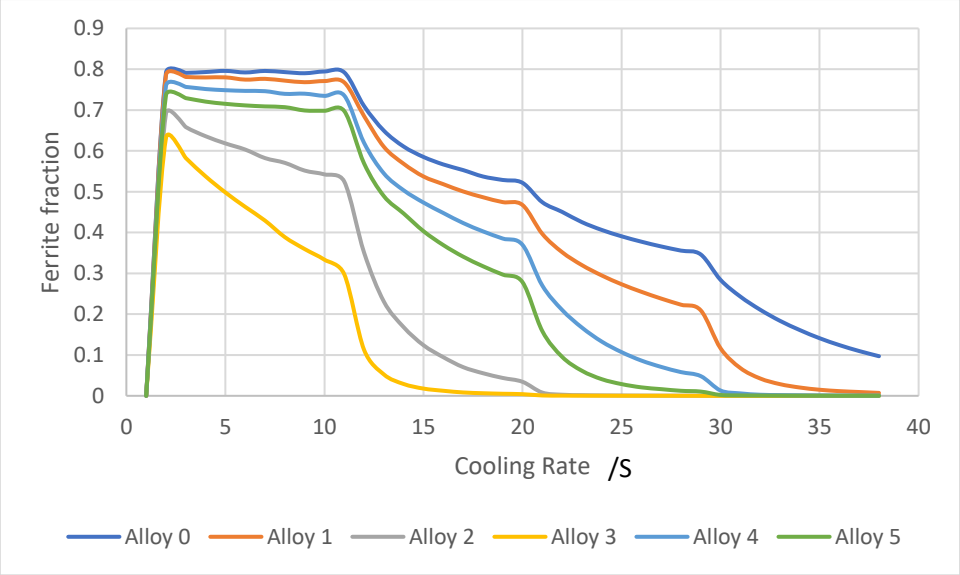

Fgure 4.5.1 Ferrite fraction vs cooling rate

As a result, the ferrite fraction decreases. It is also observed that the ferrite fraction gradually reduced as the amount of molybdenum increased in the Figure. The lowest ferrite fraction is found in Alloy 3, which has the most Mo. In case of alloy 4, the ferrite fraction increased compared to alloys 2 and 3. Alloy 4 has both molybdenum and chromium alloying elements. Chromium atoms prevent carbon atoms from diffusing, reducing the thickness of grain boundary ferrite. With increasing chromium content, the number of fractions of high-angle grain boundaries increases [87]. As a result, the overall ferrite fraction increases. However, for alloy 5 the fraction again decreases than alloy 4 as more Cr is added. In the study [88], the influence of Cr on transformation and microstructure was investigated, and it was discovered that Cr significantly inhibits ferrite transformation. However, the ferrite fraction decreased for alloy 5.

4.5.2 Pearlite Fraction

From the Figure 4.5.2 It is seen that the pearlite fraction initially increased with increasing cooling rate and then declined after a particular cooling rate. Alloy 0 has the lowest amount of pearlite fraction. As alloying element was added, the pearlite fraction drastically changed. Besides chromium, titanium, aluminum, nickel, copper, and manganese, molybdenum has been one of the alloying elements that can delay the transformation of ferrite and/or pearlite [89]. The pearlite content increases as the molybdenum content increases.

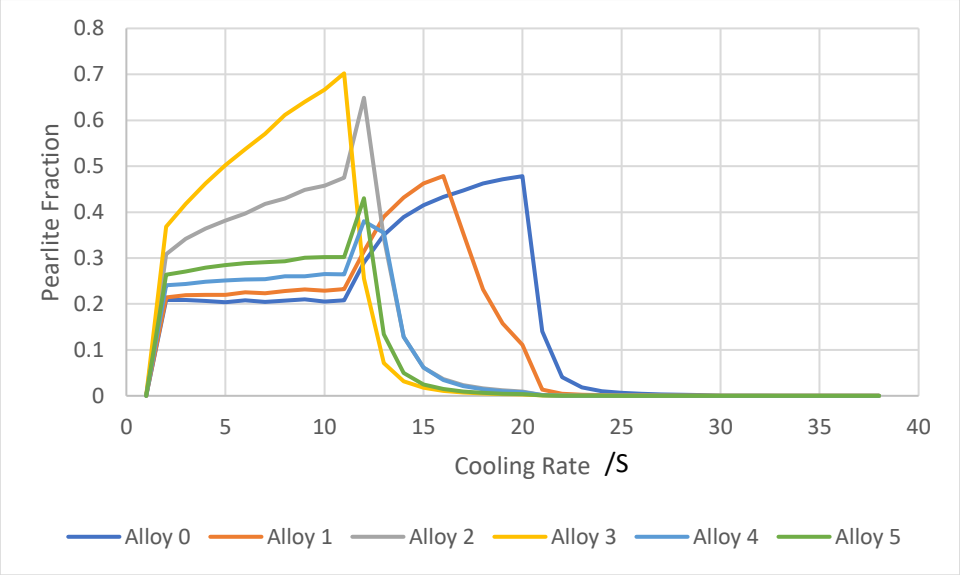

Figure 4.5.2 Pearlite fraction vs cooling rate

Similar to this, in the Figure 4.5.2 it is shown that, with the increasing content of Mo, the pearlite fraction increased for alloy 1,2,3 respectively. For alloy 4, addition of chromium caused progressively reduction in the curve of pearlite fraction. As Cr concentration rises, the values of Ac1 and Ac3 rise as well [90,91]. In addition, the Cr content increased the amount of information on transformation kinetics. As a result, the pearlite fraction is decreased for alloy 4. However, by maintaining proper alloying percentage, the fraction can be increased. The pearlite proportion rose in alloy 5 with a 0.25% increase in Cr over alloy 4.

4.5.3 Bainite Fraction

The Figure 4.5.3 depicts that, alloy 0 has the lowest bainite fraction. As Mo content increased, the bainite fraction increased. When upper bainite forms during cooling, molybdenum has a greater impact on characteristics. For isothermal lower bainite production, the influence of molybdenum on strength and ductility is negligible [92]. The inclusion of Mo boosts the quantity of isothermal bainite transition and speeds up the kinetics of bainite transformation [93]. As shown in the graph, the bainite fraction increased for alloy 1, 2 and 3 respectively as the Mo content is increased. As demonstrated in the Figure, when Cr is added to the alloy 4, the bainite fraction decreases. The addition of Cr may cause the bainitic process to take longer transformation [94]. In this Figure, similar type of behavior of Cr was observed on alloy 4. However, for excess presence of Cr in the alloying element, with the increasing cooling rate, the bainite fraction is seen to be increased.

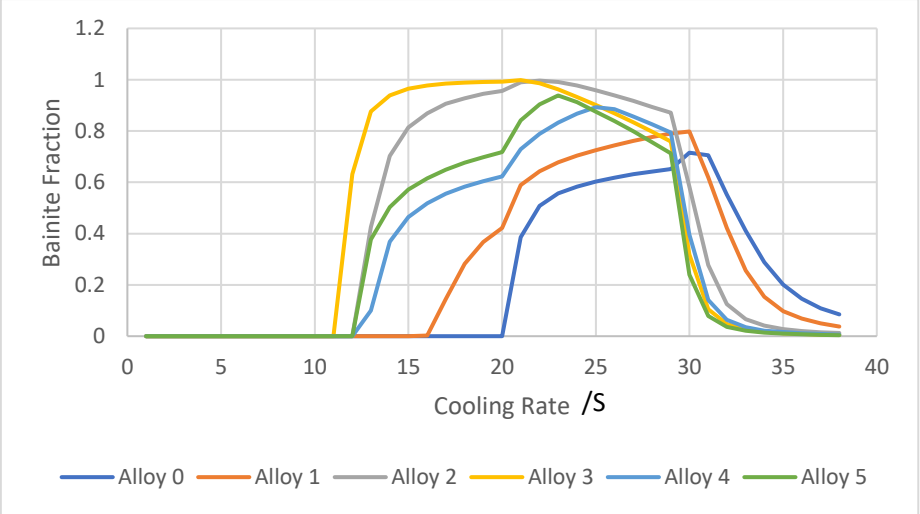

Figure 4.5.3 Bainite fraction vs cooling rate

4.5.4 Austenite Fraction

From the Figure 4.5.4, with the increasing cooling rate, the austenite fraction increased. With the longest initial cooling rate, alloy 0 has the lowest fraction. In general, the molybdenum-containing alloy has far more austenite fractions and is less sensitive to partitioning time than the base alloy [95]. The austenite fraction enhanced with increasing cooling rate as the Mo content of the alloying element increased. Alloy 4 has slightly lower austenitic fraction than alloy 3. Cr is an efficient carbide producing element for refining pearlitic structure. As a result, as the Cr concentration rises, the number of austenite nucleation sites rises, contributing to austenite production and growth [91]. Even though alloy 4 did not follow the traditional course, alloy 5 did.

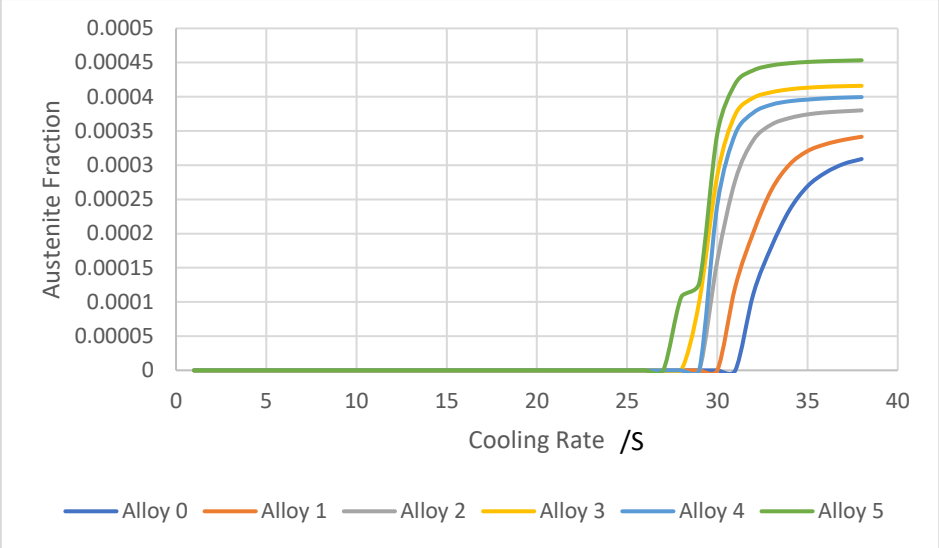

Figure 4.5.4 Austenite fraction vs cooling rate

4.5.5 Martensite Fraction

Figure 4.5.5 depicts that for a certain period of time, the martensite fraction remained constant with the increasing cooling rate. After a certain period, with the increasing cooling rate, the martensite fraction increased. Figure 4.1.4, which depicted austenitic fraction curves, is strikingly similar to this one. Alloy 0 has the lowest martensitic fraction. The addition of Mo allows for the development of low-temperature transition products such bainite and martensite [96]. For the increasing Mo content, the martensite fraction is seen to be increased. Cr is important in contemporary heat treatment procedures, which rely mostly on the martensitic transition [97]. As the Cr content is added as the alloying element in alloy 4 and 5, the martensitic fraction increased with the cooling rate

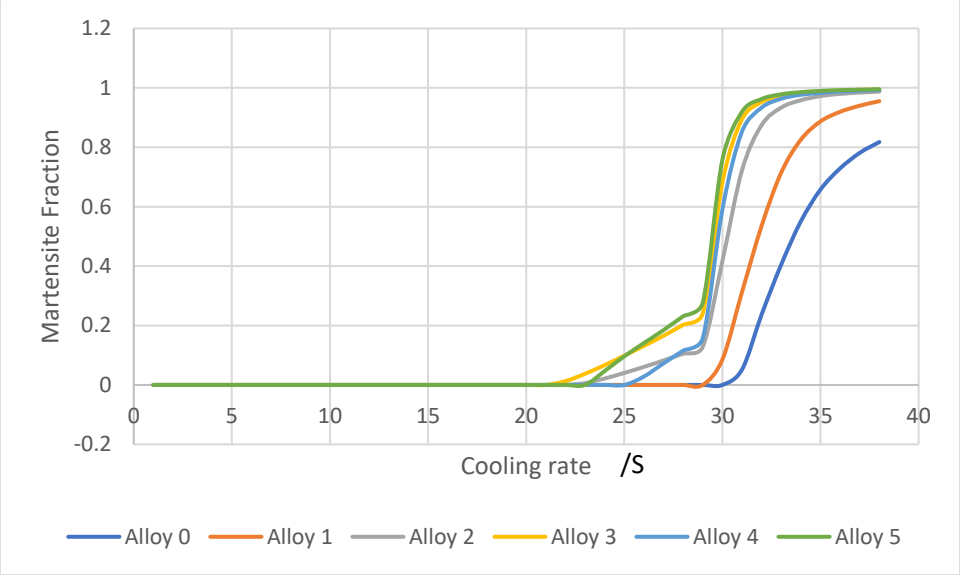

Figure 4.5.5 Austenite fraction vs cooling rate

4.6 Equilibrium Phase formation on Temperature Dependence

TTT diagram is an abbreviation for "time-temperature-transformation diagram." It's also known as an isothermal transformation diagram. TTT graphs show the kinetics of isothermal conversions. Isothermal transformation diagrams (also known as time-temperature-transformation (TTT) diagrams) are temperature vs. time charts (usually on a logarithmic scale).

4.6.1 Bainite formation

Figure 4.6.1 shows a complex curve of bainite formation (1%) with the increase in the temperature. In a study [98] it is stated that the isothermal bainitic transformation kinetics in lean medium-Mn steels are highly influenced by temperature. Due to the enhanced driving power of the transformation at 350 °C, a greater amount of bainite is generated during the isothermal step. In this Figure a scenario is found where with the increasing temperature the bainite formation is decreased. Alloy containing Mo has a higher bainite formation than the base alloy.

The addition of Mo boosts the strength of low-carbon bainitic steel by producing more and finer bainite plates. Also as stated earlier that by adding Mo to a low-carbon steel increases its tensile qualities by delaying the creation of high-temperature products during the continuous cooling process.

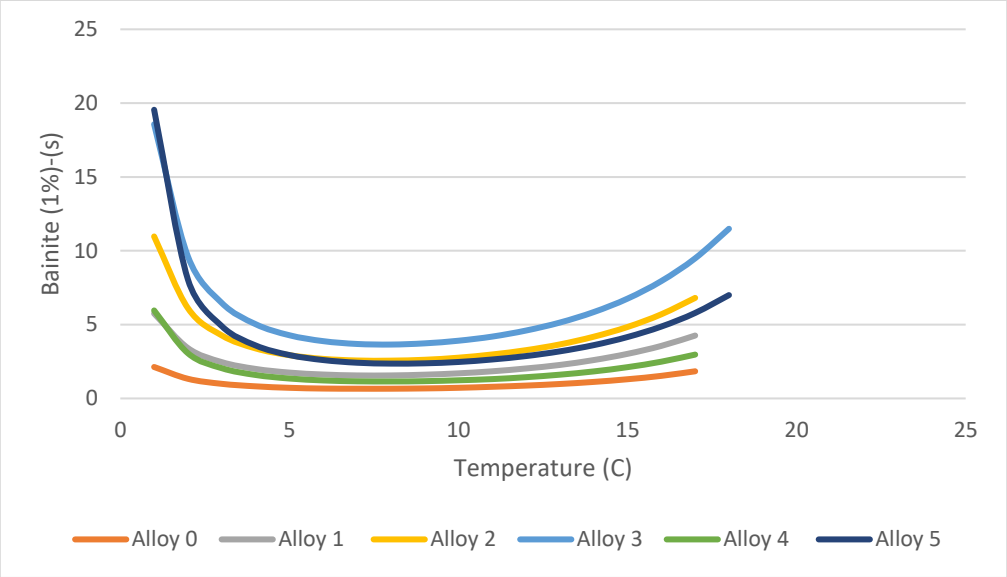

Figure 4.6.1 Bainite formation (1%) vs Temperature

After adding chromium, the bainite is seen to be lesser than the previous alloys. Cr is usually used to enhance hardenability and, as a result, to encourage the production of bainite by inhibiting the creation of high-temperature transition products [99-105].

4.6.2 Ferrite formation

Figure 4.6.2 shows a complicated graph of ferrite formation as a function of temperature. Alloy 5 is seen to have the highest amount of formed ferrite while alloy 0 is negligible. For alloy 1,2 and 3 the formation percentage increased as the alloying element is added. With an increase in Mo content, the amount of ferrite steadily increases. In case of chromium, in the study [106] it is investigated that increased Cr content of up to 0.6 percent speeds up ferrite recrystallization, which, combined with the presence of Cr-rich carbides, facilitates austenitization primarily through the nucleation process, resulting in finer austenite grains.

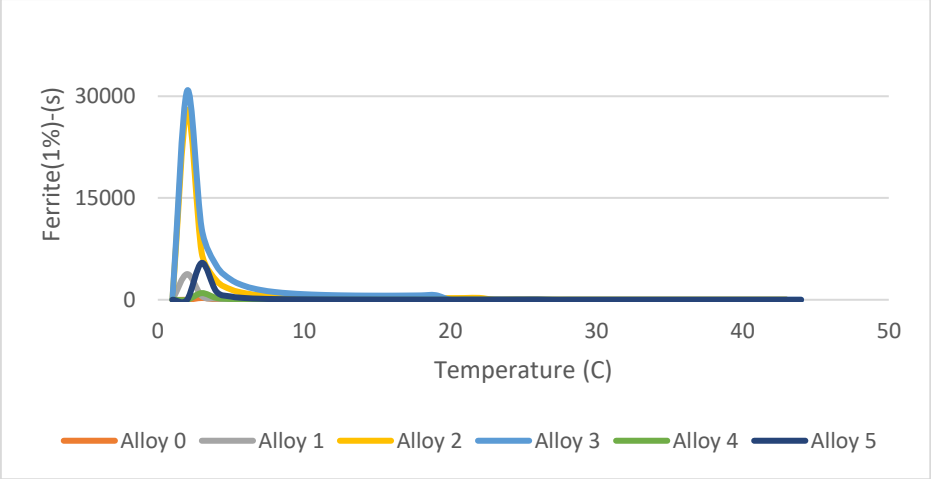

Figure 4.6.2 Ferrite formation (1%) vs Temperature

4.6.3 Pearlite formation

A sophisticated graph of perlite formation as a function of temperature is shown in Figure 4.6.3. The formation of pearlite is shown to rise with rising temperature at a specific temperature. After passing that degree, the formation decreases as the temperature rises. By adding alloying element Mo, the pearlite formation is seen to be negligible for a long temperature range of about 610 to 650ºC. After passing around 690ºC the curve is seen to be suppressing. However, by adding Cr a significant increase in the pearlite formation within a certain temperature range. After that at higher temperature the pearlite formation is decreased.

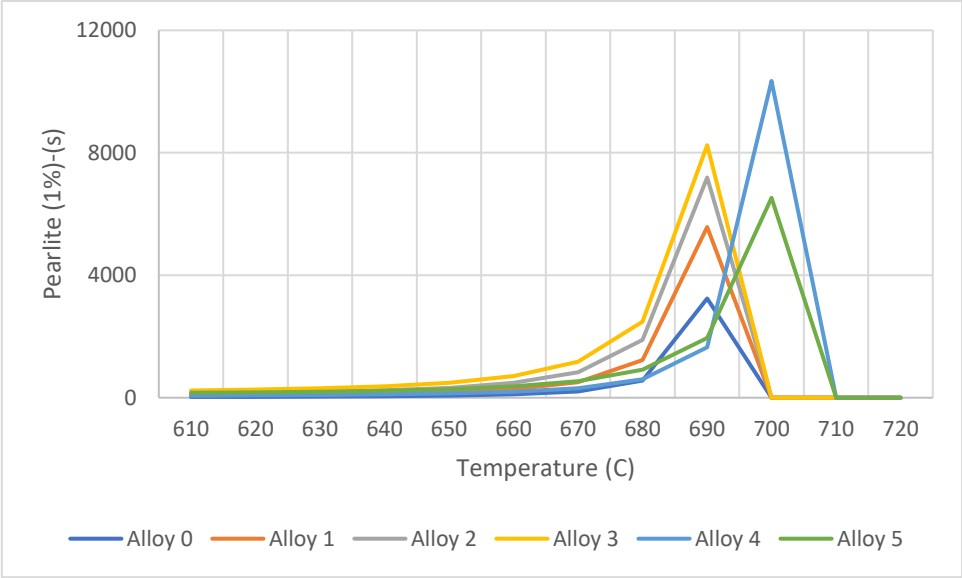

Figure 4.6.3 Perlite formation (1%) vs Temperature

4.7 Non-equilibrium Phases – Precipitation Amount

Precipitation may form in a number of ways, depending on the temperature and rate of cooling. The amount of precipitation is strongly influenced by the alloying elements added to the base metals or alloys.

4.7.1 Precipitation Amount for MC:

Figure 4.7.1 shows that all of the alloys have had the same pattern after a certain amount of time. After a particular period of time, the amount of carbide precipitation remains constant. In comparison to alloy 0, alloy 1 takes longer to precipitate carbide. Because Nb, Mo, and W create strong carbides, the chemical composition of precipitates changes. Type MC can be referred to Noibium carbides (Nb) which precipitates in massive forms that were not dissolved during the austenitization process. For the selected austenitization condition, however, the niobium addition had no effect on secondary precipitation [107]. As addition of molybdenum has influence on the dissolving during austenitization, it takes more time to precipitate for alloy 1. In the instance of alloy 2, 0.25 % more Mo is added, causing precipitation to take longer. As discussed earlier because of molybdenum affecting recrystallization activity, the alloying is effective in causing austenite formation to be delayed which can be seen in case of alloy 2. The precipitation amount curves for alloys 3 and 4 are identical.

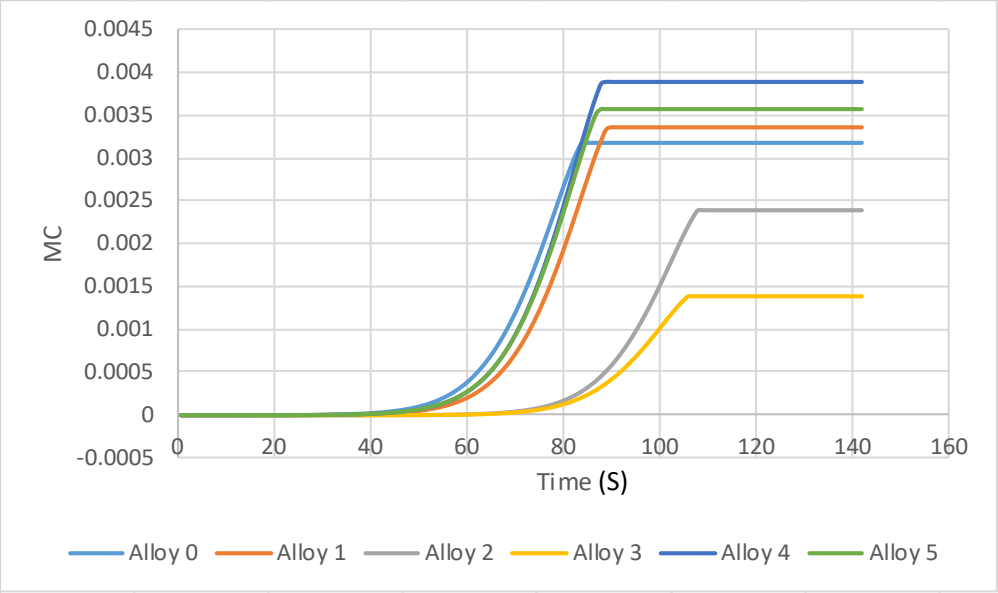

Figure 4.7.1 Precipitation amount of MC with time

After the recrystallization was done for adding certain amount of molybdenum, further adding 0.25% Mo caused alloy 3 to precipitate more quickly. When 0.50 percent of Mo was removed and 0.25 percent of Cr was added to alloy 4, the curve did not alter when compared to alloy 3. Secondary and also eutectic carbides characteristics are heavily influenced by the primary elements' composition (C, Cr). Secondary carbides that precipitate in matrix regions improve matrix strength by improving dispersion and refining microstructure [108]. This influences of chromium affects the precipitating amount of carbides. When 0.25 % extra chromium was added to the elemental composition, it required almost the same amount of time as alloys 3 and 4, but precipitated far less carbide.

Maximum amount of precipitation forms in case of Alloy 4. But adding more amount of Cr and Al, Ti causes to reduce the precipitation amount. Thus maximum amount of MC forms in case of alloy 4. It can be predicted that addition of Mo and Cr are responsible to increase MC but Cr>0.25 results to decrease the amount. But when L and Ti is added then the amount of MC again increases but the alloy 4 shows maximum precipitation amount.

4.7.2 Precipitation Amount for M_2C:

Figure 4.7.2 shows the changes in the carbide precipitation (M_2C) curve for several alloys. The precipitation amount for alloy 0 upholds no resemblance to that of other alloys. The addition of molybdenum and chromium causes significant changes in the curves. Micro-alloy additives such as Nb, Ti, Mo, and V refine grain size, inhibit recrystallization, and produce fine carbide or carbo-nitride precipitates, all of which increase mechanical characteristics [109]. However, such additions have an effect on the austenite to ferrite transition rates, and thus on interphase precipitation. The additions of Ti, V, and Nb speed up the transformation kinetics, whereas Cr, Mo, and W have the reverse effect and slow it down [110]. From the Figure, Mo has a great impact on the M_2C precipitation amount with time. Alloy 1, with the least amount of Mo, undergoes an average amount of precipitation of M_2C. As the amount of Mo in alloy 2 increases, the precipitation increases, but not as much as like alloy 3 with the highest Mo.

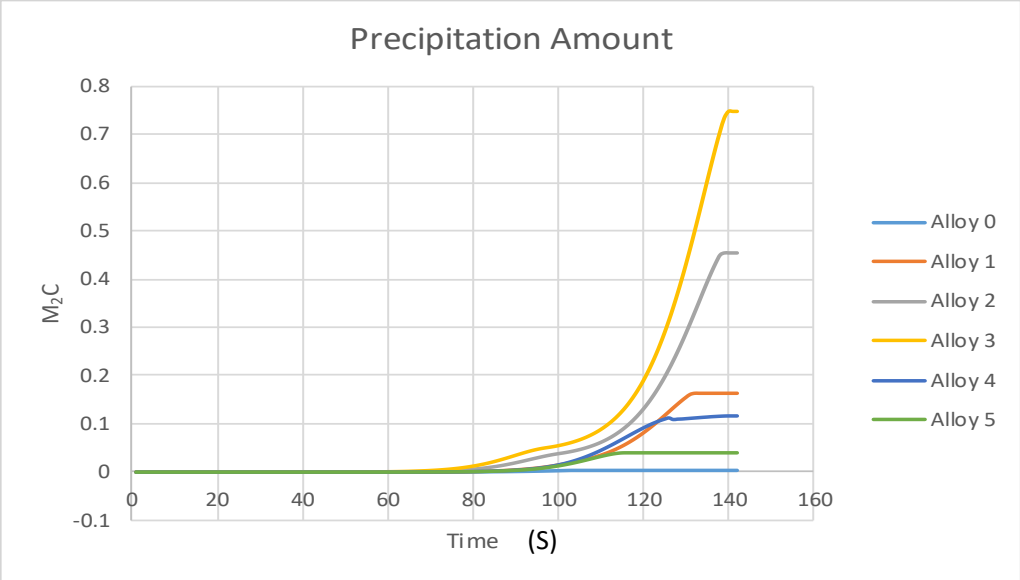

Figure 4.7.2 Precipitation amount of M_2C with time

However, chromium also has an impact on this graphical changes for alloy 4 and 5. As the amount of chromium in the alloy increases, the precipitation reduces. In comparison to alloy 3, in case of alloy 4 about 0.50% of Mo is reduced and 0.25 % chromium is added. As previously stated, the recrystallization behavior of Mo also could be a factor in this. When it comes to alloy 5, it's evident that as the chromium content rises, precipitation decreases compared to the prior alloy. So Mo appears to be less dissolved than chromium because of its fine carbide formation characteristic. However, M_2C, on the other hand, has more amount of precipitation than MC. The explanation for greater M_2C precipitation than MC can be deduced

from the study [111-113], where it is shown that depending on the Cr/C ratio, Mo additions to High Chromium Cast Irons result in the creation of M_2C or M_6C type carbides.

From the Figure 4.3.2, it can be predicted that, addition of Mo rapidly increase the M_2C. As Mo has better affinity for C. On the other hand further addition of Cr, Al, Ti retards to form M_2C.

4.7.3 Precipitation Amount for M_3C:

Figure 4.7.3 depicts that with the increasing time, the amount of M_3C precipitation is decreased. The base alloy precipitation remains constant over time. By adding molybdenum, the precipitation amount is decreased progressively for alloy 1,2 and 3. Tempering time and temperature affect the quantity of each carbide precipitated, resulting in a reduction in carbide volume fraction and coarsening of boundary carbides [114]. In this Figure, Mo has reverse impact on the precipitation amount of M_3C. The curve has drastically lowered as Cr is added to the alloys. Alloy 5 has the lowest amount of M_3C precipitation.

Likewise, the case of MC formation, M_3C shows the same mechanism. Here like the MC, Alloy 4 forms maximum amount of M_3C.

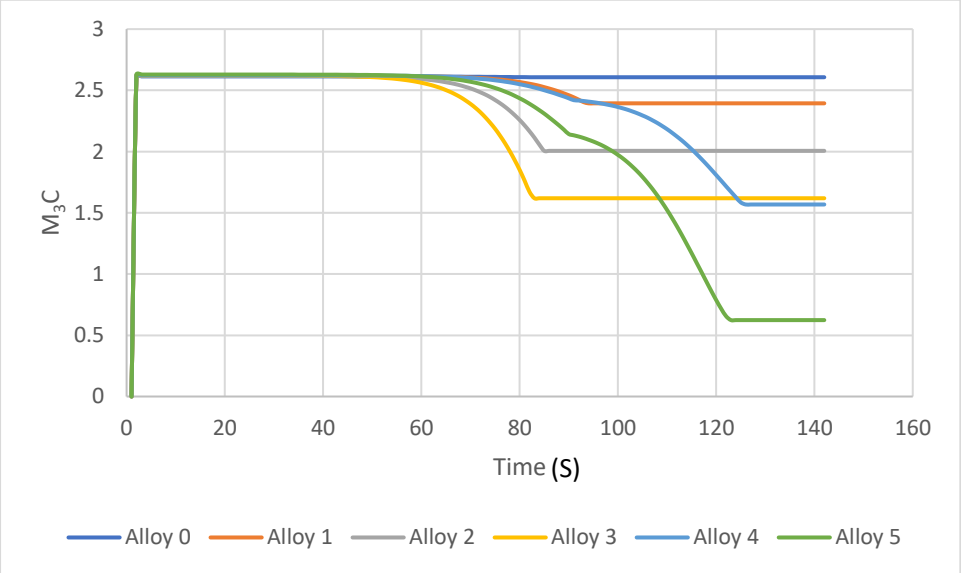

Figure 4.7.3 Precipitation amount of M_3C with time

4.7.4 Precipitation Amount for M_7C_3:

Figure 4.7.4 shows that, like the precipitations of MC and M_2C discussed previously, the amount of precipitation for M_7C_3 varies with Mo and Cr. As the Mo content increases the

precipitation amount of M_7C_3 increases. This behavior is observed previously in a study [115] where it is clear that the concentration of Mo and W in the carbide grew as the cast iron's Mo or W content increased, whereas the concentration of Fe reduced. The XRD data of that study also revealed that as the Mo or W content was raised, the lattice constant of M_7C_3 carbide changed, and the volume of a unit cell did grow. In the Figure 11, alloy 3 with the highest number of Mo, has the highest amount of M_7C_3 precipitation with time. The addition of molybdenum alters the crystal structure and atomic radii, which contributes to the amount of the precipitation [115]. Despite the fact that alloys 1 and 4 have the same quantity of Mo, alloy 4 has the least amount of precipitation since it contains 0.25 % chromium. However, when the Cr content of alloy 5 is raised by 0.25%, the precipitation amount curve rises somewhat. Both alloys 4 and 5 have a curve that shows a consistent precipitation amount after a particular amount of time. This consistent value is thought to be induced by the addition of chromium. The most popular notion is that M_7C_3 precipitation is mostly influenced by Cr atom concentration [116,117]. Because Cr enriches cementite to around 20% [118], only a limited quantity of Cr is present in solid solution in the martensite of low Cr steels [116], resulting in in-situ cementite precipitation. However, the Cr content of cementite increases with tempering time, which could explain the M_7C_3 formation delay [119]. Moreover, when compared to the precipitating amounts of MC and M_2C in Figures 4.7.1 and 4.7.2, M_7C_3 is significantly higher.

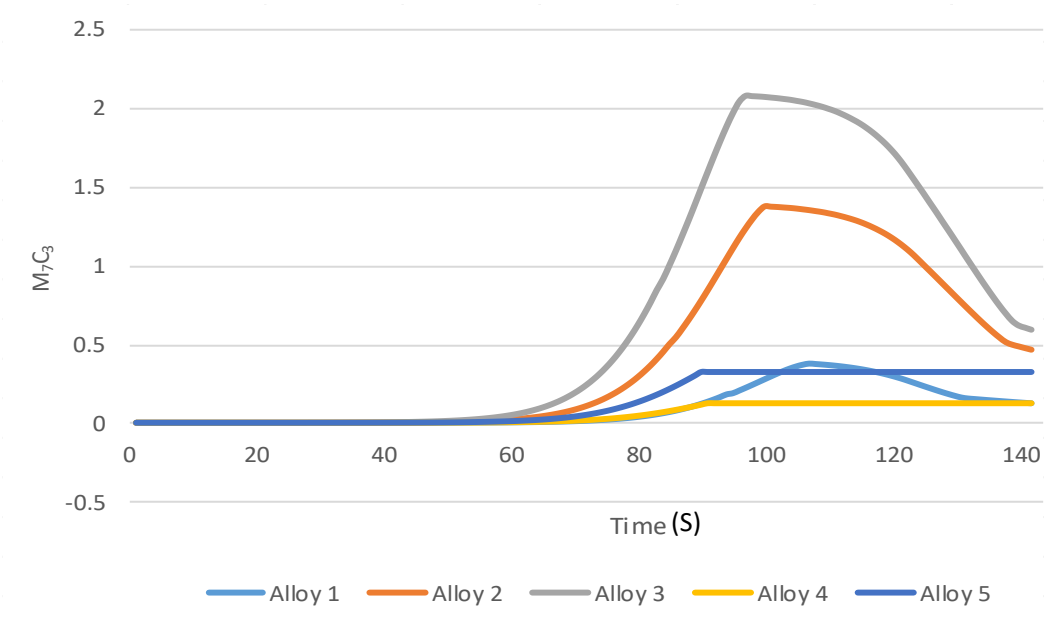

Figure 4.7.4 Precipitation amount of M_7C_3 with time

From Figure 4.7.4, it can be predicted that, Alloy 3 forms maximum M_7C_3. Thus further addition of Cr, Al, Ti retard the formation of M_7C_3. Addition of Mo influences to form the carbide whereas Cr, Al, Ti retards the formation of M_7C_3.

4.7.5 Precipitation Amount for $M_{23}C_6$:

Figure 4.7.5 depicts $M_{23}C_6$ precipitation, which illustrates that as the rate of chromium increases, so does the amount of precipitation. It is interesting to note that from figures (4.7.2-4.7.4), alloy 3 has the largest precipitation amount, but it has the lowest here, or in other words, the precipitation amount tends to zero. The curve of alloy 3 is also identical to alloy 2 as well. Alloy 5, having the highest amount of Cr concentration, has the highest precipitation amount. The study [120] has suggested that secondary carbides (M_7C_3) originate from austenite and are difficult to transition into $M_{23}C_6$carbides as the temperature drops in the air. Primary carbides were resistant to heat treatment and thermal deformation once they were created, whereas secondary carbides were. Form the study [121], it is also observed that the grain boundary character and interfacial energy were found to have a significant impact on the $M_{23}C_6$ carbide behavior.

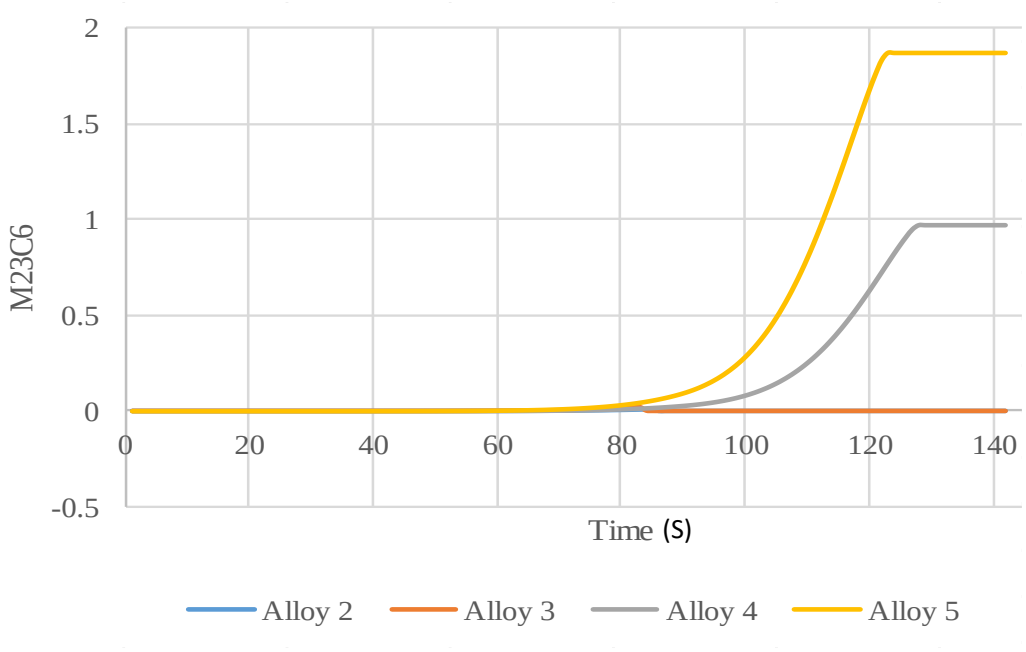

Figure 4.7.5 Precipitation amount of $M_{23}C_6$ with time

However, though there has been extensive research on interphase precipitation enhanced steels, there is still much that is unknown in the interphase precipitation process, such as the role of a variety of elements, especially Mo. The addition of Mo to the austenite to ferrite transformation

kinetics was shown to be greatly reduced, especially for the V steel [122]. As the elemental composition changes, the behavior of distinct carbide precipitations can be observed in various alloys.

Alloy 5 forms maximum amount of $M_{23}C_6$. Thus it can be predicted that addition of Mo, Cr helps to form more $M_{23}C_6$.

4.7.6 Precipitation Amount for M_6C:

The precipitation of M_6C is increased for a period of time in Figure 4.7.6, and then it decreases after reaching a specific point. As Mo is added, the precipitation of M6C increased. Alloy 3 has the most precipitation as it contains the most Mo. It is shown in the study [123] that long-term aging resulted in the formation of M_6C type carbide with a high Mo content. In case of alloy 4 and 5, the reduction of the precipitation amount of M_6C is observed. So the influence of Cr is clearly seen in both of alloy 4 & 5.

As the Cr content increased, the precipitation amount decreased compared to other alloys. In a study [124], it is investigated that in low chromium steels, only M6C precipitates, but in high chromium steels, numerous carbides precipitate and a considerable quantity of molybdenum stays in solution in the matrix. It is also stated that M_6C develops a primary precipitate in steels with less than 8% Cr over prolonged periods of time. So, it is obtained that steel with less Cr content has higher precipitation amount. In Figure 4.7.6, the curve also showed relevant result with this outcome.

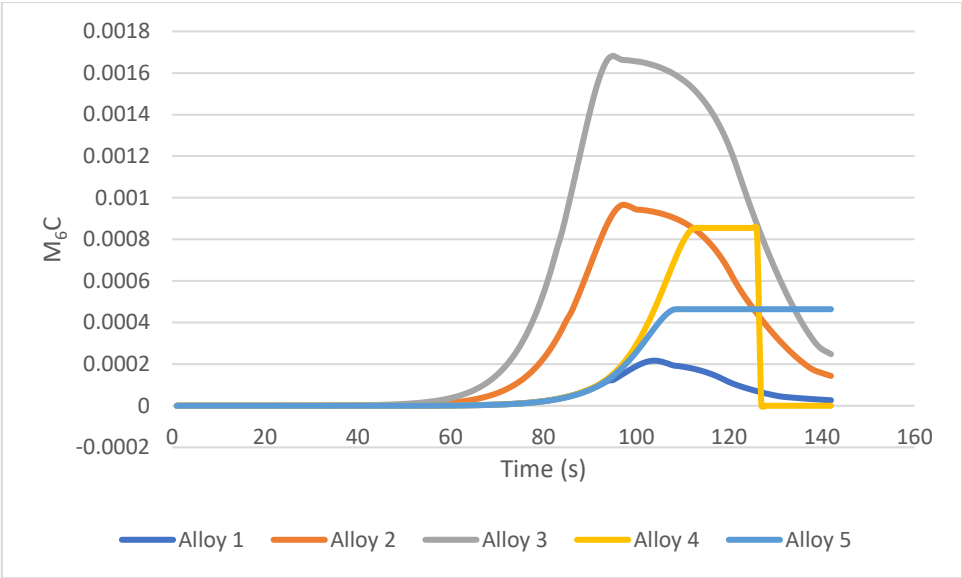

Figure 4.7.6 Precipitation amount of M_6C with time

4.7.7 Precipitation Amount for M(C,N):

Alloy 4 shows the maximum amount of carbon and nitrogen solubility. On the other hand Alloy 5 also has closely similar types of solubility.

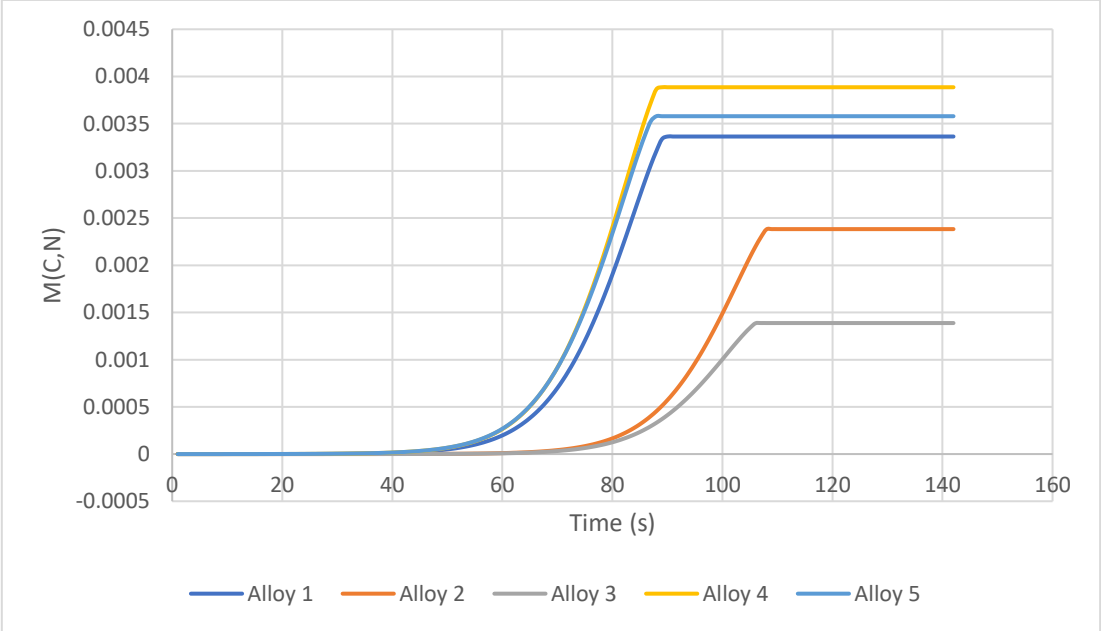

Figure 4.7.7 Precipitation amount of M(C,N) with time

Table 4.7.1 shows that, the alloying elements that Mo and Cr minimize the carbide size. And the lowest size of the carbide is present mainly in Alloy 3 and Alloy 4.

Table 4.7.1 Summary of the effect of alloying element on Precipitation amount

Precipitation (Carbide)	Presence Maximum in Alloy	Element Responsible to form particular carbide	Element Responsible to retard particular carbide
MC	4	Mo, Cr<0.25	Al, Ti, Cr>0.5
M_2C	3	Mo	Al, Ti, Cr
M_3C	4	Mo, Cr<0.25	Al, Ti, Cr>0.25
M_7C_6	3	Mo	Al. Ti, Cr
$M_{23}C_6$	5	Mo and Cr	Al, Ti
M_6C	3	Mo	Al, Ti, Cr

4.8 Non-equilibrium phases- Precipitation Size

Depending on the temperature and rate of cooling, precipitation can develop in a variety of ways. The alloying elements added to the base metals or alloys have a significant impact on the magnitude of precipitation.

4.8.1 Precipitation Size for MC:

The changes in MC precipitation size for different alloys may be seen in the Figure 4.8.1. It was also observed that the size of precipitation stayed constant after a certain time period. The initial addition of molybdenum in alloy 1 caused a minor change in the curve with respect to alloy 0. From the study [125] a similar behavior was evaluated that with increasing particle size and isothermal holding time, the concentration of Mo in the precipitates decreases. Additionally, it is stated that after a lengthy period of isothermal holding in the austenite zone, these precipitates can become quite coarse, losing their advantage in microstructure refinement and precipitation strengthening. In this Figure, it was noticed that with the increasing amount of molybdenum, the precipitation size decreases. In general, the particle size in Mo-containing steel is lower than in Mo-free steel [125]. In a study [126], it is found that the addition of 0.2 wt% Mo to a Ti micro-alloyed steel increases the nucleation of MC precipitates and delays coarsening in the austenite matrix. However, it can be indicated from the Figure that it took

longer for alloys 3 and 4 to reach a stable precipitation size value. When compared to other alloys, alloy 4 has the largest size of precipitation because the amount of molybdenum has been reduced and chromium has been added.

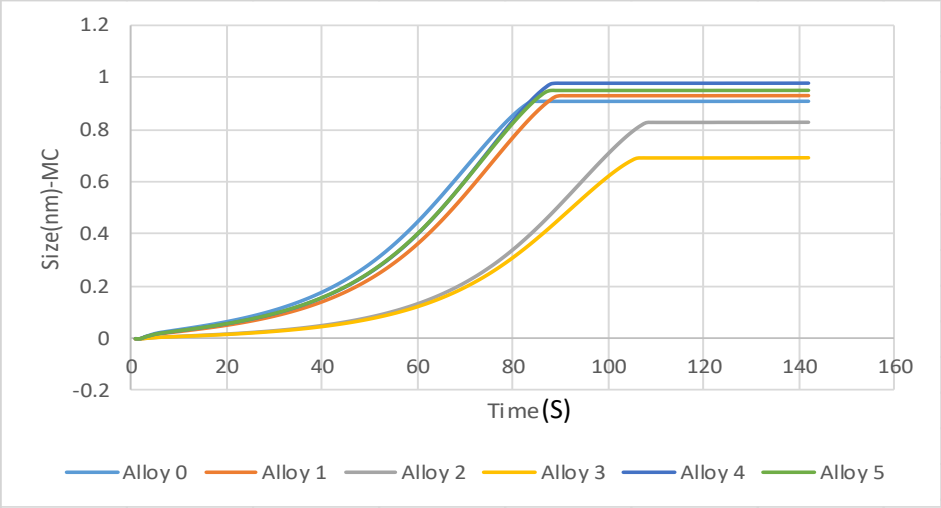

Figure 4.8.1 Precipitation size of MC with time

As a result, molybdenum can be stated to play a role in reducing the size of MC precipitation. When more chromium was added to alloy 5, however, the size of the precipitation was reduced marginally when compared to alloy 4. Chromium is a powerful carbide former, forming a complex succession of carbide structures in the presence of carbon and iron [127]. So from the Figure it is evident that alloys containing the alloying element chromium have larger precipitation sizes than others.

4.8.2 Precipitation Size for M_2C:

Figure 4.8.2 depicts various changes in alloy curves as alloying elements are changed. With the increasing amount of molybdenum, the precipitation size gets larger. Among all the alloys, Alloy 3 with the highest amount of molybdenum has the largest precipitation size. So with respect to MC precipitation, the effect of molybdenum is reverse here in M_2C precipitation. Mo has a tendency for forming Mo_2C or M_2C type carbides with a high hardness [128, 129]. This is why, in Figure 4.8.2, the amount of M_2C precipitation was substantially higher than the amount of other carbide precipitations. It has been indicated that [130] as the M_2C carbides in the 0.03Nb-0.6Mo steel are relatively large, exceeding 20nm in size, and scattered at grain boundaries, they do not appear to produce precipitation hardening. The molybdenum content

is lowered to 0.50 % and 0.25 % chromium is added in alloy 4, resulting in a smaller precipitation size than alloys 1-3 with higher molybdenum level.

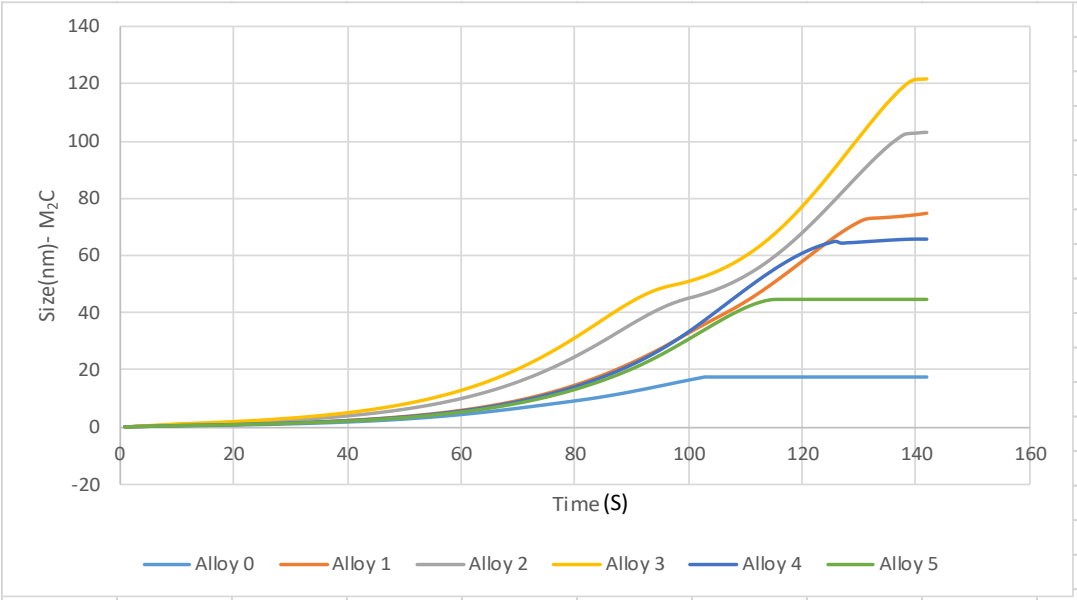

Figure 4.8.2 Precipitation size of M_2C with time

When alloying elements such as Si, Cr and W are present in steels, coarsening of cementite in the tempering temperature range 400-700°C, which represents the fourth stage of tempering, can be successfully prevented [131]. However, with the increasing content of chromium, the precipitation size gets smaller. In alloy 5, the precipitation size is the lowest despite of having 0.25% of molybdenum.

4.8.3 Precipitation Size for M_7C_3:

Figure 4.8.3 shows that molybdenum-containing alloys have greater precipitation sizes. Carbides with complex crystal structures and low formation heats, such as M_7C_3, M_6C, and $M_{23}C_6$, tend to produce coarse suspensions [132]. Here in the Figure, Mo content rises, the curve rises as well, with alloy 3 having the largest precipitation size of all. The study [129] indicates that Mo is distributed into both the austenitic matrix and M_7C_3 eutectic carbides at lower Mo levels, improving the alloy hardness by dissolving in the austenite and also by increasing the secondary precipitation of Mo. Mo dissolved in M_7C_3 carbides, on the other hand, improves the hardness of the carbides themselves. However, Mo has a great impact in the precipitation size of secondary carbide as discussed earlier. In M_7C_3 precipitation molybdenum caused larger sized precipitation. In the study [131], it is stated that continuous

softening in a 2 wt% Cr-0.2 wt% C steel will generally occur on tempering between 500°C and 700°C, while addition of other alloying elements, such as Mo, will minimize the rates of coarsening of Cr_7C_3 steel.

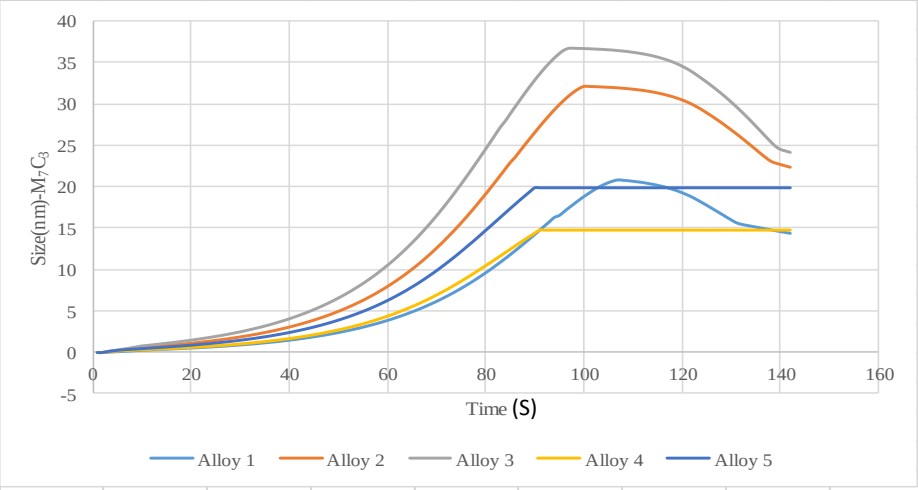

Figure 4.8.3 Precipitation size of M_7C_3 with time

However, when considering having chromium in the alloy, it is obvious that alloy having chromium content has smaller precipitation size. Furthermore, [133] reported that secondary carbides of the M_7C_3 type will form more easily in HCCI alloys with reduced Cr content. The study also has shown that the size of secondary M_7C_3 carbides rises with increasing temperature and time, according to the size distribution of secondary carbides. Moreover, alloy with Cr content have a constant precipitation size after certain time.

4.8.4 Precipitation Size for $M_{23}C_6$:

Figure 4.8.4 illustrates the curves for precipitation size of $M_{23}C_6$ which shows a complex orientation. In the Figure, some peaks are predicted in some positions of the continuous functional curve. $M_{23}C_6$ is the primary precipitate in several austenitic stainless steel grades [134]. Some alloying elements have a significant impact on $M_{23}C_6$ carbide precipitation and molybdenum and chromium are one of those. However, alloy 2 and 3 with the molybdenum content has a marginal difference in the curve. Both alloys show that after a certain time period there was no precipitation found. As demonstrated and discussed in Figure 4.8.4, the precipitation amount of $M_{23}C_6$ for molybdenum is very low or tends to zero. Meanwhile in case of chromium the precipitation size is very large as can be seen for alloy 4 and 5.

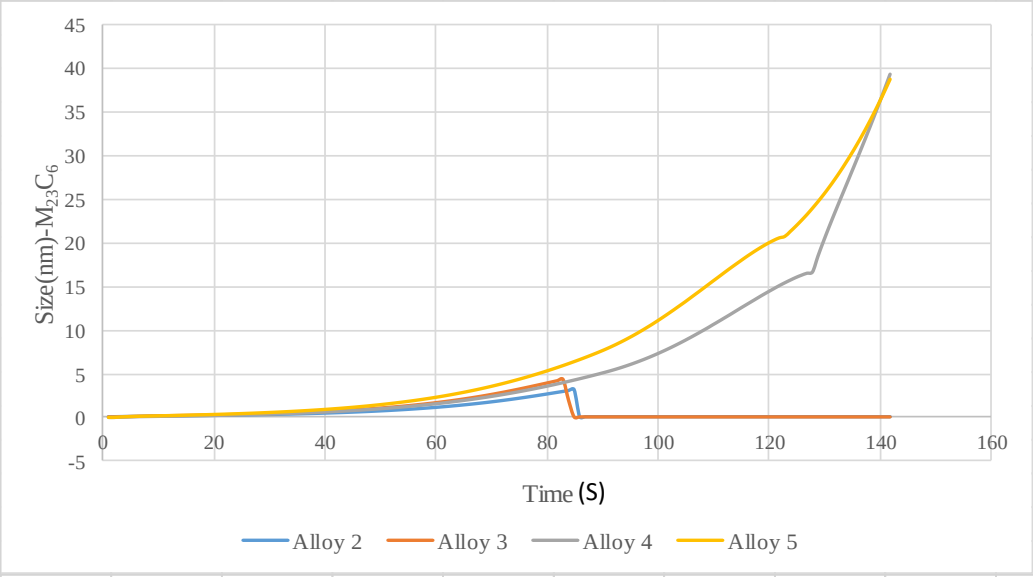

Figure 4.8.4 Precipitation size of $M_{23}C_6$ with time

The study [133] suggested that secondary carbides of the $M_{23}C_6$ type will occur more frequently in HCCI alloys with more Cr. From another study it is indicated that the inclusion of Cr increases the strength of the steel during tempering, and the addition of Mo produces a strong secondary hardening peak. Because alloys 4 and 5 contain modest amounts of molybdenum, the effect is visible as a peak in the curve [135]. However, secondary hardening peaks do not form in tempering curves for steels containing up to 9% Cr [131].

4.8.5 Precipitation Size for M_6C:

For certain time period Alloy 3 shows maximum precipitation size. The precipitation of M_6C results in the deformation of the common structural steels at the elevated temperature. When catastrophic fire happens on the steel then different precipitates forms on the sample. With the addition of various alloying element it is targeted to lessen the precipitated amount. Thus for Alloy 5, it is seen that it depicts least precipitation size. A comparable process has been studied in [136] carbon alloy, in which M_6C precipitates on a much coarser scale, allowing detailed measurements on the transformation from solid to liquid.

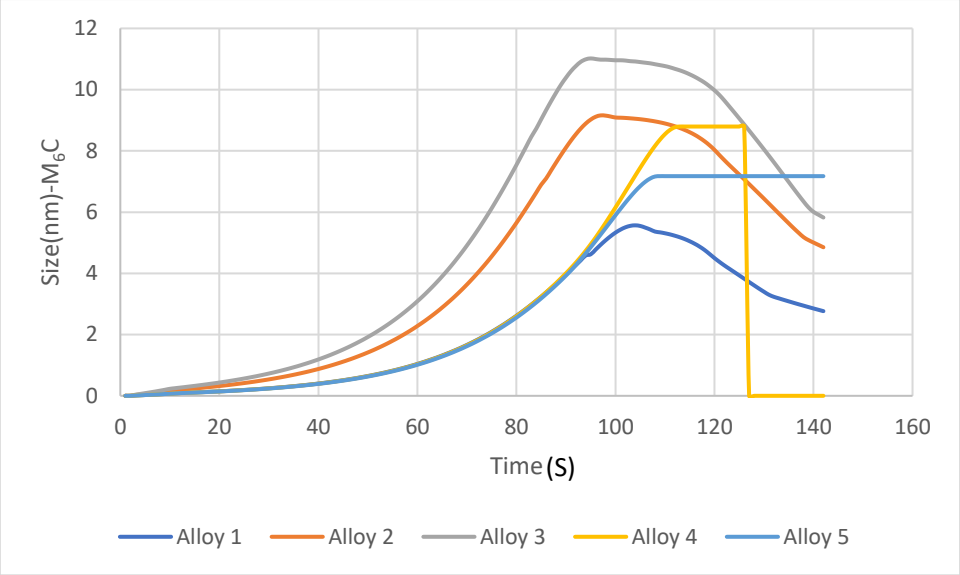

Figure 4.8.5 Precipitation size of M_6C with time

Table 4.8.1 shows the summary of the contribution of the alloying elements and the particular alloys responsible to form particular carbides.

Table 4.8.1 Summary of the effect of alloying element on precipitation size

Carbide	Lowest Size in Alloy	Element responsible to reduce precipitation size
MC	3	Mo
M_2C	4	Mo and Cr<0.25
M_7C_3	4	Mo and Cr<0.25
$M_{23}C_6$	3	Mo
M_6C	4	Mo and Cr<0.25

4.9 Transformation Temperature

Transformation temperature refers to the temperature at which a substance transforms between phases. This transformation occurs over a broad temperature range (known as the transformation range) rather than at a single temperature in alloys such as steel. The minimum and maximum transformation temperatures indicate the upper and lower boundaries of the transformation range [137].

4.9.1 Upper transformation temperature:

During heating or cooling, the temperature at which a reaction or transformation completes or begins is refer as Upper Transition Temperature. The Upper Transition Temperature is represented by the A_3 and A_{cm} lines on the iron-carbon phase diagram. While heating, it indicates the transition about which austenite and ferrite, or austenite and cementite, consummate their conversion to pure austenite. After cooling, this temperature indicates when pure austenite begins to transform into a mixture of austenite and ferrite or austenite and cementite [138].

4.9.2 Lower transformation temperature:

During heating or cooling, the temperature at which a reaction or change takes place or ends. The lower transition temperature is defined as the temperature at wherein ferrite, cementite, pearlite, or a combination of these minerals begins to change into austenite when heated. When austenite, or a combination of austenite and ferrite or cementite, starts to cool to this temperature, it completely changes into ferrite, cementite, or pearlite.

4.10 Formation temperature and time:

The formation of ferrite, perlite, bainite, austenite and cementite varies with the temperature and time. The temperature and time of formation alter as the alloying characteristics change.

4.10.1 A1 & A3 Temperature:

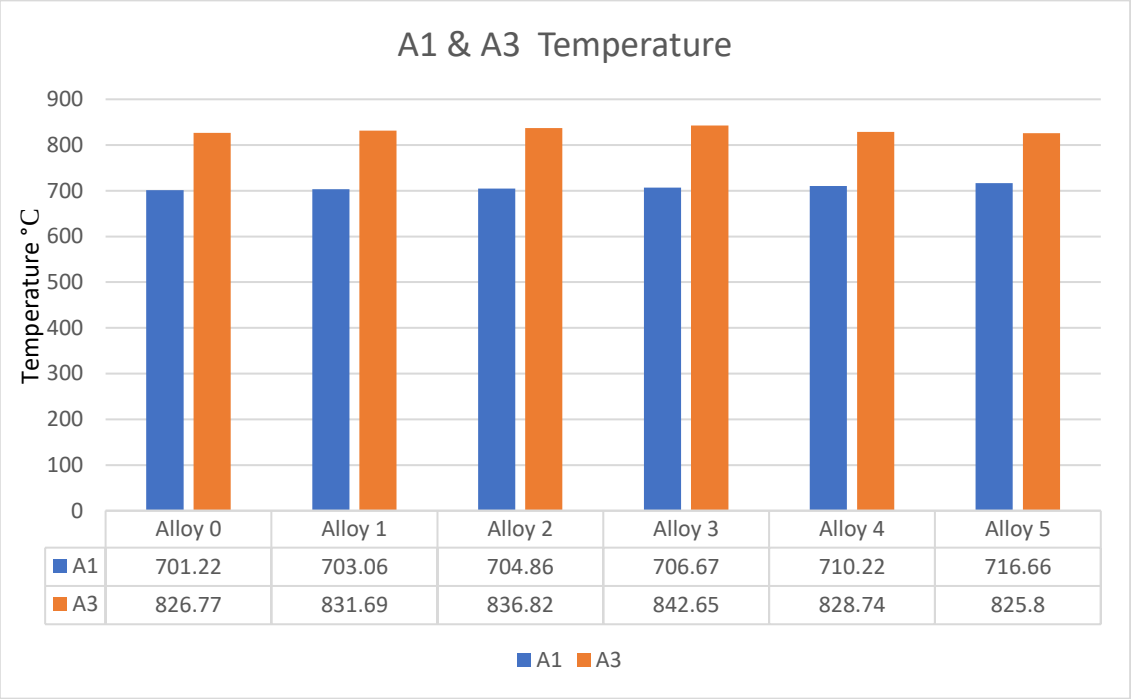

Figure 4.10.1 Difference between A1 & A3 temperature

A_1 and A_3 are the transformation temperature. Following this, the temperature phases change. It is predicted that with the addition of Mo, both the transformation temperature and the transformation time will rise. Alloys will be stable up to a particular temperature when the transformation temperature rises. Much research is being conducted in order to make the alloys stable at greater temperatures. As can be seen, the Mo addition has little effect on the shift of transition temperature to somewhat higher temperature. Figure 4.10.1 indicates that the A_1 and A_3 temperatures are roughly comparable in each alloy composition. With the addition of molybdenum, the temperature is seen to rise slightly. However, of all alloys, alloy 3 has the maximum A1 and A3 temperatures.

4.10.2 Transformation Temperature Crossing Time (A_1 line)

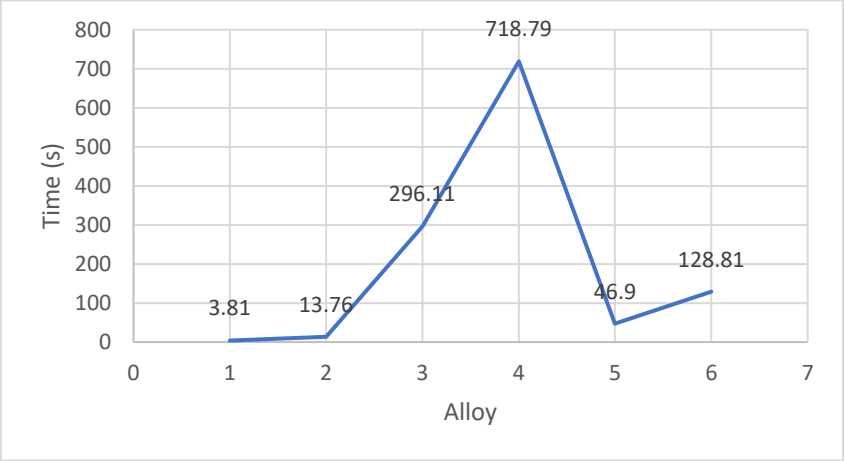

Figure 4.10.2 Time of crossing A_1 line

For Alloy 0, the time necessary to cross the A_1 line is the shortest. The time required to overcome the A1 line increases as the amount of Mo increases. Alloy 4 with 0.25 % Mo and 0.25 % Cr seems to have the highest required time to cross the A_1 line. The required time is drastically reduced to 46.9s from 718.79s just after excessive amount of Chromium was added. The necessary time lengthens as more alloying elements, such as Ti and Al, are introduced.

4.10.3 Initial Formation Temperature for Pearlite and Ferrite:

Mo has an impact on ferrite formation [139]. The amount of ferrite gets higher as the Mo content rises. As a consequence, the initial formation temperature should be lower as the amount of Mo grows. In comparison to alloy 0, alloy 1 and alloy 3 have a lower formation temperature. Nevertheless, the initial ferrite formation temperature for alloy 2 steadily rises, which differs from alloys 1 and 3. These statistics is somehow looks anomaly from the traditional patterns. As a result, with the addition of Mo, the stability of ferrite is expected to be lower than that of the base alloys. Thus adding alloying elements the initial formation temperature of each phases reduces.

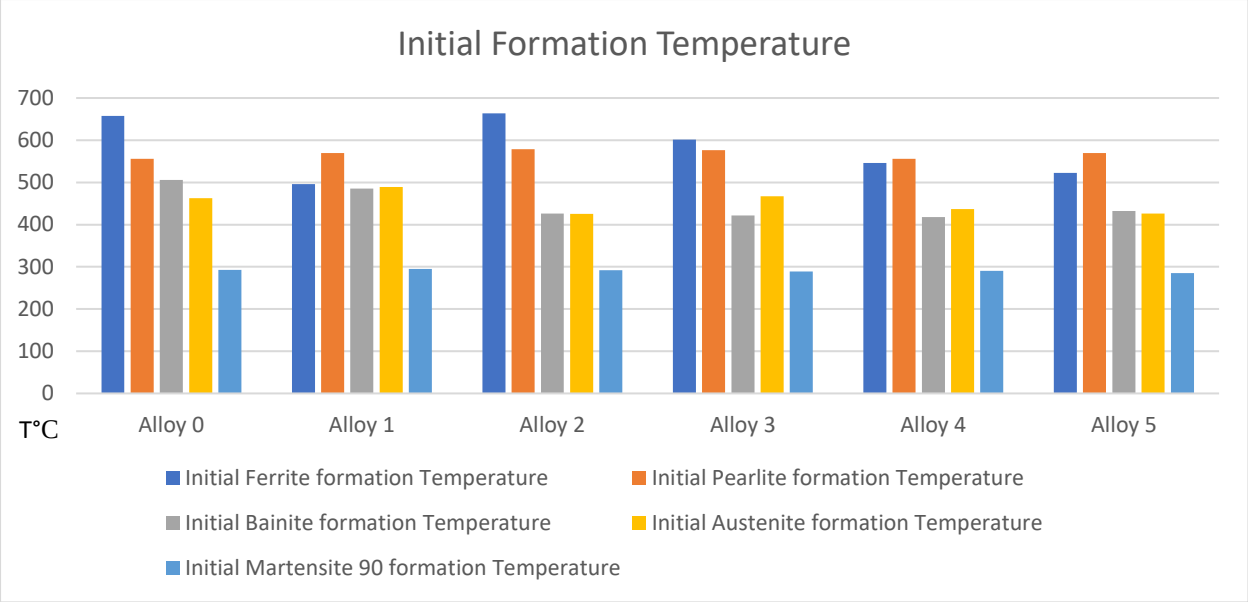

Figure 4.10.3 Initial formation temperature of pearlite, ferrite, bainite, austenite and martensite

Ferrite has a low carbon content and is stable at low temperatures. It has magnetic characteristics below 768°C. Ferrite is softer than pearlite, bainite, and martensite in terms of physical properties. As a result, the presence of ferrite in alloys functions as a shock absorber and, to some extent, a crack blunter. Alloy 0 has a lower formation temperature than the other alloys when it comes to pearlite formation. Pearlite forms at specific temperatures and compositions when quenched from high temperatures at a specific cooling rate. The temperature at which initial pearlite occurs climbs steadily when Mo is added. As a result, when cool down from a high temperature, pearlite forms at a higher temperature. As a result, pearlite should form in much less time without increasing the cooling rate. At the same time with increasing content of Mo, pearlite remains stable at the higher temperature.

4.10.4 Initial Formation Temperature for Bainite:

In the case of phase transformation, they transform to another phases by diffusion process or composition variance. Sometimes the transformation results due to the cooling rate or by the impacts of certain elements. Mo promotes the transformation of pearlite into bainite [140]. This element has the ability to change the transformation temperature and as a result, the mechanical properties of bainite improves.

To achieve granular bainite, other alloying elements that can delay ferrite formation are also needed. Other alloying elements such as Mn, Ni can prevent the formation of ferrite in order to achieve granular bainite [141]. This explains why some alloys seem to take longer to form.

Thus Mo addition significantly causes the formation of bainite at elevated temperature. Thus stability of bainite increases at lower temperature due to Mo addition.

4.10.5 Initial Formation Temperature for Austenite and Martensite:

The thermodynamic behavior of the four alloys is almost identical for initial formation temperature of martensite 90% completion but formation temperature of austenite is varied with Mo contents. In this study [142], on the basis of phase diagrams, the changes in the formation temperature of austenite for adding Mo are seen. In Figure, alloy 0 requires 462.26 °C to form austenite, which is lower than the temperatures needed for alloy 1 and alloy 3, which are 489.15 °C and 467.47 °C, respectively. Whereas alloy 2 is needed much lower temperature than alloy 0 to start the formation. Austenite pancaking becomes more pronounced as the molybdenum content rises. Simultaneously, from Mo-free to Mo added steel, the transition varies [143]. These alloys have close values for initial martensite 90 formation temperature.

By adding molybdenum, the additional benefits include microstructural refinement, tempering resistance, delayed crack resistance and synergy effects with other alloying elements [143]. As discussed earlier, at lower cooling rate Mo effectively suppresses ferrite formation and stimulates bainite formation and enhances martensite formation at higher cooling rates while also lowering the critical cooling rate of martensite.

A basic difference in each formation can be seen in Figure 4.10.3 by comparing all of the data to alloy 0. Successive addition of molybdenum is added to the base alloy. With the addition of Mo, a significant change is predicted on the formation of different phases. Phases form in the alloy due to change in temperature and compositions that certainly effects on respective physical and mechanical properties of such alloys.

4.10.6 Initial Formation Time for Austenite, Pearlite and Ferrite:

Figure 4.10.4 shows a significant difference in time in the formation of ferrite, austenite, and perlite. The initial formation time increases as the molybdenum content increases. The majority of these products require a combination of steel strengthening mechanisms cutting, shaping, and joining operations, as well as their effect on durability. Adding 0.15 wt% Mo results in a significant increase in the time to delayed fracture, indicating a synergistic effect [143]. Molybdenum has a significant impact on recrystallization activity as a result the alloying is efficient in causing delayed formation time of austenite, pearlite and ferrite [144]. As discussed

earlier, since molybdenum inhibits the formation of pearlite and ferrite, they take longer to form in the first place. This is why pearlite and ferrite have the fastest formation times, at 472.76s and 431.02s, respectively.

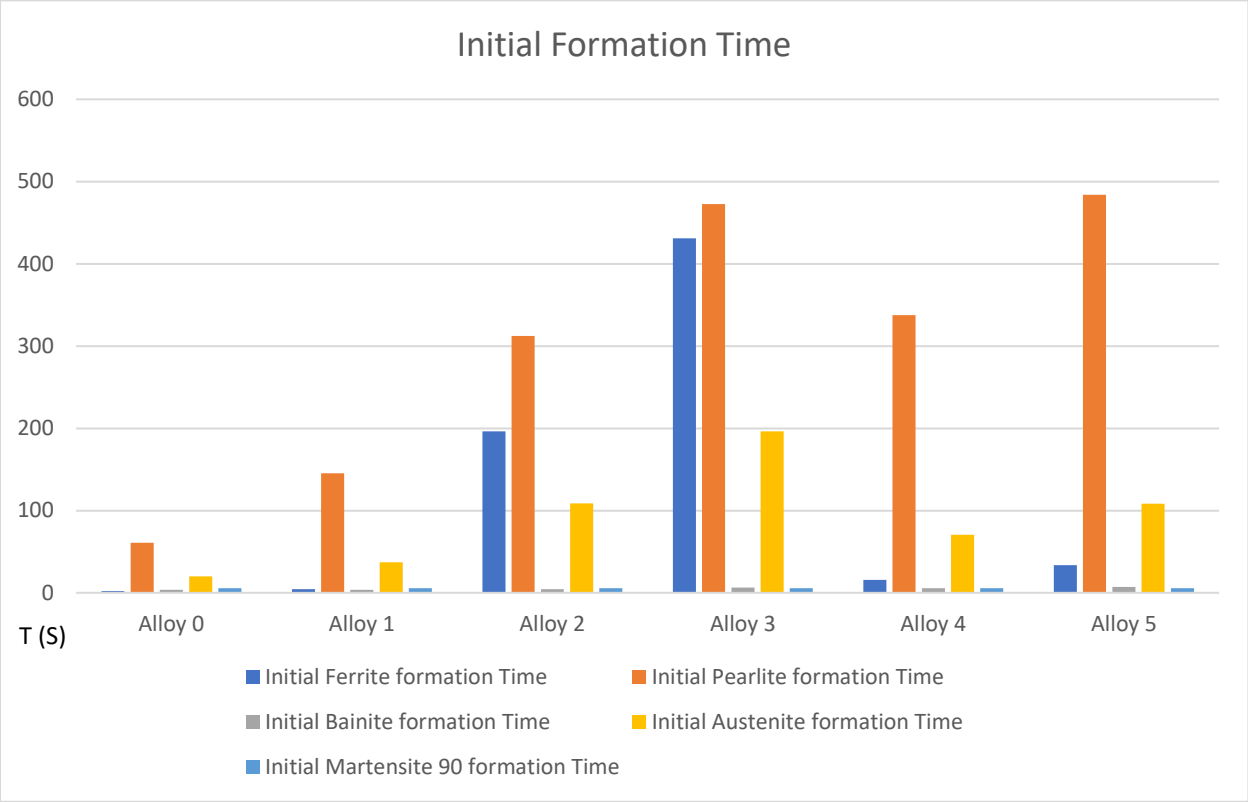

Figure 4.10.4 Initial formation time for austenite, pearlite and ferrite, bainite and martensite

In the case of ferrite and bainite when quenched form elevated temperature the transformation to ferrite and bainite happens at lower temperature than that of the base alloys due to the addition of Mo. And the time required for the initial formation of ferrite and bainite requires more time with the increased Mo. Thus, it can be predicted that the Mo addition in any way increases both the high temperature stability and time to form while cooling from elevated temperature. Pearlite and Austenite remain stable at higher temperature with the increase of the Mo. Time to form initial Pearlite and Austenite also increases duly. In that case Mo passively increases the cooling rate for the formation of the Pearlite and Cementite if considered other constraints as constants.

4.10.7 Initial Formation Time for Bainite and Martensite:

Figure 4.10.4 illustrates a very slight change in the formation time. In martensite 90, it can be barely differentiated among the alloys. Inside the austenite grains, the martensitic

transformation occurs and the amount of martensite produced in a steel is not affected by time [145]. Moreover, since there is no diffusion and it is solely dependent on the thermodynamic driving force, which is approximated by the difference in temperature between Ms and the lowest quench temperature. So for martensite, the formation times are nearly identical. However, bainite is formed when austenite decomposes at a temperature higher than MS but lower than that at which fine pearlite forms and molybdenum tends to form bainite more easily. Even if the cooling rate was not too fast, the deformed austenite would turn into finer bainite [146]. While the formation times do not vary significantly, alloy 3 with the highest molybdenum content takes longer to shape bainite than the others.

4.11 Mechanical properties on cooling rate

The changes in mechanical properties of objects deformed at different temperatures and chilled at the same time show that increasing the deformation temperature increases the yield strength, ultimate strength, and hardness. The cooling rate has a significant impact on these properties. Higher cooling rates impede atomic diffusion, resulting in smaller ferrite grains and the formation of fine phases with high strength, hardness, dislocation density, and fine phases. Polygonal ferrite converts to soft, coarse, and less dislocated phases while cooled slowly [147].

4.11.1 Tensile stress

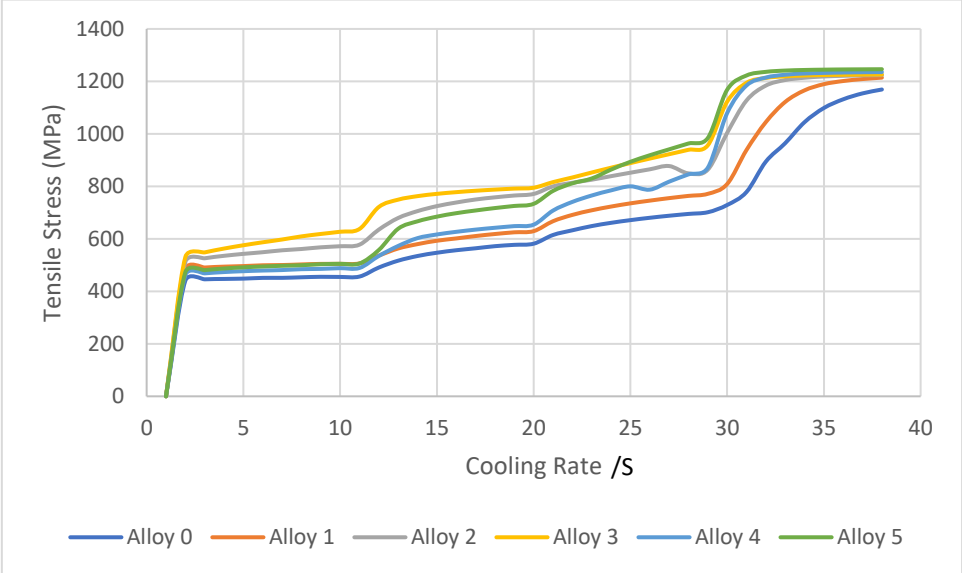

Figure 4.11.1 Tensile stress vs cooling rate

From the Figure 4.11.1, with the increasing cooling rate the tensile stress is increased. Tensile stress is greatest in Alloy 3, which contains the most molybdenum. Mo addition efficiently

delays the production of high-temperature products during the continuous cooling process, improving the tensile characteristics of low-carbon steels. For this reason, the tensile stress is increased for alloy 1, 2 and 3 respectively. However, for alloy 0, the tensile stress is the lowest as it doesn't contain any molybdenum. For alloy 4 and 5, the tensile stress is also higher than alloy 0. Alloy 4 and 5 contains 0.25% and 0.50% Cr respectively. Cr improves the hardenability of metastable austenite, refines the size of bainite-ferrite laths, and improves bainite micro-hardness. The result indicated that adding Cr has a considerable impact on mechanical characteristics that improves the tensile properties. In Figure 4.11.1, the alloy containing chromium has also shown considerably high tensile stress.

4.11.2 Hardness

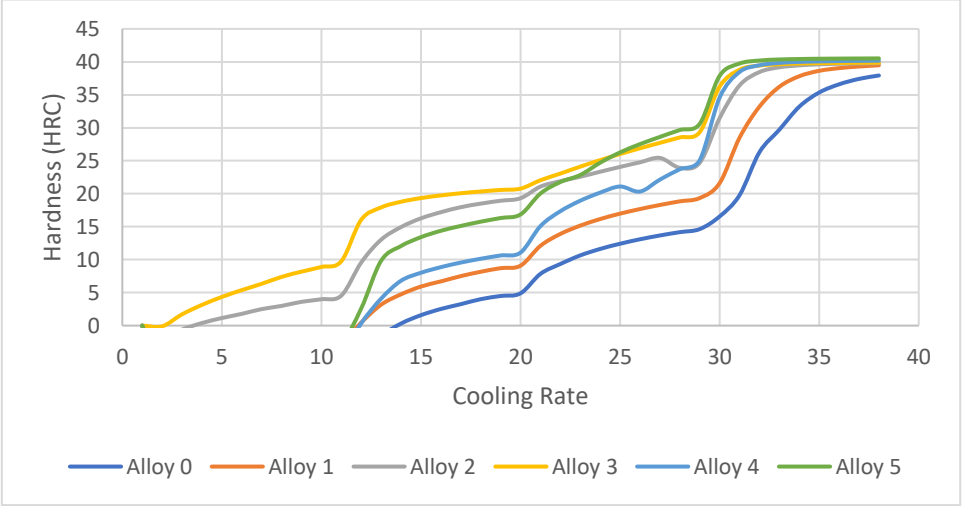

Figure 4.11.2 Hardness vs cooling rate

Figure 4.11.2 indicates that with the increasing cooling rate the hardness is increased. Alloy 0 has the lowest hardness. By adding alloying elements, the changed curve of hardness for different alloy is shown. At a wide range of cooling rates, Alloy 3 has the highest hardness. In study [148], it is investigated that the solid solution strengthening effect is improved by increasing Mo content, which is advantageous to matrix hardness enhancement. In the Figure it is observed that with the increasing amount of Mo, the hardness is increased. For alloy 4 and 5, chromium content played an important role for the enhancement of the hardness. In the study [149], it is investigated that as the alloy Cr content grew, the hardness and tensile strength also increased. In another study [150], it is showed that from first-principles calculations and testing, the alloys' strength and hardness were improved as the Cr content was increased.

However, when Cr is added to alloys 4 and 5, the resulting graph shows a higher hardness. Besides, alloy 3 with the highest Mo content has the highest hardness. This means that Mo is more effective than Cr at increasing hardness. In a study [151], it is investigated that when compared to the base material (without Mo), Mo gives a major increase in hardness of 20%, whereas Cr only delivers a slight hardening impact. However, after a minimum cooling rate, the graphs reveal that the hardness of various alloys is nearly identical.

4.12 Mechanical Properties on Temperature

Due to the unique deteriorating feature in material properties under fire environment and associated reduction in mechanical performance of members, it is critical to clarify the high-temperature mechanical properties in the design of cold-formed steel (CFS) structures under fire conditions. The coupons were cut from original coils of planned full annealed steels (S350 and S420, with nominal yielding strengths of 280 and 350 MPa, respectively) and suggested stress relieving annealed steels (G500, with nominal yielding strength of 500 MPa) for CFS constructions with thickness of 1.0 mm and 1.2 mm, and a total of nearly 50 tensile tests were carried out by steady-state test method for temperatures ranging from 20 to 700°C. Material properties such as yield strengths, ultimate strengths, the elasticity modulus, and the stress-strain curve were obtained as a result of the tests. In the meantime, the ductility of steels for CFS structures was debated. The temperature-dependent retention factors of yield strengths and elasticity modulus were then compared to those supplied by design codes and previous studies. Finally, based on existing test results, a set of prediction equations for the mechanical properties of steels for CFS constructions at increased temperatures was presented.

4.12.1 High Temperature Yield Strength:

Figure 4.12.1 illustrates how the high temperature yield strength of different alloys varies from one another. The 0.2% proof stress steadily increases as the strain rate increases. The high temperature yield strength of the alloys increases as the proportion of molybdenum increases. For many high strain rate applications, such as kinetic energy penetrators, molybdenum and its alloys are the preferred candidates [152,153]. However, the most of molybdenum's applications occur at high temperatures. From a similar study [154] showed comparison to the fully martensitic, air hardening 9 Cr-1 Mo steel, an increase in molybdenum brought delta ferrite into the microstructure of the steel, improving weld-ability. However, it was also shown earlier that the amount of ferrite continuously increases as the Mo content rises. As alloy 0 doesn’t

contain any molybdenum, it has the lowest yield strength than other alloys. A very slight change in the curve is observed for alloy 2 and alloy 5. Cr has effect on transformation kinetics, proving that adding Cr to metastable austenite improves hardenability [155, 156]. Individual Cr additions enhance the amount of ultimate bainite transformation.

By increasing the amount of bainite transformation, improves the strength of low-carbon bainite steel [157]. As a result, alloy 5 has a marginally higher yield strength than alloy 2. Alloy 3 contains only highest percentages of molybdenum. An increase in molybdenum content has a minor effect on the position of the line that marks the beginning of ferrite formation, but it affects the line that marks the beginning of pearlite creation and the conclusion of transition dramatically [158].

Similarly, the ascending curve can be seen as the amount of Mo increases. Since alloy 3 has the most Mo, it has the maximum yield strength. A little amount of chromium, like molybdenum, enables a dramatic delay of pearlite synthesis while only slightly slowing the formation of free ferrite.

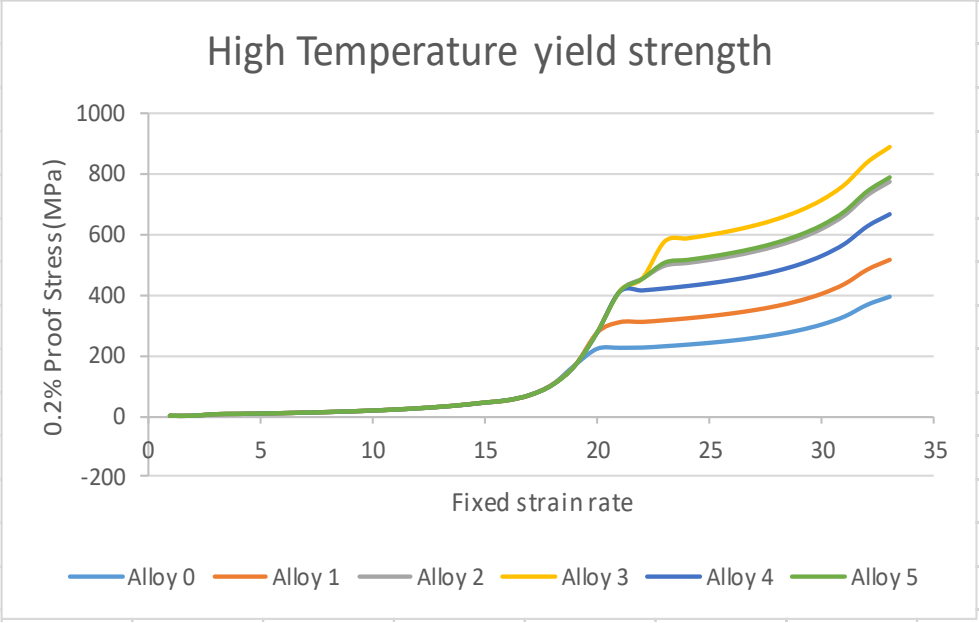

Figure 4.12.1 High Temperature Yield Strength for alloy

As a result, by studying [159] it was apparent the excess ferrite production is clearly reflected in the kinetic isothermal transformation diagram for austenite in low-carbon steels having up to 1.5 percent chromium. So in case of alloy 4, adding chromium up to 0.25% to the alloy and lowering 0.50% of molybdenum from the alloy results in a yield strength decline. Moreover, the formation of high-carbon bainite within the structure is facilitated by molybdenum rather

than chromium, which is likely due to the differing effects of these elements on carbon diffusion in the test alloys [158].

The addition of Mo and Cr increases the precipitation amount at the same time they are responsible to reduce the precipitation size. Thus Alloy 3 has the maximum yield stress at the elevated temperature.

4.13 Stress-Strain Curve

A stress–strain curve for a material is used in engineering and materials science to show the relationship between stress and strain. It's calculated by progressively adding load to a test coupon and measuring deformation, from which stress and strain may be calculated (see tensile testing). Many properties of a material are revealed by these curves, including the Young's modulus, yield strength, and ultimate tensile strength.

Stress-strain curves are, in general, curves that depict the relationship between stress and strain in any sort of deformation. Normal, shear, or mixed stress and strain can be uniaxial, biaxial, or multiaxial, and can even alter over time. Compression, stretching, torsion, rotation, and other types of deformation are all possible. The relationship between axial normal stress and axial normal strain of materials determined in a tension test is referred to as the stress–strain curve unless otherwise stated.

4.13.1 SS Curve 600^{o}C

Figure 4.13.1 is showing how the stress is changing with the change in the strain. At 6000C temperature, the true stress value almost stays the same as the strain increases. But with addition of alloying element, the curve is gradually increased. Alloys with chromium content shows more enhancement in the true stress than the alloys with molybdenum content. In the study [160], similar result is stated that when molybdenum is added, the compressive yield strength improves without fracture at a compressive strain of 60 percent. In the findings of a study [161] shows that Cr variation has a major impact on the high entropy alloy system's tensile properties. It indicates that when the Cr content grew, the hardness increased as well.

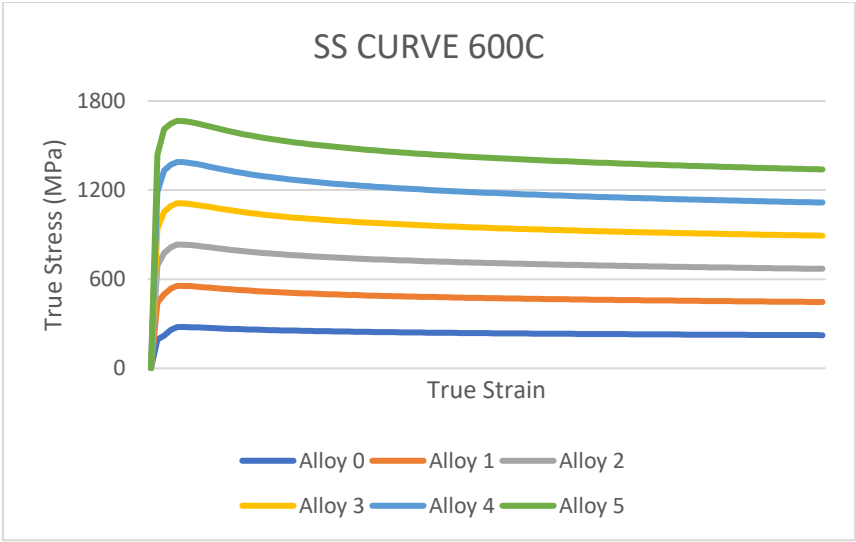

Figure 4.13.1 Stress- strain curve at 600ºC

4.13.2 SS Curve 800ºC

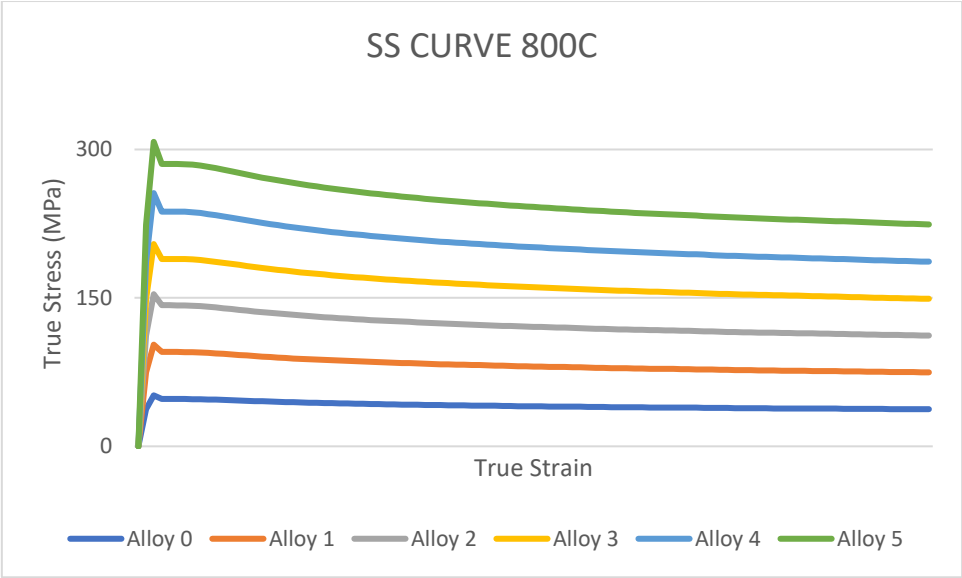

Figure 4.13.2 Stress- strain curve at 800ºC

Figure 4.13.2 upholds the stress-strain curve at 800ºC. A decline in the stress value as the temperature increased in comparison to Figure 4.13.1. In general, when temperature rises, strength and stiffness decrease, whereas elongation at break, a strong relative measure of ductility, rises [162]. In Figure 4.13.2, the same behavior as discussed earlier for alloying

element Mo and Cr. With the increasing amount of those alloying element, the stress value is increased.

4.13.3 SS Curve 1000^{o}C

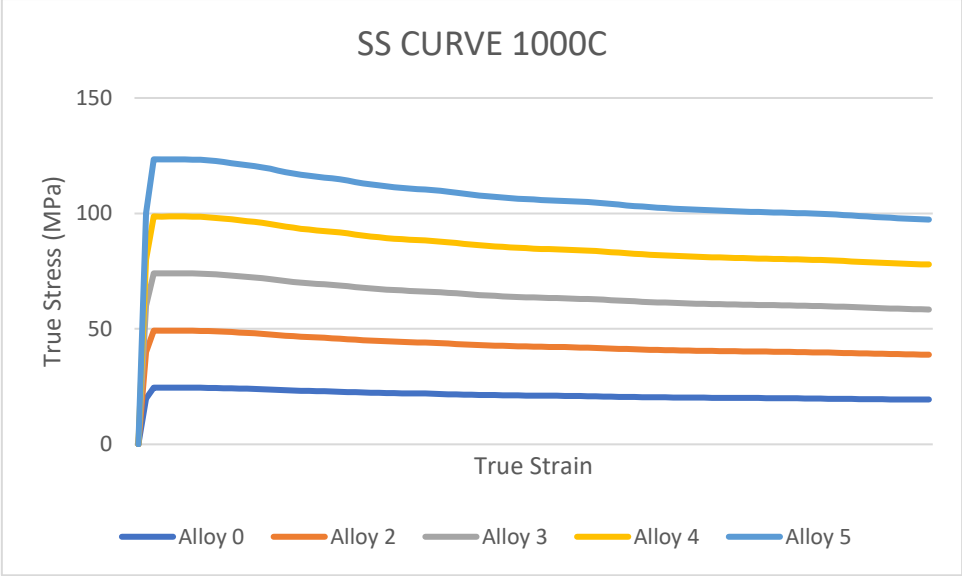

Figure 4.13.3 Stress- strain curve at 1000^{o}C

In Figure 4.13.3, the value of true stress is more decreased as the temperature is risen to 1000^{o}C. For the base alloy the curve shows the lowest value of stress. As Mo and Cr is added, the curve progressively increased.

Table 4.13.1 Effect of Alloying elemnt on True Stress at the different temperatures

Alloy	True Stress at 600◦C, 800◦C, 1000◦C	Predictions
5	**Alloy5>Alloy4>Alloy3>Alloy2>Alloy1>Alloy0**	1) Ti itself increases the yield strength at room temperature and it performs explicitly at elevated temperature. Thus Alloy 5 shows maximum room temperature and elevated temperature YS. Ti Helps to withstand the common structural steels at the elevated temperature.
4		2) Mo and Cr addition to some extent are responsible to increase the precipitation amount by forming different carbides. And at the same they are responsible to reduce the precipitation size. Thus at the elevated temperature it due to precipitation hardening it tries to with stand and shows better YS than the base alloys.
3		
2		
1		
0		

4.14 Precipitation Formation

The characteristics of structural state generation, phase precipitates, and qualities for rolled product of complicated V–Nb–Ti–Mo micro alloyed low carbon steels of the ferritic class when melted in the laboratory, it has been demonstrated that at low temperatures for strip winding on a coil, the development of interphase and ferritic precipitates, which contribute significantly to strength qualities, is significantly limited. The steel cooling rate after rolling, which is equal

to 20°C/sec, is insufficient for creating a fully block (acicular) ferrite (AF) structure with improved strength qualities. A decrease in this causes a decrease in the AF fraction, but has no effect on the temperature at the end of rolling. According to the findings of a study of rolled products produced at higher temperature 650°C and a cooling rate of 25°C/sec, the possibility of simultaneously forming an AF structure and a system of nanoscale interphase and ferrite precipitates is demonstrated, allowing for significant increases in steel strength and other service properties.As a result, precipitation forms in various combinations of temperature and cooling pace.

4.15 Stacking Fault Energy

The stacking-fault energy is a property of a material on a very small scale. It is abbreviated as SFE in units of energy per area. A stacking defect develops when the usual stacking sequence of atomic planes is interrupted in a close-packed crystal structure. The energy of these interruptions is similar to that of a stacking fault. As a result, the stacking-fault energy has some influence on the equilibrium width. When the SFE is high, dividing a full dislocation into two partials is energy inefficient, therefore the material deforms by dislocation glide or cross-slip [163].

From Figure 4.15.1, as the temperature increases, the stacking fault energy is increased. In the study [164], the effect of temperature on stacking fault energy is investigated. It is stated that as the temperature rises, the stacking fault energy rises, resulting in smaller and smaller partial dislocation separation. Dislocation glide can occur at low SFEs when two dissociated Shockley partials with a small separation distance glide together. The SFE is lowest for alloy 0. With the increasing amount of molybdenum, the value of SEF is seen increasing with temperature. Because of their high atomic size, which prevents dislocation flow, Mo and W are known to contribute additional strength to the matrix in the Satellite family of Co-based alloys [165]. In case of alloy 4 and 5, as the chromium content increases the SFE curve also increases.

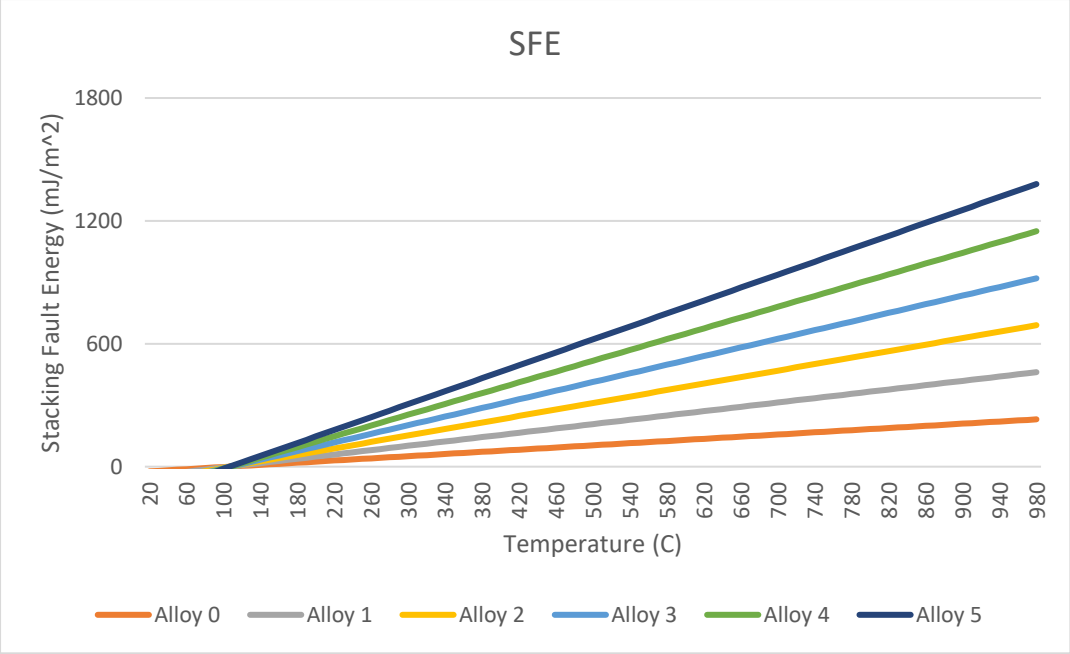

Figure 4.15.1 Stacking Fault energy vs Temperature

4.16 Summary of the effects of alloying elements on fire resistance steel

4.16.1 Molybdenum:

- **Transformation temperature:** The addition of Mo has a minor effect on the temperature shift of transformation (A_1 and A_3) to somewhat higher temperatures. With the addition of Mo, both the transformation temperature and the transformation time will rise.
  The time required to overcome the A_1 line grows as the amount of Mo increases. Thus, elevated temperature stability of the steel improves.
- **Initial formation temperature:** Mo has an effect on ferrite formation. The amount of ferrite continuously increases as the Mo content rises. Because of the addition of Mo, the high temperature stability of ferrite becomes lower than that of the base alloys and the temperature at which initial pearlite occurs improves steadily. Mo encourages the conversion of pearlite to bainite. Thus, the inclusion of Mo causes the development of bainite at high temperatures. As previously stated, Mo effectively suppresses ferrite formation and encourages bainite production at lower cooling rates, while also lowering the critical cooling rate of martensite.

The inclusion of Mo is expected to have a substantial impact on the creation of distinct stages. Changes in temperature and composition cause phases to form in the alloy, which have a significant impact on the physical and mechanical properties of such alloys.

Microstructural refinement, tempering resistance, delayed crack resistance, and synergistic effects with other alloying elements are only some of the extra benefits of adding molybdenum.

- **Initial formation time:** As the molybdenum content rises, so does the initial formation time. As a result of molybdenum's strong effect on recrystallization activity, the alloying is effective in causing austenite, pearlite, and ferrite formation to be delayed. With higher Mo, the time necessary for the initial formation of ferrite and bainite takes longer. In any case, the addition of Mo improves both the high temperature stability. With a rise in Mo, pearlite and austenite stay stable at higher temperatures. If other restrictions are considered as constants, Mo passively increases the cooling rate for the creation of Pearlite and Cementite. For martensite 90% formation, molybdenum does not have any significant impact. Molybdenum is more prone to forming bainite. The distorted austenite will develop into finer bainite even if the cooling rate is not excessively rapid.

  Thus, during firing it retards the mechanical properties failure.

- **Ferrite fraction:** Molybdenum, an alloying element, decreases carbon activity, delaying procedures that rely on carbon diffusion. The ferrite fraction decreases as a result of this.
- **Pearlite fraction:** The pearlite content increases as the molybdenum content increases.
- **Bainite fraction:** Molybdenum has a higher impact on properties when upper bainite occurs during cooling. The effect of molybdenum on strength and ductility in isothermal lower bainite production is insignificant. The addition of Mo increases the quantity of isothermal bainite transition and accelerates bainite transformation kinetics. As the Mo concentration rises, the bainite proportion rises as well.
- **Austenite fraction:** The molybdenum-containing alloy has much more austenite fractions than the base alloy and is less susceptible to partitioning time. As the Mo content of the alloying element rose, the austenite fraction increased with increasing cooling rate.

- **Martensite fraction:** The molybdenum-containing alloy has much more austenite fractions than the base alloy and is less susceptible to partitioning time. As the Mo content of the alloying element rose, the austenite fraction increased with increasing cooling rate.
- **Tensile stress:** Mo addition improves the tensile properties of low-carbon steels by delaying the development of high-temperature products during the continuous cooling process.
- **Hardness:** Increased Mo concentration improves the solid solution strengthening effect, which is beneficial to matrix hardness enhancement. The hardness of the material increases as the amount of Mo increases. When it comes to improving hardness, Mo outperforms Cr. When compared to the base material (without Mo), Mo provides a significant 20 percent improvement in hardness, whereas Cr only has a minor hardening effect. The graphs, however, show that the hardness of various alloys is approximately comparable after a minimal cooling rate.
- **High temperature yield strength:** The alloys' high-temperature yield strength increases as the molybdenum content increases. Molybdenum and its alloys are the favored candidates for many high strain rate applications, such as kinetic energy penetrators. The majority of molybdenum's applications, however, take place at high temperatures.
- **Precipitation Amount for MC with time:** Since the inclusion of molybdenum affects the dissolving during austenitization, it takes longer for the precipitate to form. Because the inclusion of molybdenum affects the dissolving during austenitization, it takes longer for the precipitate to form.
- **Precipitation Amount for M_2C with time:** Mo has a significant effect on the amount of M2C precipitation throughout time. The alloy with the least amount of Mo experiences M2C precipitation on average. As the amount of Mo grows, so does the amount of precipitation.
- **Precipitation Amount for M_3C with time:** The amount of precipitation reduces as molybdenum is added. Mo has the opposite effect on the amount of M3C precipitation.
- **Precipitation Amount for M_6C with time:** As Mo is added, the precipitation of M6C increases.
- **Precipitation Amount for $M_7C_3$with time:** As the Mo content increases the precipitation amount of M_7C_3 increases. The inclusion of molybdenum changes the crystal structure and atomic radii, which affects the precipitation quantity.

- **Precipitation size of MC with time:** The concentration of Mo in the precipitates decreases as particle size and isothermal holding time increase. Furthermore, it is suggested that these precipitates can become rather coarse after a long time of isothermal retention in the austenite zone, losing their advantage in microstructure refinement and precipitation strengthening.
- **Precipitation size of M_2C with time:** With the increasing amount of molybdenum, the precipitation size gets larger. Mo has a proclivity for generating high-hardness Mo2C or M2C carbides. This is why M2C precipitation is significantly higher than other carbide precipitations.
- **Precipitation size for M_6C with time:** As molybdenum content is added progressively for alloy, the precipitation size is seen to be increased.
- **Precipitation size for M_7C_3 with time:** Precipitation sizes are larger in molybdenum-containing alloys. Carbides like M7C3, M6C, and M23C6, which have complicated crystal structures and low formation temps, generate coarse suspensions.
- **Precipitation size for $M_{23}C_6$ with time:** For molybdenum, the precipitation quantity of M23C6 is very low or close to nil. When Mo is added, a prominent secondary hardening peak emerges.
- **Stacking fault energy:** The value of SEF increases with temperature as the amount of molybdenum increases. Mo and W are known to offer significant strength to the matrix in the Stellite family of Co-based alloys due to their large atomic size, which limits dislocation flow.
- **SS Curve 600ºC:** The true stress increases as the Mo alloying element is added. At a compressive strain of 60%, the compressive yield strength improves without breakage when molybdenum is added.
- **SS Curve 800ºC:** With the increasing amount Mo, the stress value is increased.
- **SS Curve 1000ºC:** The stress value rises as the amount of Mo increases.

4.16.2 Chromium

- The necessary time to overcome the A1 line alters dramatically as a result of adding too much chromium.
- **Ferrite fraction:** Carbon atoms are prevented from spreading by chromium atoms, lowering the thickness of grain boundary ferrite. The number of fractions of high-angle

grain boundaries increases as the chromium level increases. Thus Cr hinders ferrite transformation in a significant way.

- **Pearlite fraction:** When the concentration of Cr rises, the values of Ac1 and Ac3 rise as well. The amount of information on transformation kinetics was also increases due to the Cr content. As a result, the fraction of pearlite falls. The fraction can be raised by maintaining a correct alloying percentage.
- **Bainite fraction:** The bainite fraction decreases when Cr is introduced. The inclusion of Cr may induce the bainitic transition to take longer. However, when there is an excess of Cr in the alloying element, the bainite fraction increases as the cooling rate increases.
- **Austenite fraction:** Cr is a good carbide-producing element for pearlitic structure refinement. As a result, the number of austenite nucleation sites increases as Cr concentration increases, contributing to austenite creation and growth.
- **Martensite Fraction:** Cr is essential in modern heat treatment methods, which rely heavily on the martensitic transition. The martensitic fraction increases with the cooling rate as Cr is supplied as an alloying element.
- **Tensile Stress:** Cr enhances the hardenability of metastable austenite, the size of bainite-ferrite laths, and the micro-hardness of bainite. adding Cr has a significant impact on mechanical properties, which improves tensile properties.
- **Hardness:** The hardness and tensile strength of an alloy improve as the Cr content increases. The strength and hardness of the alloys improve when the Cr content is raised, according to first-principles calculations and tests. When Cr is added to alloys, however, the hardness increases.
- **High temperature yield strength:** The addition of Cr to metastable austenite improves hardenability by altering transformation kinetics. The amount of eventual bainite transformation is increased when individual Cr additions are made. The strength of low-carbon bainite steel is improved by increasing the amount of bainite transformation. As a result, adding Cr helps to increase the high temperature yield strength
- **Precipitation Amount for MC with time:** The composition of the parent components has a significant impact on the features of secondary and eutectic carbides (C, Cr). Secondary carbides that form in matrix regions strengthen the matrix by enhancing dispersion and refining the microstructure. The number of carbides that precipitate is affected by chromium's effect. When chromium is added to the elemental composition, it takes almost the same length of time to precipitate carbide, but it does so with significantly less carbide.

- **Precipitation Amount for M_2C with time:** In comparison to the previous alloy, it is clear that as the chromium percentage increases, precipitation decreases.
- **Precipitation Amount for M_3C with time:** With time, the precipitation amount decreases with the increasing amount of chromium
- **Precipitation Amount for M_7C_3 with time:** Cr atom concentration has the greatest impact on M7C3 precipitation. Because Cr enriches cementite to roughly 20%, only a little amount of Cr is present in solid solution in low Cr steels' martensite, causing in-situ cementite precipitation. The Cr content of cementite, on the other hand, rises with tempering time, which could account for the M7C3 production lag. Furthermore, M7C3 is much higher than the precipitating quantities of MC and M2C.
- **Precipitation Amount for $M_{23}C_6$ with time:** As the rate of chromium increases, so does the amount of precipitation.
- **Precipitation Amount for M_6C with time:** In comparison to other alloys, the precipitation amount reduced as the Cr level increased. M6C is also said to form a primary precipitate in steels containing less than 8% Cr over long periods of time. As a result, steel with a lower Cr concentration has a larger precipitation amount.
- **Precipitation size of MC with time:** In the presence of carbon and iron, chromium is a potent carbide producer, generating a complex series of carbide structures. As can be seen from the graph, alloys containing the alloying element chromium have greater precipitation sizes than those without.
- **Precipitation size of M_2C with time:** With the increasing content of chromium, the precipitation size gets smaller.
- **Precipitation size for M_6C with time:** After a period of time, the size of the precipitation for M6C is shown to stay consistent after adding Cr content. Furthermore, as compared to alloys containing Mo, the size is reduced.
- **Precipitation size for M_7C_3 with time:** When having chromium in the alloy, it can be evident that alloy having chromium content has smaller precipitation size.
- **Precipitation size for $M_{23}C_6$ with time:** In the case of chromium, the magnitude of the precipitation is enormous.
- **Stacking fault energy:** As the chromium content increases the SFE curve also increases.
- **SS Curve 600^{o}C:** True stress enhancement is greater in chromium-containing alloys than in molybdenum-containing alloys. The tensile characteristics of the high entropy alloy

system are heavily influenced by Cr fluctuation. It means that as the Cr concentration rises, the hardness rises as well.

- **SS Curve 800ºC:** With the increasing amount Cr, the stress value increases.
- **SS Curve 1000ºC:** The stress value rises as the amount of Cr increases.

4.16.3 Other Alloying Elements

- In order to create granular bainite, other alloying elements like as Mn and Ni can hinder the production of ferrite.
- The chemical composition of precipitates varies as Nb and W form strong carbides. Niobium carbides (Nb) precipitate in vast amounts that were not dissolved during the austenitization process, giving rise to Type MC. However, the niobium addition had no influence on secondary precipitation under the chosen austenitization setting.

5 Conclusions

The aim of the research work is to find the composition of common structural steels by adding different alloying elements so that it can withstand at the elevated temperature. When different alloying elements are successively added then it shows different microstructural, physical and mechanical properties. Firstly, Mo is added from 0.25% to 0.75% successively to the base alloy. Then Cr is added about 0.25% to 0.5%, followed by Al and Ti – to observe or predict the properties at the elevated temperature. The successive addition of such alloying elements to the base alloys are responsible to form different phases both in equilibrium and non-equilibrium condition. At the same time, it has also shown some distinctive properties of the formation of different carbides and different alloying elements have also played an important role in controlling the carbide precipitation size. This formation of precipitation and control over its growth is an important factor in determining the tensile properties at the elevated temperature. Few alloying elements also affect the shifting of the transformation temperature line. Some important findings have been revealed in this work.

1. Microstructural evolution at equilibrium condition states that the addition of Mo and Cr retards the formation of cementite at the elevated temperature. It is known that the cementite is brittle in nature. Thus, cementite may reduce overall mechanical properties at the elevated temperature as it has already tended to enter the melting range. On the other hand, addition of alloying elements cannot significantly influence the austenite formation. But successive addition of the Mo, Cr, Al, and Ti widens the melting range. As a result, considering equilibrium cooling from an elevated temperature, it gets ample time to reform the uniform microstructure. And at the same the liquidus line shifts higher. Thus, high temperature properties enhanced.
2. Equilibrium phases forms due to certain cooling rate. In the case of the formation of the ferrite phase considering cooling rate as constant the base alloy contains maximum amount of ferrite. For lower cooling rate, addition of Mo increases the pearlite% and in base alloy least pearlite forms. Interestingly, opposite scenario is seen in the case of the higher cooling rate. Similar case is seen in the case of the bainite also. But in the case of bainite the addition of Mo increases the bainite% for all the cooling rates. For lower

cooling rate austenite and martensite formation is close to null. But the addition of Mo and Cr with higher cooling rate forms maximum phases of austenite and martensite. Thus, addition of Mo and Cr and higher cooling rate forms martensite and other important phases that are important for enhancement of the mechanical properties.

Another scenario can be predicted that the addition of Mo initiates the bainitic, pearlite and austenitic growth. And Cr retards the initial growth of such phases.

3. The addition of Mo shifts the A_1 and A_3 line upwards. But Cr shifts the A_1 line upwards but lowers the A_3 line. When cooling from an elevated temperature, Mo addition increase the formation time of ferrite. On the other hand, cooling from an elevated temperature Mo addition increase the pearlite formation time but Cr decrease the pearlite formation time. Thus, it can be predicted that Mo addition increase the time to phase transformation, but Cr lowers the transformation time. The more the transformation time the less the residual stress develop on the structure. Thus, Mo addition to some extent enhance the properties.
4. Mo and Cr addition are responsible to the formation of precipitation like different stoichiometric ratios of carbides. The successive addition of Mo and Cr increase the amount of carbide. But interestingly, the addition of Mo and Cr retards the growth of the carbides. As a result, it can be predicted that, when catastrophic fire build on the structure then the structure containing common structural steels with such alloying elements have precipitates like carbides on its microstructure that has high melting point thus it helps the structure to withstand at the elevated temperature. Thus, it is further seen that the common structural steels with the Mo and Cr has significantly perform higher mechanical properties at the elevated temperature. Common structural steels with Ti also show such type of extrinsic properties.

In this research work firstly the impact of Mo on the common structural steels has been studied. The main concern was to meet the economic perspective. As a result Cr is added over the Mo to see the impact if it is close to the singly added Mo and found a positive result. The price of Mo is much higher and Cr can be the alternative in this matter. Later Ti and Al is added to see the impact but all the properties have not been measured due to the computational difficulties. But it is predicted that it also influences the high temperature properties of the common structural steels. It can break the tip of iceberg to extend the further research work. Experimentation of such research will give more authenticity of this research. Authors tried to find out the effects of alloying

elements on the phase formation and microstructural evaluation at different temperature to predict some important decision.

5.1 Scope for Future Work

The research that has been done can break the tip of iceberg to extend the further research work. Experimentation of such research will give more authenticity of this research. Few initial data have been validated but more data needs to be validated for experimentation.

- This research work has play with a lot of statistical data. And it is predicted that the addition of Mo can improve the high temperature stability of the common structural steels. And at the same time by reducing the amount of Mo and adding Cr over Mo can be satisfactory alternative. Moreover, Ti and Al addition also provides a better prediction in this matter. Experimentation on this basis can be a great impact on the research. It will also validate the existing results.
- For more explicit and exclusive conclusion of the research work more alloy combination can be taken into consideration. More precisely only Cr addition over the base alloy can be done to see the influence of Cr solely.
- There are more scopes to generate statistical data for the alloy 6. Then more predictions and conclusion may come to an end.

Reference

1. Wu, Z., Shi, C., He, W., & Wu, L. (2016). Effects of steel fiber content and shape on mechanical properties of ultra high performance concrete. *Construction and building materials*, *103*, 8-14.
2. Fischer, E. C., & Varma, A. H. (2017). Fire resilience of composite beams with simple connections: Parametric studies and design. *Journal of Constructional Steel Research*, *128*, 119-135.
3. Gao, J., Fu, P., Liu, H., & Li, D. (2015). Effects of rare earth on the microstructure and impact toughness of H13 steel. *Metals*, *5*(1), 383-394.
4. Llewellyn, D., & Hudd, R. (1998). *Steels: metallurgy and applications*. Elsevier.
5. Loffredo, S., Paternoster, C., & Mantovani, D. (2019). Iron-Based Degradable Implants.
6. Raghavan, V. (2015). *Physical metallurgy: principles and practice*. PHI Learning Pvt. Ltd.
7. Ha, H. Y., Lee, T. H., Bae, J. H., & Chun, D. W. (2018). Molybdenum effects on pitting corrosion resistance of FeCrMnMoNC austenitic stainless steels. *Metals*, *8*(8), 653.
8. de Andrés, C. G., Capdevila, C., Madariaga, I., & Gutierrez, I. (2001). Role of molybdenum in acicular ferrite formation under continuous cooling in a medium carbon microalloyed forging steel. *Scripta materialia*, *45*(6), 709-716.
9. Bogucki, R., & Pytel, S. M. (2014). Influence of molybdenum addition on mechanical properties of low carbon HSLA-100 steel. *Archives of Metallurgy and Materials*, *59*(3), 859-864.
10. Gundlach, R. B. (1979). Elevated-temperature properties of alloyed gray irons for diesel engine components.
11. Bepari, M. M. A., & Shorowordi, K. M. (2004). Effects of molybdenum and nickel additions on the structure and properties of carburized and hardened low carbon steels. *Journal of materials processing technology*, *155*, 1972-1979.

12. Papaefthymiou, S., Bouzouni, M., & Petrov, R. H. (2018). Study of carbide dissolution and austenite formation during ultra-fast heating in medium carbon chromium molybdenum steel. *Metals*, *8*(8), 646.
13. Kong, J., & Xie, C. (2006). Effect of molybdenum on continuous cooling bainite transformation of low-carbon microalloyed steel. *Materials & design*, *27*(10), 1169-1173.
14. Jung, S., Jeon, C., Jo, Y. H., Choi, W. M., Lee, B. J., Oh, Y. J., ... & Lee, S. (2016). Effects of tungsten and molybdenum on high-temperature tensile properties of five heat-resistant austenitic stainless steels. *Materials Science and Engineering: A*, *656*, 190-199.
15. JEKEL, A. N. (2012). Influence of molybdenum on the hot-tensile properties of austenitic stainless steels. *Materiali in tehnologije*, *46*(6), 649-655.
16. Tomashchuk, I., Grevey, D., & Sallamand, P. (2015). Dissimilar laser welding of AISI 316L stainless steel to Ti6–Al4–6V alloy via pure vanadium interlayer. *Materials Science and Engineering: A*, *622*, 37-45.
17. Rajan, T. V., Rajan, T. S., Sharma, C. P., & Sharma, A. (2011). *Heat treatment: principles and techniques*. PHI Learning Pvt. Ltd.
18. Pawar, P. B., & Utpat, A. A. (2016). Effect of chromium on mechanical properties of A487 stainless steel alloy. In *Proceedings of 3rd International Conference on Recent Innovations in Science, Engineering and Management* (pp. 119-125).
19. Sun, B., Zuo, X., Cheng, X., & Li, X. (2020). The role of chromium content in the long-term atmospheric corrosion process. *npj Materials Degradation*, *4*(1), 1-9.
20. Maximov, J. T., Anchev, A. P., Duncheva, G. V., Ganev, N., & Selimov, K. F. (2017). Influence of the process parameters on the surface roughness, micro-hardness, and residual stresses in slide burnishing of high-strength aluminum alloys. *Journal of the Brazilian Society of Mechanical Sciences and Engineering*, *39*(8), 3067-3078.
21. Zhang, X., Fan, L., Xu, Y., Li, J., Xiao, X., & Jiang, L. (2015). Effect of aluminum on microstructure, mechanical properties and pitting corrosion resistance of ultra-pure 429 ferritic stainless steels. *Materials & Design (1980-2015)*, *65*, 682-689.
22. Rahimian, M., Parvin, N., & Ehsani, N. (2010). Investigation of particle size and amount of alumina on microstructure and mechanical properties of Al matrix composite made by powder metallurgy. *Materials Science and Engineering: A*, *527*(4-5), 1031-1038.

23. Jones, R. M. (1998). *Mechanics of composite materials*. CRC press.
24. Gateman, S. M., Stephens, L. I., Perry, S. C., Lacasse, R., Schulz, R., & Mauzeroll, J. (2018). The role of titanium in the initiation of localized corrosion of stainless steel 444. *npj Materials Degradation*, *2*(1), 1-8.
25. Ahmed, W., Elhissi, A., Jackson, M., & Ahmed, E. (2012). Precision machining of medical devices. *The Design and Manufacture of Medical Devices*, 59-113.
26. Gelfi, M., Gorini, D., Pola, A., & La Vecchia, G. M. (2016). Effect of titanium on the mechanical properties and microstructure of gray cast iron for automotive applications. *Journal of Materials Engineering and Performance*, *25*(9), 3896-3903.
27. Stipp, M., StuÈnitz, H., Heilbronner, R., & Schmid, S. M. (2002). The eastern Tonale fault zone: a 'natural laboratory'for crystal plastic deformation of quartz over a temperature range from 250 to 700 C. *Journal of structural geology*, *24*(12), 1861-1884.
28. Matsumura, O., Sakuma, Y., & TakeChi, H. (1987). Enhancement of elongation by retained austenite in intercritical annealed 0.4 C-1.5 Si-O. 8Mn Steel. *Transactions of the Iron and Steel Institute of Japan*, *27*(7), 570-579.
29. Xu, C. L., & Jiang, Q. C. (2006). Morphologies of primary silicon in hypereutectic Al–Si alloys with melt overheating temperature and cooling rate. *Materials Science and Engineering: A*, *437*(2), 451-455.
30. Zhu, S., Yang, H., Guo, L. G., & Fan, X. G. (2012). Effect of cooling rate on microstructure evolution during α/β heat treatment of TA15 titanium alloy. *Materials Characterization*, *70*, 101-110.
31. Rasouli, D., Asl, S. K., Akbarzadeh, A., & Daneshi, G. H. (2008). Effect of cooling rate on the microstructure and mechanical properties of microalloyed forging steel. *Journal of materials processing technology*, *206*(1-3), 92-98.
32. Manson, S. S. (1953). *Behavior of materials under conditions of thermal stress* (Vol. 2933). National Advisory Committee for Aeronautics.
33. Tsai, C. W., Tsai, M. H., Yeh, J. W., & Yang, C. C. (2010). Effect of temperature on mechanical properties of Al0. 5CoCrCuFeNi wrought alloy. *Journal of Alloys and Compounds*, *490*(1-2), 160-165.
34. Shin, I., & Carter, E. A. (2011). Orbital-free density functional theory simulations of dislocations in magnesium. *Modelling and Simulation in Materials Science and Engineering*, *20*(1), 015006.

35. Kyvelou, P., Slack, H., Mountanou, D. D., Wadee, M. A., Britton, T. B., Buchanan, C., & Gardner, L. (2020). Mechanical and microstructural testing of wire and arc additively manufactured sheet material. *Materials & Design*, *192*, 108675.
36. Hodge, S. M., & Bain, E. C. (1948). Functions of alloying elements in steel. *Metals Handbook ASM*, *453*.
37. Totten, G. E. (Ed.). (2006). *Steel heat treatment: equipment and process design*. CRC Press.
38. Zhao, J., & Jin, Z. (1992). Isothermal decomposition of supercooled austenite in steels. *Materials science and technology*, *8*(11), 1004-1010.
39. Cozar, R., & Pineau, A. (1973). Morphology of y'and y" precipitates and thermal stability of inconel 718 type alloys. *Metallurgical Transactions*, *4*(1), 47-59.
40. Imam, M. A. (2018). *Phase equilibria and reaction kinetics of borides based high-temperature thermoelectric materials* (Doctoral dissertation, The University of Alabama).
41. Kaufman, L., & Bernstein, H. (1970). Computer calculation of phase diagrams. With special reference to refractory metals.
42. Sundman, B., Lukas, H. L., & Fries, S. G. (2007). *Computational thermodynamics: the Calphad method*. New York: Cambridge university press.
43. Gurao, N. P., & Biswas, K. (2017). In the quest of single phase multi-component multiprincipal high entropy alloys. *Journal of Alloys and Compounds*, *697*, 434-442.
44. Lee, J. E., Kim, K. S., Inoue, M., Jiang, J., & Suganuma, K. (2008). Effects of Ag and Cu addition on microstructural properties and oxidation resistance of Sn–Zn eutectic alloy. *Journal of Alloys and Compounds*, *454*(1-2), 310-320.
45. Xiong, W. (2015). CALPHAD-based integrated computational materials engineering research for materials genomic design. *JOM*, *67*(8), 1864-1865.
46. Ritter, N. C., Sowa, R., Schauer, J. C., Gruber, D., Goehler, T., Rettig, R., ... & Singer, R. F. (2018). Effects of solid solution strengthening elements Mo, Re, Ru, and W on transition temperatures in nickel-based superalloys with high γ′-volume fraction: Comparison of experiment and CALPHAD calculations. *Metallurgical and Materials Transactions A*, *49*(8), 3206-3216.
47. Andersson, J. O., Helander, T., Höglund, L., Shi, P., & Sundman, B. (2002). Thermo-Calc & DICTRA, computational tools for materials science. *Calphad*, *26*(2), 273-312.

48. Yang, S., Lu, J., Xing, F., Zhang, L., & Zhong, Y. (2020). Revisit the VEC rule in high entropy alloys (HEAs) with high-throughput CALPHAD approach and its applications for material design-A case study with Al–Co–Cr–Fe–Ni system. *Acta Materialia*, *192*, 11-19.

49. Kattner, U. R. (2016). The Calphad method and its role in material and process development. *Tecnologia em metalurgia, materiais e mineracao*, *13*(1), 3.

50. Ågren, J. (1982). Numerical treatment of diffusional reactions in multicomponent alloys. *Journal of Physics and Chemistry of Solids*, *43*(4), 385-391.

51. Andersson, J. O., & Ågren, J. (1992). Models for numerical treatment of multicomponent diffusion in simple phases. *Journal of applied physics*, *72*(4), 1350-1355.

52. Lu, X. G., Selleby, M., & Sundman, B. (2005). Theoretical modeling of molar volume and thermal expansion. *Acta materialia*, *53*(8), 2259-2272.

53. Liu, Z. K., Zhang, H., Ganeshan, S., Wang, Y., & Mathaudhu, S. N. (2010). Computational modeling of effects of alloying elements on elastic coefficients. *Scripta Materialia*, *63*(7), 686-691.

54. Uche, O. A., & Muhammad, I. H. (2014). Probabilistic Sensitivity Assessment of Composite Steel Beam Exposed to Fire. *American Journal of Civil and Structural Engineering*, *55*, 61.

55. Ketabdari, H., Daryan, A. S., & Hassani, N. (2019). Predicting post-fire mechanical properties of grade 8.8 and 10.9 steel bolts. *Journal of Constructional Steel Research*, *162*, 105735.

56. Choe, L., Varma, A. H., Agarwal, A., & Surovek, A. (2011). Fundamental behavior of steel beam-columns and columns under fire loading: experimental evaluation. *Journal of Structural Engineering*, *137*(9), 954-966.

57. Bertolini, L., Elsener, B., Pedeferri, P., Redaelli, E., & Polder, R. B. (2013). *Corrosion of steel in concrete: prevention, diagnosis, repair*. John Wiley & Sons.

58. Kim, S. H., Kim, H., & Kim, N. J. (2015). Brittle intermetallic compound makes ultrastrong low-density steel with large ductility. *Nature*, *518*(7537), 77-79.

59. Digges, T. G., Rosenberg, S. J., & Geil, G. W. (1966). *Heat treatment and properties of iron and steel*. NATIONAL BUREAU OF STANDARDS GAITHERSBURG MD.

60. Wang, W. Y., Liu, B., & Kodur, V. (2013). Effect of temperature on strength and elastic modulus of high-strength steel. *Journal of materials in civil engineering*, *25*(2), 174-182.
61. Huang, L., Li, G. Q., Wang, X. X., Zhang, C., Choe, L., & Engelhardt, M. (2018). High temperature mechanical properties of high strength structural steels Q550, Q690 and Q890. *Fire technology*, *54*(6), 1609-1628.
62. Khan, F., & Rashed, H. M. (2020). Phase Transformation in Micro-Alloyed Steels. In *Engineering Steels and High Entropy-Alloys*. IntechOpen.
63. Gong, P., Liu, X. G., Rijkenberg, A., & Rainforth, W. M. (2018). The effect of molybdenum on interphase precipitation and microstructures in microalloyed steels containing titanium and vanadium. *Acta Materialia*, *161*, 374-387.
64. Bain, E. C., & Paxton, H. W. (1966). Alloying elements in steel. *1966*, *291 P. AMERICAN SOCIETY FOR METALS, METALS PARK, OHIO*.
65. Campbell, K., & Honeycombe, R. W. K. (1974). The isothermal decomposition of austenite in simple chromium steels. *Metal Science*, *8*(1), 197-203.
66. Maalekian, M. (2007). The effects of alloying elements on steels (I).
67. Thibault, D., Bocher, P., Thomas, M., Lanteigne, J., Hovington, P., & Robichaud, P. (2011). Reformed austenite transformation during fatigue crack propagation of 13% Cr–4% Ni stainless steel. *Materials Science and Engineering: A*, *528*(21), 6519-6526.
68. Jang-Jaccard, J., & Nepal, S. (2014). A survey of emerging threats in cybersecurity. *Journal of Computer and System Sciences*, *80*(5), 973-993.
69. Néron, A., Lantagne, G., & Marcos, B. (2012). Computation of complex and constrained equilibria by minimization of the Gibbs free energy. *Chemical engineering science*, *82*, 260-271.
70. Kangas, P., Hannula, I., Koukkari, P., & Hupa, M. (2014). Modelling super-equilibrium in biomass gasification with the constrained Gibbs energy method. *Fuel*, *129*, 86-94.
71. Saunders, N., & Miodownik, A. P. (Eds.). (1998). *CALPHAD (calculation of phase diagrams): a comprehensive guide*. Elsevier.
72. Koukkari, P., & Pajarre, R. (2006). Calculation of constrained equilibria by Gibbs energy minimization. *Calphad*, *30*(1), 18-26.
73. Luo, A. A. (2015). Material design and development: From classical thermodynamics to CALPHAD and ICME approaches. *Calphad*, *50*, 6-22.

74. Luo, Q., Zhai, C., Sun, D., Chen, W., & Li, Q. (2019). Interpolation and extrapolation with the CALPHAD method. *Journal of Materials Science & Technology*, *35*(9), 2115-2120.

75. Shi, R., & Luo, A. A. (2018). Applications of CALPHAD modeling and databases in advanced lightweight metallic materials. *Calphad*, *62*, 1-17.

76. Cha, S. C., Hong, S. H., Kim, M. Y., Park, J., Shim, J. H., Jung, W. S., ... & Kozeschnik, E. (2016). CALPHAD-based alloy design for advanced automotive steels–Part II: Compositional and microstructural modification for advanced carburizing steels. *Calphad*, *54*, 172-180.

77. Zhang, Y. H., Li, M., Godlewski, L. A., Zindel, J. W., & Feng, Q. (2017). Effective design of new austenitic cast steels for ultra-high temperature automotive exhaust components through combined CALPHAD and experimental approaches. *Materials Science and Engineering: A*, *683*, 195-206.

78. Kaufman, L., & Cohen, M. (1956). The martensitic transformation in the iron-nickel system. *JOM*, *8*(10), 1393-1401.

79. Campbell, C. E., Kattner, U. R., & Liu, Z. K. (2014). The development of phase-based property data using the CALPHAD method and infrastructure needs. *Integrating Materials and Manufacturing Innovation*, *3*(1), 158-180.

80. Emel'yanenko, V. N., Verevkin, S. P., & Heintz, A. (2007). The gaseous enthalpy of formation of the ionic liquid 1-butyl-3-methylimidazolium dicyanamide from combustion calorimetry, vapor pressure measurements, and ab initio calculations. *Journal of the American Chemical Society*, *129*(13), 3930-3937.

81. Kattner, U. R. (1997). The thermodynamic modeling of multicomponent phase equilibria. *Jom*, *49*(12), 14-19.

82. Mitchell, R. J., Preuss, M., Tin, S., & Hardy, M. C. (2008). The influence of cooling rate from temperatures above the γ′ solvus on morphology, mismatch and hardness in advanced polycrystalline nickel-base superalloys. *Materials Science and Engineering: A*, *473*(1-2), 158-165.

83. Rao, G. A., Kumar, M., Srinivas, M., & Sarma, D. S. (2003). Effect of standard heat treatment on the microstructure and mechanical properties of hot isostatically pressed superalloy inconel 718. *Materials Science and Engineering: A*, *355*(1-2), 114-125.

84. Hosseini, V., Hurtig, K., Eyzop, D., Östberg, A., Janiak, P., & Karlsson, L. (2019). Ferrite content measurement in super duplex stainless steel welds. *Welding in the World*, *63*(2), 551-563.

85. Eckstein, H. J., Fennert, M., & Ohser, J. (1993). Application of thermodynamic computations to the solution behaviour of niobium and vanadium carbonitrides. *Steel research*, *64*(3), 143-147.

86. Lee, S. J., Matlock, D. K., & Van Tyne, C. J. (2011). An empirical model for carbon diffusion in austenite incorporating alloying element effects. *ISIJ international*, *51*(11), 1903-1911.

87. Liu, Y., Sun, Y. H., & Wu, H. T. (2021). Effects of chromium on the microstructure and hot ductility of Nb-microalloyed steel. *International Journal of Minerals, Metallurgy and Materials*, *28*(6), 1011-1021.

88. ZHOU, L. Y., LIU, Y. Z., FANG, Y., Huang, Q. W., & SONG, R. B. (2009). Effect of Cr on transformation of Ferrite and bainite dual phase steels [J]. *Journal of Iron and Steel Research*, *21*(7), 37-41.

89. Gogolin, J. A., & Tonn, B. (2018). Impact of Molybdenum on Heat-Treatment and Microstructure of ADI. In *Materials Science Forum* (Vol. 925, pp. 188-195). Trans Tech Publications Ltd.

90. Dekker, L. (2015). *Anwendung neuer Methoden in der Legierungsentwicklung am Beispiel eines warmfesten Gusseisens mit Kugelgraphit: Erkenntnisse zur Wirkung des Legierungselementes Molybdän*. Papierflieger Verlag GmbH.

91. Kong, L., Liu, Y., Song, Y., Li, S., Zhang, R., Li, T., & Liang, Y. (2015). The influence of chromium on the pearlite-austenite transformation kinetics of the Fe–Cr–C ternary steels. *Journal of Alloys and Compounds*, *648*, 494-499.

92. Ackermann, M., Resiak, B., Buessler, P., Michaut, B., & Bleck, W. (2020). Effect of molybdenum and cooling regime on microstructural heterogeneity in bainitic steel wires. *steel research international*, *91*(11), 1900663.

93. Chen, Z., Qi, J., Liu, H., Sun, L., Wei, H., & Wang, G. (2020). Bainitic Transformation and Mechanical Properties of Low-Carbon High-Strength Bainitic Steels with Mo Addition. *Journal of Materials Engineering and Performance*, *29*(4), 2428-2439.

94. Chance, J., & Ridley, N. (1981). Chromium partitioning during isothermal transformation of a eutectoid steel. *Metallurgical Transactions A*, *12*(7), 1205-1213.

95. De Moor, E., & Speer, J. G. (2017). Bainitic and quenching and partitioning steels. *Automotive steels*, 289-316.
96. Mohrbacher, H. (2018). Property optimization in as-quenched martensitic steel by molybdenum and niobium alloying. *Metals*, *8*(4), 234.
97. Jirková, H., Kučerová, L., & Mašek, B. (2015). The effect of chromium on microstructure development during QP process. *Materials Today: Proceedings*, *2*, S627-S630.
98. Morawiec, M., Ruiz-Jimenez, V., Garcia-Mateo, C., & Grajcar, A. (2020). Thermodynamic analysis and isothermal bainitic transformation kinetics in lean medium-Mn steels. *Journal of Thermal Analysis and Calorimetry*, *142*(5), 1709-1719.
99. Caballero, F. G., Bhadeshia, H. K. D. H., Mawella, K. J. A., Jones, D. G., & Brown, P. (2001). Design of novel high strength bainitic steels: Part 1. *Materials Science and Technology*, *17*(5), 512-516.
100. Caballero, F. G., Bhadeshia, H. K. D. H., Mawella, K. J. A., Jones, D. G., & Brown, P. (2001). Design of novel high strength bainitic steels: Part 2. *Materials Science and Technology*, *17*(5), 517-522.
101. Caballero, F. G., & Bhadeshia, H. K. D. H. (2004). Very strong bainite. *Current opinion in solid state and materials science*, *8*(3-4), 251-257.
102. Caballero, F. G., Santofimia, M. J., García-Mateo, C., Chao, J., & De Andres, C. G. (2009). Theoretical design and advanced microstructure in super high strength steels. *Materials & design*, *30*(6), 2077-2083.
103. Hasan, H. S., Peet, M. J., Avettand-Fènoël, M. N., & Bhadeshia, H. K. (2014). Effect of tempering upon the tensile properties of a nanostructured bainitic steel. *Materials Science and Engineering: A*, *615*, 340-347.
104. Yao, Z., Xu, G., Hu, H., Yuan, Q., Tian, J., & Zhou, M. (2019). Effect of Ni and Cr addition on transformation and properties of low-carbon bainitic steels. *Transactions of the Indian Institute of Metals*, *72*(5), 1167-1174.
105. Tian, J., Xu, G., Zhou, M., Hu, H., & Wan, X. (2017). The Effects of Cr and Al Addition on Transformation and Properties in Low-Carbon Bainitic Steels. *Metals*, *7*(2), 40.
106. Silva, J. F. D., Oliveira, C. A. S. D., Fonstein, N., Girina, O., Miranda, F. J. F., Drumond, J., ... & Afonso, C. R. M. (2016). Effect of Cr additions on ferrite

recrystallization and austenite formation in dual-phase steels heat treated in the intercritical temperature range. *Materials Research*, *19*, 258-266.

107. Michaud, P., Delagnes, D., Lamesle, P., Mathon, M. H., & Levaillant, C. (2007). The effect of the addition of alloying elements on carbide precipitation and mechanical properties in 5% chromium martensitic steels. *ACTA materialia*, *55*(14), 4877-4889.

108. Guitar, M. A., Suárez, S., Prat, O., Guigou, M. D., Gari, V., Pereira, G., & Mücklich, F. (2018). High chromium cast irons: destabilized-subcritical secondary carbide precipitation and its effect on hardness and wear properties. *Journal of Materials Engineering and Performance*, *27*(8), 3877-3885.

109. Bikmukhametov, I., Beladi, H., Wang, J., Hodgson, P. D., & Timokhina, I. (2019). The effect of strain on interphase precipitation characteristics in a Ti-Mo steel. *Acta Materialia*, *170*, 75-86.

110. Ginzburg, V. (1989). Steel-rolling technology. Theory and Practice, 328.

111. Imurai, S., Thanachayanont, C., Pearce, J. T. H., Tsuda, K., & Chairuangsri, T. (2014). Effects of Mo on microstructure of as-cast 28 wt.% Cr–2.6 wt.% C–(0–10) wt.% Mo irons. *Materials characterization*, *90*, 99-112.

112. DeMello, J. D. B., Durand-Charre, M., & Hamar-Thibault, S. (1983). Solidification and solid state transformations during cooling of chromium-molybdenum white cast irons. *Metallurgical Transactions A*, *14*(9), 1793-1801.

113. Ikeda, M., Umeda, T., Tong, C. P., Suzuki, T., Niwa, N., & Kato, O. (1992). Effect of molybdenum addition on solidification structure, mechanical properties and wear resistivity of high chromium cast irons. *ISIJ international*, *32*(11), 1157-1162.

114. Senior, B. A. (1988). A critical review of precipitation behaviour in 1Cr□ Mo□ V rotor steels. *Materials Science and Engineering: A*, *103*(2), 263-271.

115. Yamamoto, K., Inthidech, S., Sasaguri, N., & Matsubara, Y. (2014). Influence of Mo and W on high temperature hardness of M7C3 carbide in high chromium white cast iron. *Materials Transactions*, F-M2014801.

116. Yu, J., & McMahon, C. J. (1980). The effects of composition and carbide precipitation on temper embrittlement of 2.25 Cr-1 Mo steel: Part I. Effects of P and Sn. *Metallurgical Transactions A*, *11*(2), 277-289.

117. Clark, R. A., & Thomas, G. (1975). Design of strong tough Fe/Mo/C martensitic steels and the effects of cobalt. *Metallurgical Transactions A*, *6*(5), 969-979.

118. Eggeler, G. (1989). The effect of long-term creep on particle coarsening in tempered martensite ferritic steels. *Acta Metallurgica*, *37*(12), 3225-3234.

119. Mesquita, R. A., & Kestenbach, H. J. (2011). M3C and M7C3 Carbide Precipitation in Modified H11 Tool Steel. In *Solid State Phenomena* (Vol. 172, pp. 414-419). Trans Tech Publications Ltd.

120. Zhu, Q. T., Li, J., Shi, C. B., Yu, W. T., Shi, C. M., & Li, J. H. (2017). Precipitation behavior of carbides in high-carbon martensitic stainless steel. *International Journal of Materials Research*, *108*(1), 20-28.

121. Lee, T. H., Lee, Y. J., Joo, S. H., Nersisyan, H. H., Park, K. T., & Lee, J. H. (2015). Intergranular M 23 C 6 carbide precipitation behavior and its effect on mechanical properties of Inconel 690 tubes. *Metallurgical and Materials Transactions A*, *46*(9), 4020-4026.

122. Zhang, Y. J., Miyamoto, G., Shinbo, K., & Furuhara, T. (2020). Weak influence of ferrite growth rate and strong influence of driving force on dispersion of VC interphase precipitation in low carbon steels. *Acta Materialia*, *186*, 533-544.

123. Jiang, L., Marceau, R. K., Dorin, T., Yin, H., Sun, X., Hodgson, P. D., & Stanford, N. (2020). The Effect of Molybdenum on Precipitation Behaviour in Austenite of Strip-Cast Steels Containing Niobium. *Metals*, *10*(10), 1330.

124. FUJITA, T., ASAKURA, K., & MIYAKE, H. (1982). Effect of Chromium on Creep Rupture Strength and Microstructure of 10Cr-2Mo-V-Nb Heat Resisting Steels. *Transactions of the Iron and Steel Institute of Japan*, *22*(1), 13-21.

125. Jiang, L., Marceau, R. K., Dorin, T., Hodgson, P. D., & Stanford, N. (2019). Effect of molybdenum on phase transformation and microstructural evolution of strip cast steels containing niobium. *Journal of materials science*, *54*(2), 1769-1784.

126. Wang, Z., Zhang, H., Guo, C., Liu, W., Yang, Z., Sun, X., ... & Jiang, F. (2016). Effect of molybdenum addition on the precipitation of carbides in the austenite matrix of titanium micro-alloyed steels. *Journal of materials science*, *51*(10), 4996-5007.

127. Colás, R., & Totten, G. E. (Eds.). (2016). *Encyclopedia of iron, steel, and their alloys (Online version)*. CRC Press.

128. Inthidech, S., & Matsubara, Y. (2008). Effect of alloying elements on variation of micro-hardness during heat treatment of hypoeutectic high chromium cast iron. *Materials transactions*, *49*(10), 2322-2330.

129. Inthidech, S., Boonmak, K., Sricharoenchai, P., Sasaguri, N., & Matsubara, Y. (2010). Effect of repeated tempering on hardness and retained austenite of high chromium cast iron containing molybdenum. *Materials transactions*, *51*(7), 1264-1271.

130. Lee, W. B., Hong, S. G., Park, C. G., & Park, S. H. (2002). Carbide precipitation and high-temperature strength of hot-rolled high-strength, low-alloy steels containing Nb and Mo. *Metallurgical and Materials Transactions A*, *33*(6), 1689.

131. Maalekian, M. (2007). Early Stages of Precipitation.

132. Porter, D. A., & Easterling, K. E. (2009). *Phase transformations in metals and alloys (revised reprint)*. CRC press.

133. Liu, Q., Shibata, H., Hedström, P., Jönsson, P. G., & Nakajima, K. (2013). Dynamic precipitation behavior of secondary M7C3 carbides in Ti-alloyed high chromium cast iron. *ISIJ international*, *53*(7), 1237-1244.

134. Gharehbaghi, A. (2012). Precipitation study in a high temperature austenitic stainless steel using low voltage energy dispersive x-ray spectroscopy.

135. Leslie, W. C. (1981). The physical metallurgy of steels. *Hemisphere Publishing Corp., 1981*, 396.

136. Davenport, A. T., & Honeycombe, R. W. K. (1971). Precipitation of carbides at γ─α boundaries in alloy steels. *Proceedings of the Royal Society of London. A. Mathematical and Physical Sciences*, *322*(1549), 191-205.

137. Liu, Y., & Galvin, S. P. (1997). Criteria for pseudoelasticity in near-equiatomic NiTi shape memory alloys. *Acta materialia*, *45*(11), 4431-4439.

138. Liu, G., Dai, Z., Yang, Z., Zhang, C., Li, J., & Chen, H. (2020). Kinetic transitions and Mn partitioning during austenite growth from a mixture of partitioned cementite and ferrite: Role of heating rate. *Journal of Materials Science & Technology*, *49*, 70-80.

139. Mohrbacher, H. (2013). Reverse metallurgical engineering towards sustainable manufacturing of vehicles using Nb and Mo alloyed high performance steels. *Advances in manufacturing*, *1*(1), 28-41.

140. Mohrbacher, H., Spöttl, M., & Paegle, J. (2015). Innovative manufacturing technology enabling light weighting with steel in commercial vehicles. *Advances in Manufacturing*, *3*(1), 3-18.

141. Wang, S. C., & Kao, P. W. (1993). The effect of alloying elements on the structure and mechanical properties of ultra low carbon bainitic steels. *Journal of materials science*, *28*(19), 5169-5175.

142. Jung, S., Jo, Y. H., Jeon, C., Choi, W. M., Lee, B. J., Oh, Y. J., ... & Lee, S. (2017). Effects of Mn and Mo addition on high-temperature tensile properties in high-Ni-containing austenitic cast steels used for turbo-charger application. *Materials Science and Engineering: A*, *682*, 147-155.

143. Uranga, P., Shang, C. J., Senuma, T., Yang, J. R., Guo, A. M., & Mohrbacher, H. (2020). Molybdenum alloying in high-performance flat-rolled steel grades. *Advances in Manufacturing*, *8*(1), 15-34.

144. Mohrbacher, H. (2010). Principal effects of Mo in HSLA steels and cross effects with microalloying elements. *Central Iron and Steel Research Institute (CISRI)*, 75-96.

145. Krauss, G. (2015). *Steels: processing, structure, and performance*. Asm International.

146. Kong, J., & Xie, C. (2006). Effect of molybdenum on continuous cooling bainite transformation of low-carbon microalloyed steel. *Materials & design*, *27*(10), 1169-1173.

147. Rasouli, D., Asl, S. K., Akbarzadeh, A., & Daneshi, G. H. (2008). Effect of cooling rate on the microstructure and mechanical properties of microalloyed forging steel. *Journal of materials processing technology*, *206*(1-3), 92-98.

148. Chen, Z., Miao, S., Kong, L., Wei, X., Zhang, F., & Yu, H. (2020). Effect of Mo concentration on the microstructure evolution and properties of high boron cast steel. *Materials*, *13*(4), 975.

149. Qi, K., Yang, Y., Liang, W., Jin, K., & Xiong, L. (2021). Influence of the anomalous elastic modulus on the crack sensitivity and wear properties of laser cladding under the effects of a magnetic field and Cr addition. *Surface and Coatings Technology*, *423*, 127575.

150. Lepíková, K. (2015). Vliv podmínek technologie výroby na vlastnosti niklových superslitin.

151. Ledermueller, C., Pratiwi, H. I., Webster, R. F., Eizadjou, M., Ringer, S. P., & Primig, S. (2020). Microalloying effects of Mo versus Cr in HSLA steels with ultrafine-grained ferrite microstructures. *Materials & Design*, *185*, 108278.

152. Zamora, K. O., Sevillano, J. G., & Perez, M. F. (1992). Fracture toughness of W heavy metal alloys. *Materials Science and Engineering: A*, *157*(2), 151-160.

153. Lennon, A. M., & Ramesh, K. T. (2000). The thermoviscoplastic response of polycrystalline tungsten in compression. *Materials Science and Engineering: A*, *276*(1-2), 9-21.

154. Grobner, P. J., & Hagel, W. C. (1980). The effect of molybdenum on high-temperature properties of 9 pct Cr steels. *Metallurgical Transactions A*, *11*(4), 633-642.

155. Kong, L., Liu, Y., Song, Y., Li, S., Zhang, R., Li, T., & Liang, Y. (2015). The influence of chromium on the pearlite-austenite transformation kinetics of the Fe–Cr–C ternary steels. *Journal of Alloys and Compounds*, *648*, 494-499.

156. Zhang, G. H., Chae, J. Y., Kim, K. H., & Suh, D. W. (2013). Effects of Mn, Si and Cr addition on the dissolution and coarsening of pearlitic cementite during intercritical austenitization in Fe-1mass% C alloy. *Materials characterization*, *81*, 56-67.

157. Tian, J., Xu, G., Zhou, M., Hu, H., & Wan, X. (2017). The Effects of Cr and Al Addition on Transformation and Properties in Low-Carbon Bainitic Steels. *Metals*, *7*(2), 40.

158. Tkachuk, M. A., Golovin, S. V., Efron, L. I., & Il'inskii, V. I. (2016). Effect of Alloying with Molybdenum and Chromium on Pipe Steel of Strength Category X65 Properties. *Metallurgist*, *60*(5), 483-490.

159. Tkachuk, M. A., Golovin, S. V., Efron, L. I., & Il'inskii, V. I. (2016). Effect of Alloying with Molybdenum and Chromium on Pipe Steel of Strength Category X65 Properties. *Metallurgist*, *60*(5), 483-490.

160. Wang, W., Wang, J., Yi, H., Qi, W., & Peng, Q. (2018). Effect of molybdenum additives on corrosion behavior of (CoCrFeNi) 100− xMox high-entropy alloys. *Entropy*, *20*(12), 908.

161. Wu, H., Huang, S., Zhu, C., Zhu, H., & Xie, Z. (2020). Influence of Cr content on the microstructure and mechanical properties of CrxFeNiCu high entropy alloys. *Progress in Natural Science: Materials International*, *30*(2), 239-245.

162. Gao, X. R., Li, Y., Huang, H. D., Xu, J. Z., Xu, L., Ji, X., ... & Li, Z. M. (2019). Extensional stress-induced orientation and crystallization can regulate the balance of toughness and stiffness of polylactide films: interplay of oriented amorphous chains and crystallites. *Macromolecules*, *52*(14), 5278-5288.

163. Byun, T. S., Hashimoto, N., Farrell, K., & Lee, E. H. (2006). Characteristics of microscopic strain localization in irradiated 316 stainless steels and pure vanadium. *Journal of nuclear materials*, *349*(3), 251-264.

164. Molnar, D., Sun, X., Lu, S., Li, W., Engberg, G., & Vitos, L. (2019). Effect of temperature on the stacking fault energy and deformation behaviour in 316L austenitic stainless steel. *Materials Science and Engineering: A*, *759*, 490-497.

165. Davis, J. R. (Ed.). (2000). *Nickel, cobalt, and their alloys*. ASM international.